

UNIVERSITY OF CALIFORNIA

Los Angeles

**Nonlinear Plasma Wakefield Theory and
Optimum Scaling for Laser Wakefield
Accelerator (LWFA) in the Blowout Regime**

A dissertation submitted in partial satisfaction

of the requirements for the degree

Doctor of Philosophy in Electrical Engineering

by

Wei Lu

2006

© Copyright by
Wei Lu
2006

The dissertation of Wei Lu is approved.

Steve Cowley

F.F. Chen

Chan. Joshi

Warren B. Mori, Committee Chair

University of California, Los Angeles

2006

Chasing the light

To my family for their support, understanding, and above all, love

TABLE OF CONTENTS

1	Introduction	1
1.1	Introduction	1
1.2	Plasma Based Acceleration	5
1.3	Particle-in-Cell Simulation	11
1.4	Motivation and Outline	13
2	Nonlinear Theory for Relativistic Plasma Wakefields in the Blowout Regime	16
2.1	Introduction	16
2.2	The Basic Equations for Wake Excitation	20
2.3	On Blowout and Sheet Crossing	26
2.4	Wake Excitation in the Blowout Regime	33
2.5	On the Transition between Linear Theory and the Breakdown of Fluid Theory	42
2.6	The Ultra-relativistic Blowout Regime	45
2.7	Formulas for Arbitrary Blowout Radius	47
2.8	Differences between Laser Driver and Electron Beam Driver	49
2.9	Summary	53
3	Some Applications of the Nonlinear Wakefield Theory	54
3.1	Introduction	54

3.2	The optimum Plasma Density for Plasma Wakefield Excitation in the Blowout Regime	54
3.3	Beam Loading in the Blowout Regime	61
3.4	The Transformer Ratio for a Ramped Electron Beam	65
3.5	The Electron Hosing Instability in the Blowout Regime	68
3.5.1	What is the Electron Hosing Instability?	68
3.5.2	Toward a more General Hosing Theory for a Narrow Elec- tron Beam	72
4	On Wave Breaking and Particle Trapping in Plasma Waves	81
4.1	Introduction	81
4.1.1	What Does “Wave Breaking ” Mean in One-dimensional Plasma Waves	82
4.1.2	What Does “Wave Breaking ” Mean in Multi-dimensional Plasma Waves	85
4.1.3	“Periodic ” vs. “Driven” Waves	86
4.2	General Formalism for Particle Motion in Fields with Translational Symmetry	88
4.2.1	The General Trapping Condition	93
4.2.2	The General Particle Energy Bounds	94
4.3	Wave Breaking of Driven Plasma Waves	97
5	LWFA Scaling in the Blowout Regime	103
5.1	Introduction	103
5.2	What Do We Need for a LWFA as an Useful Accelerator?	106

5.3	What Does Linear Theory Tell Us?	107
5.3.1	Stability Consideration	108
5.3.2	Efficiency Consideration: Pump to Wake	110
5.3.3	Laser Guiding	113
5.3.4	Beam Loading and Beam Quality	114
5.3.5	Summary	117
5.4	Does Nature Force Us to the Blowout Regime?	118
5.5	Physics in the Blowout Regime	122
5.5.1	Blowout and Matching Condition	123
5.5.2	Wake Excitation	126
5.5.3	Local Pump Depletion and Laser Front Etching	128
5.5.4	Guiding : Self-Guiding or Channel Guiding	133
5.5.5	Injection and Beam Loading	136
5.5.6	Possible Laser Plasma Instabilities and Laser Pulse Distortions	137
5.6	Phenomenological Scaling and Its Verification by PIC Simulations	140
5.7	Comparison with the Scaling Based on Similarity Theory	148
5.8	Parameter Design for Future	152
6	Prospects for Plasma Based Acceleration in the Blowout Regime	159
6.1	Summary	159
6.2	Future Work	162
References	165

LIST OF FIGURES

2.1 Electron charge density with the defined blowout radius $r_b(\xi)$	17
2.2 Plots of trajectories for electrons at different initial radial position for an electron beam driver with $k_p\sigma_r = 0.01$, $k_p\sigma_z = \sqrt{2}$, the beam center $\xi_0 = 5$ and with (a) $n_{b0} = 1$ (b) $n_{b0} = 10$	29
2.3 $J_z/c - \rho$ profile from a PIC simulation	36
2.4 Comparison of the trajectories of $r_b(\xi)$ and the accelerating field $E_z(\xi)$ between theoretical calculations and PIC simulations: PIC simulation(red), calculation using a constant profile (green), and calculation using a varying profile (blue). The maximum blowout radius is (a) $r_m = 4$ (b) $r_m = 4$ with two beams (c) $r_m = 2$ (d) $r_m = 0.18$	40
2.5 Plasma density plots from PIC simulations with matched and un- matched spot sizes for the same laser power P and plasma density n_p , $P/P_c = 8$ (a) matched case with $k_pW_0 = 4$ and $a_0 = 4$ (b) unmatched case with $k_pW_0 = 3$ and $a_0 = 5.3$	52
3.1 The normalized beam dimensions $k_p\sigma_r$, $k_p\sigma_z$ and the normalized blowout radius $k_p r_m$ (the driver is a bi-Gaussian beam with $N =$ 1.8×10^{19} , $\sigma_z = 32\mu m$ and $\sigma_r = 10\mu m$)	58
3.2 The normalized and absolute peak wakefield amplitudes (the driver is a bi-Gaussian beam with $N = 1.8 \times 10^{19}$, $\sigma_z = 32\mu m$ and $\sigma_r = 10\mu m$)	59

3.3	Plasma wake driven by an electron beam with a linearly ramped current profile $n_b/n_p = 100$, $k_p a = 0.5$, $L_0 = 22$ (a) plasma phase space x2x1 (b) color plot of E1 (c) lineout of E1	78
3.4	A plot of the beam on top of the plot of the ion channel in the nominal “afterburner” simulation.	79
3.5	The centroid oscillation $ x_b $ (blue curve) in a self-generated channel and the prediction (red curve) from the fluid theory for an equilibrium channel. The black line is a linear fit for the initial growth in the simulation before the nonlinearity occurs. This initial growth is one order of magnitude smaller than the result for a equilibrium channel.	79
3.6	Density plots of the beams (red) and plasma (blue) in (a) the adiabatic non-relativistic regime; (b) the adiabatic relativistic regime; (c) the non-adiabatic non-relativistic regime; (d) the non-adiabatic relativistic regime. The beams move to the left in these plots. . .	80
3.7	Hosing growth in four regimes.	80
4.1	A weakly nonlinear coherent wake field driven by an 1D electron driver: $n_b/n_p = 0.1$, $k_p \sigma_z = 1.5$ (a) color plot of E1 (b) lineout of E1 (c) lineout of ψ (d) phase space p1x1	99
4.2	A strongly nonlinear wake field driven by an 1D electron driver: $n_b/n_p = 0.1$, $k_p \sigma_z = 1.5$ (a) color plot of E1 (b) lineout of E1 (c) lineout of ψ (d) phase space p1x1 (e) ψ near -1	100

4.3 A strongly nonlinear wake field driven by an 3D electron driver: $n_b/n_p = 100$, $k_p\sigma_z = \sqrt{2}$, $k_p\sigma_r = 0.5$	(a) color plot of phase space x2x1 (b) color plot of E1(c) lineout of E1 (d) lineout of ψ (e) ψ near -1 (f) phase space p1x1	101
5.1 A laser pulse with $a_0 = 1$, $k_p c \tau = \pi$ propagating through a plasma with $n_p/n_c = 0.00287$,	(a) E3 at time $t = 400\omega_0^{-1}$ (b) E3 at time $t = 20400\omega_0^{-1}$ (c) E1 at time $t = 400\omega_0^{-1}$ (d) E1 at time $t = 20400\omega_0^{-1}$	111
5.2 A laser pulse with $a_0 = 2$, $k_p c \tau = \pi$ propagating through a plasma with $n_p/n_c = 0.00287$,	(a) E3 at time $t = 800\omega_0^{-1}$ (b) E3 at time $t = 20400\omega_0^{-1}$ (c) E1 at time $t = 800\omega_0^{-1}$ (d) E1 at time $t = 20400\omega_0^{-1}$	112
5.3 A 30fs, 6TW short laser pulse with $a_0 = 2$, $k_p c \tau = \pi$ and $k_p W_0 \approx 2.83$ propagating through a plasma channel with $n_p/n_c = 0.00287$ on axis, note that $k_p c \tau_{rise}/\pi = 0.7$ and $k_p c \tau_{fall}/\pi = 1.3$	121
5.4 Plasma density plots for matched blowout of a laser driver, $P/P_c = 1$, $a_0 = 2$, $k_p W_0 = 2\sqrt{2}$, $k_p c \tau = \pi$ and $n_p/n_c = 0.00287$,	(a) at $0.57Z_r$ (b) at $2.85Z_r$ (c) at $6.27Z_r$ (d) at $10Z_r$	127
5.5 Lineouts of E3 for 1D and 3D simulations for $a_0 = 2$ and $n_p/n_c = 0.00287$ at $t = 2500\omega_0^{-1}$	(a) 1D simulation (b) 3D simulation with laser spot size $k_p W_0 = 2\sqrt{2}$ and a plasma channel depth $\Delta n_c/n_p = 1/2$	130
5.6 Lineouts of E3 for 1D and 3D simulations for $a_0 = 40$ and $n_p/n_c = 0.04$ at $t = 12000\omega_0^{-1}$	(a) 1D simulation (b) 3D simulation with matched laser spot size $k_p W_0 = 10$	131

5.7 A sequence of 2-dimensional slices ($x - z$) reveals the evolution of the accelerating structure (electron density, blue) and the laser pulse (orange). Each plot is a rectangular of size $z = 101.7\mu m$ (longitudinal direction, z) and $x = 129.3\mu m$ (transverse direction, x). A broken white circle is superimposed on each plot to show the shape of the blown-out region. When the front of the laser has propagated a distance, (a) $z = 0.3mm$ the matched laser pulse has clearly excited a wakefield. Apart from some local modification due to beam loading effects, as seen in (b) this wakefield remains robust even as the laser beam propagates though the plasma a distance of $7.5mm$ (as seen in (c) and (d)) or 5 Rayleigh lengths. After the laser beam has propagated $2mm$ (as seen in (b)) into the plasma, one can clearly see self-trapped electrons in the first accelerating bucket. The radial and longitudinal localization of the self-trapped bunch is evident in part (c). After $7.5mm$ the acceleration process terminates as the depleted laser pulse starts diffracting. 154

LIST OF TABLES

5.1	Comparison of Different Scaling Laws	151
5.2	Parameter Design for GeV and Beyond	153

ACKNOWLEDGMENTS

First of all, I would like to express my great gratitude to Prof. Warren Mori and Prof. Chan Joshi. Without their support, understanding and instruction, it would not have been possible for me to conduct all the work in this dissertation.

I would like to thank Prof. F. F. Chen and Prof. Steve Cowley, for their very kind support as members of my committee. Their advices are very valuable for me to finish this work.

I would also like to thank many persons from both the simulation and the experiment group at UCLA for their many contributions for this work. They are Michail Tzoufras, Miaomiao Zhou, Chengkun Huang, Frank Tsung, Viktor Decyk, Chris Clayton, Ken Marsh, Fang Fang, Joe Ralph.

Last but not least I would like to thank the staff, researchers, and students who I had the pleasure to work with for making UCLA such a friendly and welcoming place.

VITA

1977	Born, Suiping, Henan, China
1998	B.S. in Engineering Physics Tsinghua University , Beijing, China
2001	M.S. in Engineering Physics Tsinghua University , Beijing , China
2006	Ph.D. in Electrical Engineering University of California, Los Angeles

PUBLICATIONS

W. Lu et al., “ On Trapping and Wave Breaking of Driven Plasma Wave”, in preparation

W. Lu, M. Tzoufras, M. Zhou and W. B. Mori, “Several Issues in the Blowout Regime: optimum Plasma Density for Wake Excitation, Beam Loading and Transformer Ratio” , in preparation

C. Huang, W. Lu, M. Zhou et al., “Hosing Instability in the Blowout Regime for Plasma Wakefield Acceleration”, to be submitted to PRL

W. Lu, M. Tzoufras, C. Joshi, F. S. Tsung, W. B. Mori, J. Vieira, R. A.

Fonseca, and L. O. Silva, “Generating Multi-GeV Electron Bunches Using Single Stage Laser Wakefield Acceleration in a 3D Nonlinear Regime”, submitted to Nature Physics

Blumenfeld et al., “Energy Doubling of 42 GeV Electrons in a Meter Scale Plasma Wakefield Accelerator”, accepted by Nature

D.K. Johnson et al., “Positron Production by X Rays Emitted by Betatron Motion in a Plasma Wiggler”, Phys. Rev. Lett. 97, 175003, 2006

C. Huang et al., “QUICPIC: A Highly Efficient Particle-in-cell Code for Modeling Wakefield Acceleration in Plasma”, Journal of Computational Physics, 217, 658-679, 2006

F. S. Tsung, W. Lu, M. Tzoufras, W. B. Mori, C. Joshi, J. M. Vieira, L. O. Silva, and R. A. Fonseca, “Simulation of monoenergetic electron generation via laser wakefield accelerators for 525 TW lasers”, Phys. Plasmas, 13, 056708, 2006

W. Lu, C. Huang, M. Zhou, M. Tzoufras, F. S. Tsung, W. B. Mori and T. Katsouleas, “A Nonlinear Theory for Multidimensional Relativistic Plasma Wave Wakefields”, Phys. Plasmas, 13, 056709, 2006

W. Lu, C. Huang, M. Zhou, W. B. Mori and T. Katsouleas, “ Nonlinear Theory for Relativistic Plasma Wakefields in the Blowout Regime” , Phys. Rev. Lett., 96, 165002, 2006

S. Deng et al., "Hose Instability and Wake Generation by an Intense Electron Beam in a Self-Ionized Gas", Phys. Rev. Lett. 96, 045001 2006

W. Lu, C. Huang, M. Zhou, W. B. Mori and T. Katsouleas, "Limits of Linear Plasma Wakefield Theory for Electron or Positron Beams ", Phys. Plasmas, 12, 063101, 2005

M. J. Hogan et al., "Multi-GeV Energy Gain in a Plasma-Wakefield Accelerator", Phys. Rev. Lett. 95, 054802 2005

W.Lu , C.Huang , M.M.Zhou , W.B.Mori , Linear Wakefield expression for Bi-Gaussian Drive Bunches, Proceedings of the 11th Advance Accelerator Workshop , 2004

S. Deng et al., "Modeling E164x experiment", AIP Conf. Proc. 737, 936, 2004

E. Oz et al., "Optical Diagnostics for Plasma Wakefield Accelerators", AIP Conf. Proc. 737, 708 , 2004

C. Huang et al., " Simulation of a 50GeV PWFA stage", AIP Conf. Proc. 737, 433 , 2004

P. Muggli et. al., "Meter-Scale Plasma-Wakefield Accelerator Driven by a Matched Electron Beam", Phys. Rev. Lett. 93, 014802 2004

B. E. Blue et al., “Plasma-Wakefield Acceleration of an Intense Positron Beam”, Phys. Rev. Lett. 90, 214801 2003

S. Deng et al., “Plasma wakefield acceleration in self-ionized gas or plasmas”, Phys. Rev. E 68, 047401 2003

M. Hogan et al., “Acceleration and Focusing of Electrons and Positron Using a 30GeV Drive Beam”, AIP Conf. Proc. 647, 3 2002

S. Deng et al., “ Modeling Ionization Physics with the PIC Code OSIRIS”, AIP Conf. Proc. 647, 219 , 2002

ABSTRACT OF THE DISSERTATION

**Nonlinear Plasma Wakefield Theory and
Optimum Scaling for Laser Wakefield
Accelerator (LWFA) in the Blowout Regime**

by

Wei Lu

Doctor of Philosophy in Electrical Engineering

University of California, Los Angeles, 2006

Professor Warren B. Mori, Chair

In this dissertation, we analyze through theory and simulation many important aspects of a highly nonlinear regime for plasma based acceleration, namely the blowout regime. In chapter 2, a nonlinear kinetic theory for multidimensional plasma wave wakes with phase velocities near the speed of light is presented. This theory is appropriate for describing plasma wakes excited in the so-called blowout regime by either electron beams or laser pulses where the plasma electrons move predominantly in the transverse direction. The theory assumes that all electrons within a blowout radius are completely expelled. These radially expelled electrons form a narrow sheath just beyond the blowout radius which is surrounded by a region which responds weakly. This assumption is reasonable when the spot size of the electron beam and laser are substantially less than the blowout radius. By using this theory one can predict the wakefield amplitudes and blowout radius in terms of the electron beam or laser beam parameters, as well as predict the nonlinear modifications to the wakes wavelength and wave form. For the laser case, the laser spot size must also be properly matched in order for a narrow

sheath to form. The requirements for forming a spherical wave form, i.e., bubble, are also discussed. The theory is also used to show when linear fluid theory breaks down and how this leads to a saturation of the logarithmic divergence in the linear Greens function.

In chapter 3, we apply the theoretical framework in chapter 2 on four different physical problems in the blowout regime. First, the optimum plasma density for maximum wakefield amplitude in the relativistic blowout regime is obtained. Then the problem of beamloading in the blowout regime is discussed. The third problem is on how to optimize the transformer ratio by using a linear ramped electron beam driver. The last problem is about the electron hosing instability in the blowout regime.

Then in chapter 4, we give an extensive analysis of electron trapping in arbitrary electromagnetic fields with translation symmetry. The general trapping condition and energy gain limits will be derived. Based on these analysis, we will discuss the physical meaning of wavebreaking limits derived from 1D fluid theory and show that these limits are not achievable in a system with a driver (laser or electron beam). Particle trapping and significant wave amplitude damping will occur far before these theoretical wave amplitude limits being reached in both 1D and multi-dimensional wakefields. These analyses clarify a subtle point that misleading the plasma physicists about the meaning of wavebreaking for many years .

In chapter 5, we discuss what is the possible parameter regime for LWFA to be useable as a real accelerator technology. We start from discussions of the necessary conditions and analyze what they suggest in the weakly nonlinear wakefield regime. Then we show the analyses in weakly nonlinear regime prefer a regime where the assumption of weakly nonlinear totally breaks down, namely

the blowout regime. We then discuss many physical aspects in this regime and derive a group of scaling laws to extrapolate this regime to higher energy (GeV and beyond).

Finally in chapter 6, we summarize the results, discuss the prospects of plasma acceleration technologies, and provide directions for further research.

CHAPTER 1

Introduction

1.1 Introduction

Physics is the science about the understanding of how matter interacts with each other. These interactions occur with their specific time, space and energy scales [1]. For any physical phenomena to be identifiable, it must have these three scales. This is so true such that in many situations we never mention them explicitly. For me, the most striking beauty of nature is that we can make accurate predictions and understand it without knowing every detail. Indeed, if this were not true, one could hardly imagine how the study of science could have ever gotten started. This is also the reason why doing science is not an overwhelming task and can be very enjoyable in many cases. So the real objective of most physical science is not to determine the “ultimate” theory valid for all scales but rather to come up with simplified models valid within restricted scales that can give the necessary explanation and effective prediction for the given phenomena. This is not only true for applied physics where specific physical systems are explored, it is also true in fundamental physics where the understanding of the interactions between the fundamental building blocks of matter is pursued [1].

Contemporary physics research has two seemingly distinct but equally important trends: one is to go deeper and deeper to identify the most basic building blocks and physical processes that underly all physical phenomena. The subjects

of elementary particle physics and cosmology belong to this category. This is the traditional trend of physics since the beginning of modern science and it remains very important. The other trend, which is becoming more and more important is to explore complex physical systems with more and more realism. For such systems, the microscopic elementary processes are all well known but these systems have enormously many degrees of freedom so their macroscopic behavior can be extremely rich and complex. Condense matter physics, fluid dynamics, plasma physics et al. are examples that belong to this category. One important common characteristic of these complex systems is that they generally have many physical processes that are coupled and occur simultaneously. Each of these processes may have very different time, space and energy scales.

The major topic of this dissertation is about the physics of how ultra-short ultra-intense lasers or particle beams interact with matter. This is an interesting and rapidly emerging subfield of physics and it can be seen as a rich example of the second category discussed above. It can also be seen as an interdisciplinary field involving nonlinear optics and plasma physics.

With the development of ultra-intense short pulse laser technology, i.e., chirped-pulse-amplification (CPA) [2, 3] and Ti:Sapphire laser systems [4, 5, 6, 7], multi-TW (10 - 100 TW) tabletop laser systems now are widely available in university scale laboratories [8, 9, 10, 11]. In addition, PW scale lasers are under construction around the world. The focused intensity of these lasers can easily exceed $10^{18} W/cm^2$ (many such systems can reach $10^{20} - 10^{21} W/cm^2$). Compared with normal matter, the energy density within these pulses is enormously large. The focused intensity of these lasers is many orders of magnitude larger than the binding force in normal matter (gas, liquid and solid) so that matter becomes fully ionized within just a few laser oscillations. Due to this reason, laser-matter

interaction at these intensities is almost equivalent to laser-plasma interaction. In vacuum the oscillating electron energy can easily reach energies exceeding 10 MeV, therefore relativistic effects become significant.

To see how rich and complex the relevant physics can be, some examples may help. Consider a simple experimental setup where a relativistically intense short laser pulse propagates through a cm long gas jet target. Imagine that we are observing the whole process: starting from the laser reaching the gas edge and ending when it leaves the target. There are many time and space scales involved, and within each scale there are distinct physical phenomena occurring.

On the shortest time scale, e.g. a few fs (a few μm in space), tunneling ionization of the gas atoms by the leading front of the laser occurs and this will form a relatively cold plasma [12, 13, 14]. The density profile can significantly differ depending on what kind of gas is used.

On a slightly longer time scale, e.g., tens of fs to a few hundreds of fs (depending on the plasma density), the laser pulse starts to interact with the plasma without significantly evolving. A plasma wave wake can be formed and THz radiation from these plasma oscillations can be generated [15].

On a ps time scale, the laser starts to evolve and many kinds of laser plasma instabilities may grow. e.g., the laser may self-focus, self-modulate or filament [16]. It can also interact and couple to the plasma wake leading to enhanced wake fields and Raman scattering [17, 18, 19]. In addition, plasma electrons can get trapped in the wake and become accelerated to very high energy. These electrons can significantly affect the wake structure, i.e, load down its amplitude [20]. X rays may also be generated by the interaction between the high energy electrons with the laser or the plasma wake [21, 22].

On an even longer time scale, i.e., 10 ps to ns, the energy deposited in the

plasma can couple into ion modes. The plasma may experience hydrodynamic expansion and may be heated by the dissipation of coherent energy, and electrons and ions may recombine and emit incoherent light[23, 24, 25].

This list is only a small fraction of the phenomena one can expect from ultra-intense laser matter interactions. But it is already enough to show the richness of relevant physics. One major goal of research in this field is to understand various physical processes and identify the usable parameter regime for real applications, e.g., compact accelerators and light sources.

Since laser pulses can be seen as a beam of photons [26], it is easy to understand that ultra-short intense relativistic charged particle beams can exhibit very similar behavior when interacting with matter. Modern large scale accelerators can provide charged particle beams of multi-GeV energy with a nC of charge. When properly focused, the charged particle beams from such machines can achieve the same energy density as in a focused PW laser. For example, the largest linear accelerator in the world (SLAC) can provide sub 100fs , 50GeV electron beams with 3nC of charge at rep rate of 1Hz . Although such a system is not widely available, they have many advantages when compared with the current state-of-the-art lasers. For example, the peak power is a few PW and the rep rate is much higher than the laser systems with the same amount of energy. The beam quality is well controlled and diagnosed. In addition, while there are similarities between beam plasma and laser plasma interactions, there are significant differences. These differences make the choice between using a laser or particle beam depend on the application.

1.2 Plasma Based Acceleration

One important potential application of the physics of a short pulse laser or charged particle beam interacting with a plasma is plasma based acceleration. This is also the major topic of this dissertation.

The application of charged particle beams in general scientific research and industry is currently much more restricted than that of lasers. The major reason is the very large cost of building and maintaining particle accelerators due to their complicated structure and large sizes. The RF-waveguide technology used in current accelerators can support accelerating gradients no more than 50MeV/m due to the breakdown of the material on the metallic wall. Therefore, to obtain significant beam energy (GeV and beyond) requires large RF-waveguides (at least tens of meters long) and to manipulate the beam by magnetic fields typically requires magnetic fields coils. For the very large beam energies needed in high energy physics (100GeV to TeV), the accelerator size based on RF technology is extremely large. For example, the 50GeV linear electron/positron accelerator at SLAC is more than two miles long and the Large Hadron Collider (LHC) is 27km in circumference. To build and to operate such gigantic machines is formidable. It requires the state of the art in engineering and management.

One obvious way to significantly reduce the size and cost of the accelerator is to use much larger accelerating fields, e.g., hundreds times larger than the material breakdown fields ($\gtrsim 10\text{GeV/m}$). One medium that can support such huge fields is plasma. Since it is fully ionized, it naturally avoids the problem of breakdown. It has been well known since 1950's that electrostatic waves in a cold plasma with relativistic phase velocities can support wave amplitudes in excess of the non-relativistic wave breaking limit, $E_{wb} \simeq \frac{mc\omega_p}{e} \simeq \sqrt{n_p}V/\text{cm}$ [66]. For a typical plasma with a density of $1 \times 10^{18}\text{cm}^{-3}$, this corresponds to a gradient

about $100\text{GV}/m$, more than one thousand times larger than the breakdown field in conventional RF structures. If such a wave can be generated and employed to accelerate charged particles, it might be possible to reduce the size of an accelerator by a factor of one thousand. In 1979, Tajima and Dawson pointed out that one way to drive such plasma waves is to use an intense short-pulse laser [27]. This paper lead to the birth of the field of plasma based acceleration. Since then, plasma based wakefield acceleration has attracted much interest and evolved into a very active research field in advanced accelerator research and basic plasma research.

After more than twenty years of extensive research, many ideas based on producing and utilizing plasma wakefields have been proposed and tested. Two kinds of drivers are typically used to produce these large plasma wakes: namely high-power short-pulse lasers and high current ultra-relativistic charged particle beams. Both can excite a plasma wake with a phase velocity very close to the speed of light, which can then be used to accelerate a injected relativistic charged particle bunch to high energy.

For the laser driven case, the ponderomotive force (radiation pressure) of laser pulse can displace plasma electrons away from the neutralizing ion background. The space charge force of the ions pulls the electrons back thereby setting up a plasma wake. Several related schemes have been proposed for using a laser to excite the plasma wave wake. Among them the following three schemes are the most well known and most explored: LWFA [27] (Laser Wake Field Accelerator), PBWA [28] (Plasma Beat Wave Accelerator) and SMLWFA [29, 30] (Self-Modulated Laser Wake Field Accelerator). It is interesting to note that all three of these schemes were originally mentioned in the 1979 paper by Tajima and Dawson. In LWFA, the laser pulse is an intense ultra-short laser pulse with a pulse

duration about half the plasma period. To operate in such a regime, extremely short pulses with very high peak power are needed. This requirement is why this simplest scheme has only recently been explored experimentally. In PBWA, two laser pulses with a frequency difference matched to the plasma frequency ω_p are used. The pulse length is several to many plasma wave lengths long. The beat of these two lasers can be viewed as a series of successive short pulses each with a length about plasma wake wave length. This is the first scheme that was explored extensively in experiments due to the reason that there was no short pulse laser available in early 1980's. Using beat wave excitation, in the 1980's the UCLA group demonstrated that relativistic plasma wakes could be generated [31] and in the early 1990's they accelerated externally injected electrons [32, 33]. Indeed these are the first two milestones in plasma based accelerator experimental research. The physics of PBWA is extremely rich because the laser pulses are long. However, this is also the reason that PBWA will most likely not be used in a practical accelerator, i.e., there are too many laser-plasma and plasma wave instabilities of long laser pulses. In the SMLWFA concept, a single intense short laser pulse of many plasma wavelengths long is utilized. As the laser propagates, it becomes unstable to Raman forward scattering. The laser then beats with the scattered light to excite the plasma wake. The self-modulation of the laser is complicated because self-focusing can also couple with the wake excitation process, leading to the breakup of the laser pulse into many beamlets and the enhancement of wake field excitation [29]. The advantage of SMLWFA compared with LWFA is that it needs much less laser power to excite large wake because very high plasma densities can be used. So it was preferred in experiments during 1990's to early 2000's. Many important experimental milestones were achieved in SMLWFA. For example, very high gradient acceleration up to 1TeV/m, large amounts of self-trapped electrons, high electron energies, up to 200MeV, and the

generation of beams with very small divergence angles [34]. However, SMLWFA excites a wake through an instability, so it is unlikely to make a real accelerator.

For the beam driven plasma wake field [35] or so called plasma wakefield accelerator (PWFA), the electromagnetic force from the beam charge and current plays a similar role as the ponderomotive force from the laser. For an ultra-relativistic electron beam moving into a plasma, the space charge force will push the plasma electrons away from the ion background. The displaced electrons then rush back after the beam has passed through thereby create a plasma wake. The most promising application of this scheme is the idea of a plasma afterburner [36], where two short plasma sections are placed before the IP of an existing linear collider to double the energy of the incoming beams. Very recently, a collaboration involving UCLA, USC and SLAC has achieved many milestones towards the demonstration of the key physics of a plasma afterburner [37, 38, 39, 40, 41, 42, 43, 44, 45, 46, 47, 48, 49, 50, 51, 52, 53, 54]. These include the first demonstration of acceleration of a positron beam by positron driven wakefields [44], the first multi-GeV energy gain for any plasma based acceleration [48], and the doubling of the energy of the tail of a 42GeV electron beam in less than one meter [54]! These exciting results are pushing accelerator physicists to seriously consider the possible application of plasmas in high energy physics.

For practical reasons, in experiments for both PWFA and LWFA, the drivers are tightly focused to achieve a large enough intensity for exciting large plasma wake. The narrow spot sizes of the drivers induce forces in the transverse dimensions that are comparable to those in the longitudinal direction. This leads to significant multi-dimensional effects that are absent in one-dimensional theories. In fact for typical situations, the drivers can completely expel the plasma electrons radially outward thereby forming a pure ion region (an ion channel)

behind it. When wakes are excited in this manner it is called the blowout regime. The identification of this regime is definitely one of the most important advances in the field of plasma based acceleration. As we will argue it is the method of choice for accelerating electrons.

A short introduction of the history of the blowout regime is in order. In 1987, Sun et al. [55] derived the equilibrium profiles of both a laser and plasma density for a self-guided laser pulse sufficiently short that the ions don't move but sufficiently long that no wake is excited. They found that for a laser power slightly larger than the critical power of relativistic self-focusing P_c , the equilibrium electron density profile becomes completely evacuated up to some radius. This phenomena was called electron "cavitation" by Sun et al. due to its similarity to fluid phenomena. Because this analysis was for relatively long pulses where wakefields are not excited, its implication for plasma based acceleration was not appreciated immediately. In addition, some assumptions regarding the radial profile for the plasma response were not correct. Nevertheless, their work indicates that an intense laser pulse with $P \sim P_c$ would self-focus until the intensity increases and the spot size decreases to the point where cavitation occurred. This work also hinted at the idea of a "matched" spot size of a given laser power for which the laser spot size would remain constant.

A few years later in 1991, Rosenzweig et al. [56] found an interesting regime for electron beam driven plasma wakefield through 2D ($r - \phi$) fluid and PIC simulations. In this regime, a short (about plasma wavelength) and narrow (spot size smaller than plasma skin depth) electron bunch with sufficient charge can expels (blows out) the plasma electrons away from its path to form a pure ion region around and behind it. This phenomenon is very similar to what Sun et al. found for a laser. Most importantly, Rosenzweig et al. pointed out that

the accelerating field inside a cylindrical symmetric channel is uniform across the transverse dimensions and that the focusing force depends linearly on the radius. Both of these properties are very attractive for an accelerator as they lead to no energy spread and no emittance growth. This regime was called the “blowout” regime.

Very soon thereafter it was recognized that similar wakes could be excited using a short laser driver. In 1991, Mori et al. [57] presented 2D PIC simulation results which showed that LWFA in this regime also had the advantages of a uniform accelerating field and a linear focusing force. However, in their paper Mori et al. also recognized that for existing lasers the power was too low and the pulse length too long to reach this regime.

During the early to late 1990’s, there were numerous experimental results on laser plasma acceleration. These experiments demonstrated extremely large acceleration gradients ($\sim 1\text{TeV}/m$) but the acceleration length was limited to 100’s of μm ’s. In response to this limitation in the acceleration length, a research program on plasma based acceleration was begun at the Stanford Linear Accelerator (SLAC) in the late 1990’s. This was a collaboration between UCLA, USC and SLAC. The goal was to demonstrate acceleration in plasma wakes over meter scale distance. While there are many similarities with how particle beams and lasers interact with plasma, there are also significant differences. To plan and interpret these PWFA experiments, a vigorous simulation and theory effort was also begun in the blowout regime. Much of this will be described later in this dissertation.

Very recently, much simulation/theory and experimental progress has been made on LWFA in the blowout regime. In 2002, Pukhov and Meyer-ter-vehn observed a very interesting phenomena in the first 3D PIC simulations of LWFA

[58]. They simulated a 300 TW 30 fs laser propagating in a $2 \times 10^{19} cm^{-3}$ plasma. They found that mono-energetic electron beams with large amount of charge can be self injected near the tail of the ion channel. They believed that this phenomena only occurred at very high laser intensity, laser power and plasma density. Furthermore, the shape of the ion channel in these simulations resembled a sphere. In a subsequent paper they coined the term “Bubble” regime. Several years later, Tsung et al.[59] showed that self-injected mono-energetic beams could also be produced at lower laser powers, intensities and plasma densities. They simulated a 16TW laser propagating in a $3 \times 10^{18} cm^{-3}$ plasma. Very soon thereafter, in 2004, three independent groups around the world reported self-generated mono-energetic electron beams with energies between $70 \sim 200 MeV$ by shooting $10 \sim 30 TW$, $30 \sim 40 fs$ laser pulses into mm scale gas jet targets [60, 61, 62]. Since then, more than 20 different groups around the world have reported similar results. A new record just came out a few months ago. The LBNL group reported a $1 GeV$ mono-energetic electron beam generated by propagating a $40 TW, 40 fs$ short laser pulse through a cm scale capillary discharge plasma wave guide [63]. With the development of more power and compact laser sources and more sophisticated diagnostic technologies, much more exciting new results will come out in the very near future.

1.3 Particle-in-Cell Simulation

Theory, experiment and simulation are three major tools in scientific research with each has its advantages and disadvantages. They are closely related in many fields of contemporary scientific activities. This is especially true for plasma physics. Plasma is a very complex state of matter and the physical processes in plasma are extremely rich and complex. Generally to fully understand some

physical phenomena in plasma, very close collaborations between theory, experiment and simulation are needed. Two most well known examples are magnetic confined fusion and inertial confined fusion.

With the advances of parallel computing, the importance of simulations continues to increase in many fields of physics. There is no where more true than in plasma physics. In many problems in plasma physics, the distribution function is far from equilibrium, collisions are infrequent, and the long range forces of individual particles are coupled. Therefore to study such problems, fully kinetic algorithms are needed. One such algorithm is the particle-in-cell method which is the method of choice for modeling intense laser and beam plasma interactions.

The idea behind the particle-in-cell (PIC) method is very straight forward [64]. The electromagnetic fields are represented on a grid with a resolution high enough to resolve the shortest spatial scales of interests. The particles move within the grid and can be thought of as finite size particles with a size equal to that of the grid. In each cycle (time step) of the simulation, the particles are first pushed to new positions and momenta according to the equation of motion with the force obtained by interpolating the fields defined at the grid locations to where the particle resides within the grid. The charge and current density are then interpolated onto the grid from the particles' positions. Last, the fields are advanced according to Maxwell equations with this current density. The simulations are run for the desired number of steps.

The PIC algorithm has been developed extensively during the past 30 years. With the rapid development of computer technology and parallel computing in the last 20 years, we now have the ability to model the full scales both in time and space of experiments in a full 3D geometry. This was unthinkable even just ten years ago. Without this powerful modeling ability, much of the theoretical

progress described in this dissertation would not have been possible.

1.4 Motivation and Outline

Despite the extensive interest in the blowout regime for both laser and electron beam drivers, many theoretical issues remained unclear until very recently. For example, no theory existed on how the wake is excited and how to parametrize the blowout regime, no methods for optimizing the wake fields for a given driver parameters or optimizing the driver shape to achieve higher transformer ratio existed, no theory for beam loading existed in this regime, and no theory for the electron hosing instability of short electron bunches existed. In addition, recent simulations and experiments in LWFA naturally lead one to ask the following questions. How does self-injection occur in a multi-dimensional wake? How can the recent experimental results be scaled to higher energy and better beam quality? What kind of instabilities can affect the realization of a practical accelerator? In the rest of this dissertation, we will try to present several recent theoretical and simulation results which might clarify many of these issues. The following is an outline of each chapter.

In chapter 2, a nonlinear kinetic theory for multidimensional plasma wave wakes with phase velocities near the speed of light is presented. This theory is appropriate for describing plasma wakes excited in the so-called blowout regime by either electron beams or laser pulses where the plasma electrons move predominantly in the transverse direction. The theory assumes that all electrons within a blowout radius are completely expelled. These radially expelled electrons form a narrow sheath just beyond the blowout radius which is surrounded by a region which responds weakly. This assumption is reasonable when the spot size of the electron beam and laser are substantially less than the blowout radius. By using

this theory one can predict the wakefield amplitudes and blowout radius in terms of the electron beam or laser beam parameters, as well as predict the nonlinear modifications to the wakes wavelength and wave form. For the laser case, the laser spot size must also be properly matched in order for a narrow sheath to form. The requirements for forming a spherical wave form, i.e., bubble, are also discussed. The theory is also used to show when linear fluid theory breaks down and how this leads to a saturation of the logarithmic divergence in the linear Greens function.

In chapter 3, we apply the theoretical framework in chapter 2 to four different physical problems in the blowout regime. First, the optimum plasma density for maximum wakefield amplitude in the relativistic blowout regime is obtained. Next, the problem of beamloading in the blowout regime is discussed. A expression is given for the number of electrons that can be loaded into a nonlinear 3D wakefield. Next, we apply the theory in chapter 2 to show that even in the blowout regime the transformer ratio is optimized for an electron beam with a linearly ramped current profile. Last, we describe how the theory can be applied to the electron hosing instability.

In chapter 4, we give an extensive analysis of electron trapping and self-injection in arbitrary electromagnetic fields with translation symmetry. The general trapping condition and limit on energy gain are derived. Based on this analysis, we will discuss the physical meaning of wavebreaking limit derived from 1D fluid theory for an infinite wave train and show that fields at this wave breaking limit are not achievable in a system with a driver (laser or electron beam). Particle trapping and significant loading of the wake will occur far before the theoretical wave breaking limit is reached for both 1D and multi-dimensional wakefields. This analysis clarifies a subtle point that has confounded plasma

physicists about the meaning of wave breaking for driven wakes for many years .

In chapter 5, we discuss what is the possible parameter regimes for LWFA that might be useable in a real accelerator. We start by considering requirements for any high energy physics accelerator regarding the stability, the number of accelerated electrons, their beam quality and the over all efficiency if one used the weakly nonlinear wakefield regime. We argue that this exercise illustrates that the assumption of a weakly nonlinear wake is inconsistent with these requirements and that the blowout regime is the natural result. We then provide a phenomenological theory for LWFA and use it to obtain expressions that can be used to extrapolate this regime to higher energies, namely 1GeV -1TeV. We also present 3D PIC simulation results that are in agreement with our theory.

Finally in chapter 6, we summarize our results and discuss directions for further research.

CHAPTER 2

Nonlinear Theory for Relativistic Plasma Wakefields in the Blowout Regime

2.1 Introduction

The theory of one-dimensional, nonlinear plasma oscillations in cold plasmas has a long history beginning with the pioneering work of Akhiezer and Polovin [65], and Dawson [66]. Akhiezer and Polovin studied purely one-dimensional (1D) longitudinal and transverse oscillations in cold plasmas including relativistic mass effects. In the work of Dawson, non-relativistic treatments of purely 1D longitudinal oscillations were studied, including radial and spherical oscillations. He showed that trajectory crossing occurs in either radial or spherical oscillations even for arbitrarily small amplitudes. However, more than 40 years later there is still no theory for multi-dimensional (3D), nonlinear plasma oscillations associated with waves with phase velocities near the speed of light, c . Such oscillations are complicated because the fields are electromagnetic, relativistic mass effects are important, and trajectory crossing occurs. Besides being of great fundamental interest, a class of these nonlinear multi-dimensional plasma waves are of great importance to plasma based acceleration.

In plasma-based acceleration, a plasma wave with a phase velocity close to the speed of light is driven by an intense particle or laser beam. When a laser beam

is used it is called laser wakefield acceleration (LWFA)[27] and when a particle beam is used it is called plasma wakefield acceleration (PWFA)[35]. Most theories to date on wakefield excitation have either been restricted to linear fluid theory [35, 49, 74] or one dimensional nonlinear fluid theory[65]. However, in recent PWFA and LWFA experiments [60, 61, 62, 48] the wakes are excited in the so-called blowout regime where neither fluid nor one-dimensional theory applies. In the blowout regime, the wake is excited by the space charge of the beam or the radiation pressure of the laser expelling plasma electrons radially outward leaving behind a “channel” of unshielded ions. These expelled, blownout, electrons form a narrow sheath just outside the ion channel. Eventually the space charge of the ions pulls the electrons back, thereby creating the plasma wave wake. This is illustrated in Fig.2.1 where the electron density is plotted from a fully nonlinear particle-in-cell (PIC) simulation using the code OSIRIS [75]. The electron beam is propagating to the left in the variable $\xi = ct - z$. The blowout or ion channel radius, r_b , is also defined in this plot. This figure makes clear that the radius of the channel is not constant, i.e., it depends on $\xi = ct - z$.

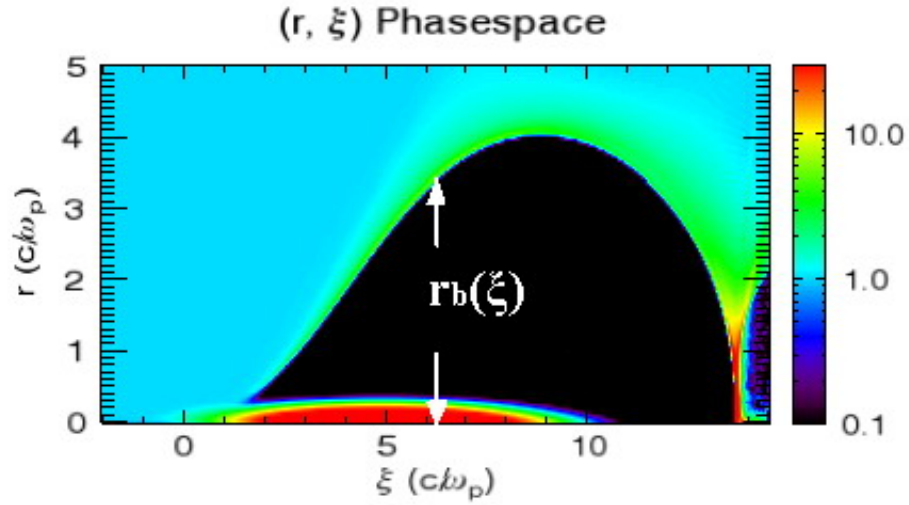


Figure 2.1: Electron charge density with the defined blowout radius $r_b(\xi)$

The blowout regime of creating wakefields was first investigated by Rosenzweig *et al.*[56] for electron beam drivers. They pointed out that these wakefields had perfectly linear focusing fields and had an acceleration gradient that was constant in radius for electrons. For sufficiently intense drivers the ion channel can have a spherical, i.e., bubble, shape. Therefore, in some of the recent work on LWFA the term bubble [58], is used. Despite this intense interest, there is little theory for how the wakefields in the blowout regime scale with the electron beam or laser beam parameters; and no theory exists for how beam loading occurs within these nonlinear multi-dimensional wakes. In addition, while there are expressions for the nonlinear frequency shift [65] for one-dimensional wakes there is no such expression for multi-dimensional wakes.

The blowout regime also has relevance to the linear theory of wake excitation. It is well known that the Green function of a relativistically moving point particle logarithmically diverges with the inverse of the radial position behind the particle. It had been argued rather nonrigorously that this divergence breaks down for r less than the Debye length[35] or the Compton wavelength[76]. In a cold plasma the Debye length is zero and since the theory is classical one should attempt to obtain a physical reason within the scope of classical theory. Simulations have shown that the wakes made by narrow bunches do indeed saturate for r smaller than a critical value[49]. The present work provides a clear explanation as to why this occurs and therefore when and why fluid theory breaks down. For any amount of charge one can shrink the beam's spot size down to a value for which blowout occurs. The linear Green's function is not valid for radii within the region void of electrons. For small blowout radius the influence of the electrons within and beyond the sheath become very important while within the blowout radius one needs a different description of plasma oscillations which this new theory provides.

Recently, Barov *et al.*[77], Lotov[78], and Kostyukov *et al.* [79] each have theoretically analyzed the limit of large blowout radius (Lotov calls it the “cavern” while Kostyukov calls it the “bubble” regime). Barov only treated the energy loss of an infinitesimally short electron beam. Lotov attempted to provide a qualitative analysis of the blowout regime for the PWFA, but his main results differ profoundly from ours. For example, he obtains the scaling between the blowout radius and the axial length L_c of the ion channel (“cavern”), $k_p L_c \propto k_p^3 r_m^3$ for large $k_p r_m$, where r_m is the maximal blowout radius; while we will show later that when $k_p r_m \gtrsim 4$, the ion channel is a sphere, i.e., $L_c = r_m$. Kostyukov observed in simulations that for laser drivers the ion channel is indeed a sphere (“bubble”) and derived the field structure for such shapes moving at the speed of light. Very recently, Gordienko and Puhkov [80] have presented a similarity theory for wake-field acceleration driven by laser drivers. This theory provides a mechanism for scaling results from one simulations or experiment to others provided that the laser profile remains same, that the relevant laser, space, and time variables are scaled properly, and that the laser intensity is very high. However, these analyses do not explain why there is a bubble, nor can they predict the field structure in wakes created by beam driver or weaker lasers.

In this chapter, we will present a predictive theoretical model for wake excitation by particle beam or laser drivers that are narrow enough to excite the wake in the blowout regime. The spot size must be less than the blowout radius and this is quantified in terms of the electron or laser beam parameters later. This theory can be used to understand the limitations of the cold fluid theory and to explore the blowout regime for either laser or particle beam drivers. The theory is valid for arbitrary blowout radius making it possible to understand why the ion column is roughly spherical for large blowout radius. The theory can also be used to develop a theory for electron hosing, for nonlinear beam loading, and for

pulse shaping. The key idea behind the theory is that the wake can be described entirely in terms of the trajectory of the blowout radius, $r_b(\xi)$. This can be done because the blownout electrons form a sheath whose thickness is narrower than the blowout radius, even for small values of r_b . This key assumption does not always hold for laser drivers. The chapter is outlined as follows. In section 2.2 the basic equations are described. In section 2.3 the condition for sheet crossing is given. In section 2.4 an equation for the blowout radius is derived. In section 2.5 and 2.6 the limits of small and large blowout radius are considered respectively. In section 2.7 formulas for arbitrary blowout radius are derived. In section 2.8 the differences between using a laser versus a particle beam driver are described and the work is summarized in section 2.9

2.2 The Basic Equations for Wake Excitation

In a theoretical description of short laser pulses or ultra-relativistic charged particle beams interacting with underdense plasmas, one needs to self-consistently treat both the electromagnetic fields and the trajectories for the plasma particles. For the electromagnetic fields, the full set of Maxwell's equations or some reduced form can be used and due to their linear origin once the currents and charge densities are known, they can be easily solved subject to appropriate boundary conditions (including no boundary at all). Therefore, the nonlinearities and complexities come from the description of plasma. Indeed this is true for all kinds of nonlinear laser matter interactions. The simplest model for a plasma is a cold fluid model, which is valid for describing laser or beam plasma interactions as long as the particle trajectories do not cross. Unfortunately particle trajectory crossing is so pervasive in laser plasma or beam plasma interactions that except for linear or weakly nonlinear cases, the single cold fluid model always breaks

down. This situation is painfully evident when multi-dimensional oscillations are considered.

In 1959, Dawson already pointed out that trajectory crossing will happen after a period of time for purely radial or spherical cold plasma oscillations, as long as very weak nonlinearities are taken into account. The reason for this is that the nonlinearities will induce initial position dependent frequency shifts, which eventually cause particles to oscillate out of phase with each other leading to trajectory crossing. Interestingly, 1D planar non-relativistic oscillations lack this kind of phase mixing due the fact that there is no frequency shifts for this case. As a result, particle crossing in 1D planar oscillations only occurs for rather large oscillation amplitudes, e.g., the 1D wavebreaking limit. As Dawson showed this is also the condition when some particles get trapped in the wave, i.e., their velocity exceeds the phase velocity of the wave. This special property for the 1D planar case leads to a confusing use of the words “wavebreaking” and “trapping” in the literature. The original meaning of “wavebreaking” in Dawson’s classic paper is closer to “trajectory crossing” than “trapping”. As we just discussed, in 1D they always happen together, however for non planar oscillations, “trajectory crossing” can happen very easily for even very small amplitude without particles getting “trapped”. In this chapter, we will adopt the term “trajectory crossing” as the meaning of “wavebreaking” to emphasize the breakdown of single cold fluid model. How particles trapping can happen in multi-dimentional plasma wakefield will be the topic of chapter 4.

In light of Dawson’s work, we can see that even for very weakly nonlinear multidimensional laser plasma or beam plasma interactions the cold fluid model can only be valid for a finite time or alternatively for a finite region in space. For example, in the cases of weak and short drivers (by weak, we only mean that the

density perturbation caused by the driver is small compared with the ambient plasma density), for the region not too far behind the driver, the fluid model is valid. This region could be many plasma wavelengths long for a weak driver. On the contrary, if the trajectory crossing happens near the driver, the fluid model breaks down totally and a model which includes the blowout regime is essential this case. For a particle beam driver, one does not necessarily need a strong driver in order to cause blowout.

From this discussion, it is clear that a particle picture must be used for a general treatment of the laser or beam plasma interaction. This is equivalent to a multi-species cold-fluid model where particles within each species execute cold laminar flow without trajectory crossing.

To analyze general multi-dimensional plasma oscillations excited by an intense particle beam or laser beam, we therefore start from Maxwell's equations in the Lorentz gauge and the equation of motion for an arbitrary number of laminar fluids:

$$\left(\frac{1}{c^2} \frac{\partial^2}{\partial t^2} - \nabla^2 \right) [\begin{array}{c} \mathbf{A} \\ \phi \end{array}] = 4\pi [\begin{array}{c} \mathbf{J}/c \\ \rho \end{array}] \quad (2.1)$$

$$\frac{1}{c} \frac{\partial \phi}{\partial t} + \nabla \cdot \mathbf{A} = 0 \quad (2.2)$$

$$\left(\frac{\partial}{\partial t} + \mathbf{V}_i \bullet \nabla \right) \mathbf{P}_i = q_i [\mathbf{E} + \frac{\mathbf{V}_i}{c} \times \mathbf{B}] \quad (2.3)$$

where $\rho = \sum_i q_i n_i$, $\mathbf{J} = \sum_i q_i n_i \mathbf{V}_i$, they satisfy the charge conservation equation:

$$\frac{\partial \rho}{\partial t} + \nabla \bullet \mathbf{J} = 0 \quad (2.4)$$

We next make several simplifications. the first one is that up stream from the laser or beam driver, each fluid can be treated as at rest or cold. For tenuous plasmas, the phase velocity of the excited wakefields is roughly the speed of light, c. Compared with this speed, all the initial thermal velocities of plasma particles can be treated as zero. The second approximation is the wavelike assumption where that fields in the wake depend on the variable $\xi \equiv (ct - z)$ where the phase velocity of the wave is essentially c. The last approximation is called the “Quasi-static approximation” [81]or “Frozen field approximation”[82], which is based on the multi timescale nature of the physical process. The driver evolves on a timescale much longer than the plasma response, so during the time it takes for a driver to pass by a plasma particle, the driver changes shape very little. This suggests that we can take the driver as non-evolving when calculating the plasma response. Therefore, the wake depends weakly on the distance the driver has moved into the plasma.

For this last approximation to be valid, we need different conditions for laser drivers and beam drivers. For the laser case, the driver evolves on a scale length roughly given by the Rayleigh length ($Z_R = \frac{\pi W_0^2}{\lambda_0}$). The laser spot size W_0 is on the order of plasma skin depth c/ω_p , so the quasi-static approximation is valid as long as $\frac{\omega_0}{\omega_p} \gg 1$. For the electron beam case, the driver evolves on a length scale roughly given by the Betatron wavelength, which is $2\pi\sqrt{2\gamma}c/\omega_p$ for a beam particle in an ion channel, So the quasi-static approximation is valid for a beam driver if $\gamma \gg 1$.

It is also worth noting that for extremely strong drivers, some plasma particles are pushed forward in front of the driver with very high parallel velocity, so it takes a rather long time for the driver to pass by these particles. For these particles, the “quasi-static approximation” will fail.

For the laser driven case there are three time scales: the high frequency laser oscillation ω_0^{-1} , plasma wakefield oscillation ω_p^{-1} and laser envelope evolution $\frac{\omega_0}{\omega_p}\omega_p^{-1}$. When calculating the wakefield excitation only the smooth motion is relevant. This smooth motion can be described by averaging out the high frequency laser oscillation from the equation of motion. The resulting smooth force from the laser is the ponderomotive force.

$$\frac{d}{dt} \mathbf{P}_{is} = \left(\frac{\partial}{\partial t} + \mathbf{V}_{is} \bullet \nabla \right) \mathbf{P}_{is} = q_i [\mathbf{E}_s + \frac{\mathbf{V}_{is}}{c} \times \mathbf{B}_s] + \mathbf{F}_p \quad (2.5)$$

In this equation, the fields \mathbf{E}_s and \mathbf{B}_s are the smooth fields produced by beam driver and plasma charge density and current. F_p is ponderomotive force of the laser,

$$\mathbf{F}_p = -\frac{q_i^2}{\bar{\gamma}_i m_i c^2} \nabla \left| \frac{\hat{A}_L}{2} \right|^2 \quad (2.6)$$

where the laser field is written as $A_{Laser} = \frac{\hat{A}_L}{2} e^{-i\frac{\omega_0}{c}\xi} + c.c.$, $\frac{e\hat{A}_L}{mc^2} \equiv a$ and $\bar{\gamma}_i = (1 + \frac{P_i^2}{m^2 c^2} + \frac{|a|^2}{2})^{\frac{1}{2}}$. A thorough derivation was performed by Mora and Antonsen [83].

At this point, we will adopt normalized units, where time is normalized to ω_p^{-1} , length to c/ω_p , velocities to the speed of light, c , mass to electron mass, m , and charge to electron charge, e , fields to $mc\omega_p/e$, potentials to mc^2/e , charge density to en_p and current density to en_pc . For convenience, we also omit the subscripts “ i ” and “ s ”.

To best utilize the quasi-static approximation, we can do a transformation from the (x, y, z, t) variables to the $(x, y, \xi \equiv ct - z, s \equiv t)$. In this group of new variables the quasi-static approximation implies $\partial_s \ll \partial_\xi$ in the field equation. Maxwell’s equations then become

$$-\nabla_{\perp}^2 \begin{bmatrix} \mathbf{A} \\ \phi \end{bmatrix} = \begin{bmatrix} \mathbf{J} \\ \rho \end{bmatrix} \quad (2.7)$$

$$\nabla_{\perp} \cdot \mathbf{A}_{\perp} = -\frac{\partial \psi}{\partial \xi} \quad (2.8)$$

where $\psi \equiv \phi - A_z$, $\nabla_{\perp} \equiv \hat{x}\frac{\partial}{\partial x} + \hat{y}\frac{\partial}{\partial y}$ and $\mathbf{A}_{\perp} = \hat{x}A_x + \hat{y}A_y$ etc. Furthermore, it can be shown that the plasma electrons evolve as[83]

$$\frac{d}{d\xi} \mathbf{P}_{\perp} = \frac{1}{1-v_z} \left[-[\mathbf{E}_{\perp} + (\mathbf{V} \times \mathbf{B})_{\perp}] - \frac{1}{\bar{\gamma}} \nabla_{\perp} \frac{|a|^2}{4} \right] \quad (2.9)$$

where $\bar{\gamma} = (1 + P^2 + \frac{|a|^2}{2})^{\frac{1}{2}}$. There is an Eq.2.9 for each laminar fluid or lagrangian fluid particle. It can also be shown that $\bar{\gamma} - P_z = 1 + \psi$ is a constant of the motion. In this equation all high frequency motion associated with the laser has been averaged out. As a consequence of the constant of the motion, we can write

$$P_z = \frac{[1 + P_{\perp}^2 + \frac{|a|^2}{2} - (1 + \psi)^2]}{2(1 + \psi)} \quad (2.10)$$

$$\bar{\gamma} = \frac{[1 + P_{\perp}^2 + \frac{|a|^2}{2} + (1 + \psi)^2]}{2(1 + \psi)} \quad (2.11)$$

$$1 - v_z = \frac{2(1 + \psi)^2}{[1 + P_{\perp}^2 + \frac{|a|^2}{2} + (1 + \psi)^2]} \quad (2.12)$$

so that once P_{\perp} is solved, the axial momentum is known. In addition, the pseudo potential ψ obeys the Poisson like equation,

$$-\nabla_{\perp}^2 \psi = 4\pi(\rho - J_z), \quad (2.13)$$

the continuity equation of electric charge becomes

$$\frac{\partial}{\partial \xi}(\rho - J_z) + \nabla_{\perp} \cdot \mathbf{J}_{\perp} = 0 \quad (2.14)$$

and the fields E_z , B_z , \mathbf{E}_{\perp} and \mathbf{B}_{\perp} can be calculated via

$$E_z = \frac{\partial \psi}{\partial \xi} \quad (2.15)$$

$$B_z = (\nabla_{\perp} \times \mathbf{A}_{\perp}) \bullet \hat{z} \quad (2.16)$$

$$\mathbf{E}_{\perp} = -\nabla_{\perp} \phi - \frac{\partial \mathbf{A}_{\perp}}{\partial \xi} \quad (2.17)$$

$$\mathbf{B}_{\perp} = \nabla_{\perp} \times (A_z \hat{z}) + \nabla_z \times \mathbf{A}_{\perp} \quad (2.18)$$

Therefore, the wakefield E_z is completely described in terms of ψ which can be obtained from a Poisson like equation whose source term depends only on the profiles of plasma charge density ρ and parallel current J_z , which in turn depend on all the fields through the equation of motion.

2.3 On Blowout and Sheet Crossing

In this section we will use the simplified sheet (ring) model of Dawson to obtain a condition for trajectory crossing which is valid for weakly driven wakefields. In the next section, we will apply the full set of equations towards describing nonlinear 3D relativistic wakefields. The trajectory crossing condition also defines the transition from the linear regime to the weakly blowout regime. Imagine electrons which begin at different radial positions. If no trajectory crossing occurs then each electron will always see other electrons at smaller radii and hence there is no region void of electrons. However, if the trajectory of an electron with a sufficiently small initial radius crosses that of another electron then for radii smaller than this it is possible for an ion column to form. So trajectory crossing

is a necessary but not sufficient condition to reach the blowout regime. As we will show it provides a very reasonable estimate.

To use the Dawson sheet or ring model we assume a cylindrically symmetric, narrow, bi-flat-top electron driver. We also start by assuming that plasma electron rings do not cross each other. We also assume that the plasma current induced fields are negligible and that the velocities of the plasma electrons remain non-relativistic. These assumptions are rigorously valid for low charge drivers and we will quantify what is meant by this later.

The charge density profile for our bi-flat-top model is $n_b(r, \xi) = n_b$ when $r < a$ and $0 < \xi < L$, otherwise $n_b(r, \xi) = 0$. L is the beam length and a is the beam spot size. In the narrow beam limit we also assume $a \ll 1$ and $L \sim 1$.

The equation of motion for an electron ring can be derived from Eq.9 by taking the non-relativistic limit ($v_z \ll v_\perp \ll 1$, $v_\perp \approx dr/d\xi$), and by assuming the total force on an electron ring is due solely to the electrostatic force from the total charge within the ring, which includes the ion charge, the electron beam charge, and plasma electron charge:

$$\frac{d^2r}{d\xi^2} = -\frac{1}{2}r + \frac{c(r_0, r, \xi)}{r} \quad (2.19)$$

Here the force term $-r/2$ comes from the uniform ion background. The force term c/r comes from the 2d cylindrical electrostatic force from the total electron charge inside the ring, where $c(r_0, r, \xi)$ is the total electron charge per unit length within the sheet with a initial position r_0 and a position r at ξ . With the assumption of no crossing, $c(r_0, r, \xi) = \frac{1}{2}r_0^2 + \int_0^r r'n_b(r', \xi)dr'$. For bi-flat-top model and a particle with $r_0 > a$, $c(r_0, r, \xi) = \frac{1}{2}(r_0^2 + n_b a^2)$.

This equation can be easily integrated numerically. Fig.2 shows two trajectory

plots for different n_{b0} for a bi-Gaussian beam driver with $k_p\sigma_r = 0.01$ and $k_p\sigma_z = \sqrt{2}$. In Fig.2.3(a) $n_b = 1.0$ and there is no trajectory crossing, while in Fig.2.3(b) $n_b = 10$, and clear trajectory crossing can be seen.

Clearly there is a transition from no-crossing to crossing. We can derive such a condition if we calculate the maximum radius $r_m(r_0)$ for an arbitrary initial radius r_0 . This is possible because the particle trajectories all oscillate with frequencies in the variable ξ that are very close to each other, so they will each reach their maxima at nearly the same value of ξ . This effect can also be seen in the above figures. Trajectory crossing occurs when $r_m(r_0)$ changes from a monotonically increasing function to a function with both a local maxima and minima.

First we treat the case $r_0 \geq a$. The equation of motion can be integrated once leading to the potential energy $\phi(r, r_0)$ for a particle with an initial radius r_0 ,

$$\phi(r, r_0) = -\frac{1}{4}r^2 + \frac{1}{4}\left(\frac{n_b a^2}{r_0^2} + 1\right)r_0^2\left(1 + 2\ln\left(\frac{r}{r_0}\right)\right) \quad (2.20)$$

A particle's velocity is 0 for both $r = r_0$ and $r = r_m(r_0)$ so the potential for these two radii should be the same :

$$\phi(r_m(r_0), r_0) = \phi(r_0, r_0) \quad (2.21)$$

This leads to the following relation between $r_m(r_0)$ and r_0 :

$$r_m^2 - r_0^2 = \left(\frac{n_b a^2}{r_0^2} + 1\right)r_0^2 \ln \frac{r_m^2}{r_0^2} \quad (2.22)$$

Rewriting this equation by normalizing the radius to a , $\bar{r}_m = r_m/a$ and $\bar{r}_0 = r_0/a$ gives,

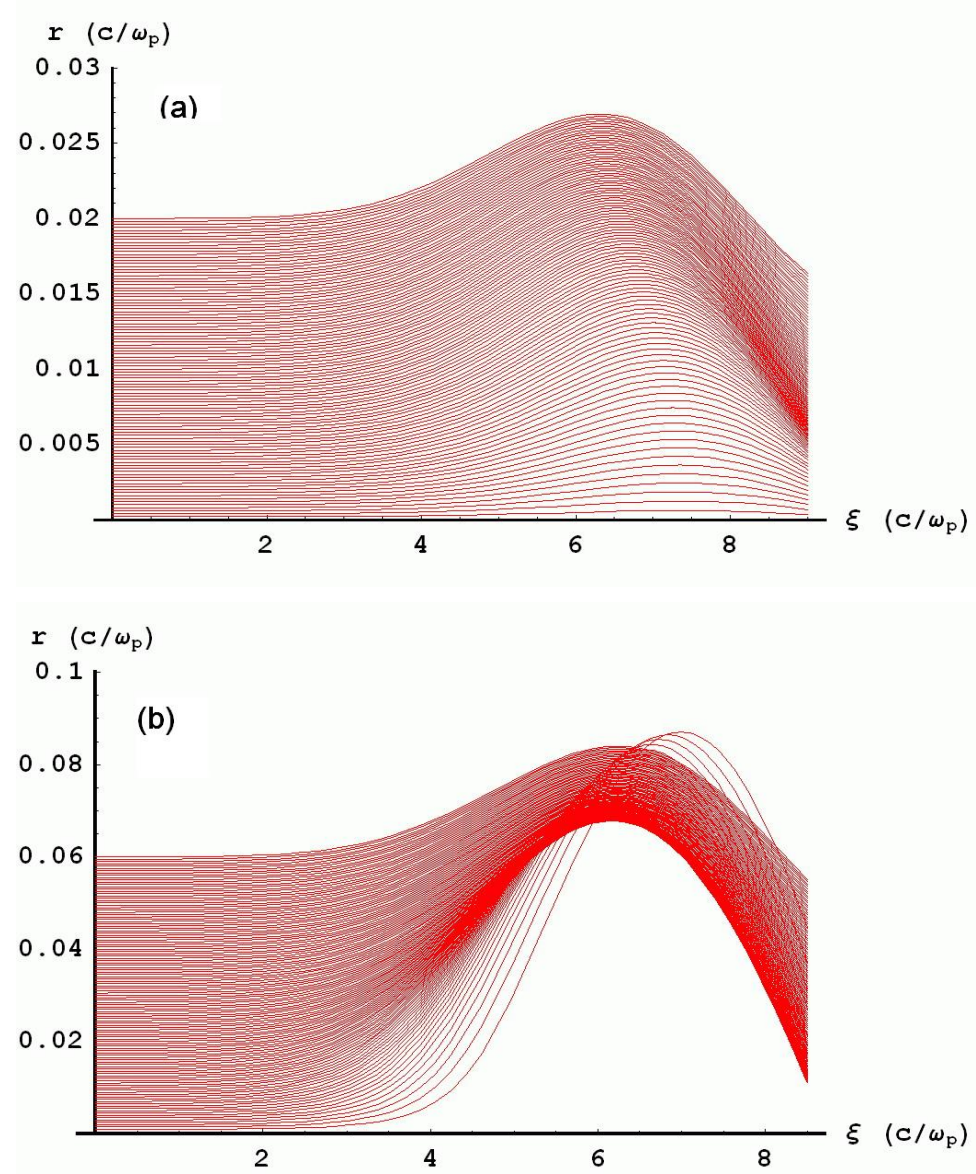


Figure 2.2: Plots of trajectories for electrons at different initial radial position for an electron beam driver with $k_p\sigma_r = 0.01$, $k_p\sigma_z = \sqrt{2}$, the beam center $\xi_0 = 5$ and with (a) $n_{b0} = 1$ (b) $n_{b0} = 10$

$$\bar{r}_m^2 - \bar{r}_0^2 = \left(\frac{n_b}{\bar{r}_0^2} + 1\right)\bar{r}_0^2 \ln \frac{\bar{r}_m^2}{\bar{r}_0^2} \quad (2.23)$$

For the non-crossing assumption to be valid, we need $\bar{r}_m(\bar{r}_0)$ to be a monotonically increasing function of \bar{r}_0 , this is equivalent to $\frac{d\bar{r}_m}{d\bar{r}_0} > 0$. By differentiating the above equation we can get :

$$\frac{d\bar{r}_m}{d\bar{r}_0} = \frac{\bar{r}_m}{\bar{r}_0} \left(\ln \frac{\bar{r}_m^2}{\bar{r}_0^2} - \frac{n_b}{\bar{r}_0^2} \right) \left(\ln \frac{\bar{r}_m^2}{\bar{r}_0^2} - \frac{n_b}{\bar{r}_0^2} + \frac{n_b}{\bar{r}_0^2} \ln \frac{\bar{r}_m^2}{\bar{r}_0^2} \right)^{-1} \quad (2.24)$$

There is no particle crossing for sufficiently large \bar{r}_0 since $d\bar{r}_m/d\bar{r}_0 \rightarrow 1$ as $\bar{r}_0 \rightarrow \infty$. We see that for $\ln \frac{\bar{r}_m^2}{\bar{r}_0^2} = \frac{n_b}{\bar{r}_0^2}$ we have $\frac{d\bar{r}_m}{d\bar{r}_0} = 0$, which defines the onset of particle crossing. We denote this critical \bar{r}_0 as \bar{r}_{0m} . Combined with the above equation, this gives \bar{r}_{0m} and $\bar{r}_m(\bar{r}_{0m})$ for a given n_b . We find that $u \equiv \frac{n_b}{\bar{r}_{0m}^2}$ satisfies the following equation :

$$\exp(u) - 1 = u(u + 1) \quad (2.25)$$

This equation has a nonzero solution $u_0 = 1.7933$. Correspondingly, $\bar{r}_{0m} = 0.747\sqrt{n_b}$ and $\bar{r}_m(\bar{r}_{0m}) = 1.831\sqrt{n_b}$. In our analysis $\bar{r}_0 \geq 1$, therefore only when $n_b \geq 1.792$ can particle crossing be possible. We can verify that at this \bar{r}_{0m} , \bar{r}_m is a minimum by checking if $\frac{d^2\bar{r}_m}{d\bar{r}_0^2} > 0$. Differentiating Eq.2.24 we get :

$$\frac{d^2\bar{r}_m}{d\bar{r}_0^2} = \frac{2\bar{r}_m\bar{r}_0^2}{n_b^2} \left(\frac{n_b}{\bar{r}_0^2} - 1 \right) \quad (2.26)$$

which is obviously greater than 0, since we have $\frac{n_b}{\bar{r}_{0m}^2} = 1.7933$.

For $r_0 < a$, a similar calculation can be carried out by taking into account the kinetic energy of the particle when it reaches $r = a$. Some particles very close to the axis will not reach $r = a$, for example, the particle with $r_0 = 0$ will just go through the beam without any deflection. This is very similar to an unstable equilibrium, where every trajectory with an initial r_0 slightly different with 0 will leave the equilibrium very quickly.

It turns out that for a beam density smaller than a critical density (surprisingly the same value $n_b = 1.792$), $r_m(r_0)$ is a monotonically increasing function. Assuming $r_0 < a$, then for $n_b > 1.792$, $r_m(r_0)$ ($r_0 < a$) will have a local maximum at some radius $r_0 = r^* < a$. If we keep increasing n_b , this r^* will move toward 0, which means more electrons inside the beam will be blown out.

Combining the results for $r_0 < a$ and $r_0 > a$, we can make the following conclusions:

1. When the beam density satisfies the condition, $n_b < 1.792$, then $r_m(r_0)$ is a monotonically increasing function. In this case, no particle crossing happens.
2. If $n_b > 1.792$, then $r_m(r_0)$ will have negative slope between $r^* < r_0 < r_{0m}$, where $r^* < a$ is a local maximum of $r_m(r_0)$, and $r_{0m} > a$ is a local minimum of $r_m(r_0)$. In addition, $r_m(r_{0m})$ is the blowout radius. Electrons with initial positions in this range will cross an electron that starts at position at r_{0m} . If n_b is large enough (e.g. $n_b = 10$), r^* will also be very close to 0, which means almost all electrons of $r_0 < r_{0m}$ will cross electrons with $r_0 < r_{0m}$, so a nearly pure ion channel will be formed .

We can rewrite the blowout radius r_{max} in normalized units as :

$$r_{max} = 1.831(n_b a^2)^{\frac{1}{2}} \quad (2.27)$$

We define Λ as normalized charge per unit length,

$$\Lambda \equiv \int_0^\infty r n_b dr \quad (2.28)$$

For a bi-flat-top beam, $\Lambda = n_{b0} a^2 / 2$, and for a bi-Gaussian beam, $\Lambda = n_{b0} \sigma_r^2$. The blowout radius then can be written as $r_{max} = 2.58 \Lambda^{\frac{1}{2}}$. This basically shows that in the blowout regime the blowout radius depends primarily on the total

charge per unit length not just the peak density. It is worth noting that for a bi-Gaussian beam ($\sigma_z \sim 1$ and $\sigma_r \ll 1$), simulations and trajectory calculations show that $r_{max} \approx 2(n_{b0}\sigma_r^2)^{\frac{1}{2}}$, which is about 20 percent smaller than the above theoretical value. The reason is that the bi-Gaussian beam has a longitudinally varying density profile, but the formula uses the maximum density leading to a larger result.

For a very short driver, e.g., $L \ll 1$, it is the initial kick from the beam that determines if blowout will happen or not. A similar calculation to that given above can be carried out. The main difference is that for this case it is the total charge of the beam that determines the condition for blowout and the blowout radius. The relation between the blowout radius and the total charge Q also has similar form, e.g., $r_{max} \propto Q^{\frac{1}{2}}$.

A direct consequence of complete blowout is the formation of a narrow electron sheath around the blowout boundary. The above method for calculating the blowout radius can also give an estimate for the width of this narrow region. We can get such an estimate by calculating the maximum radius for an electron initially located at the blowout radius, $r_0 = r_{max}$. The result is $1.287r_{max}$. Therefore, 0.287 can be a rough estimate of the ratio between the width of narrow sheath and the blowout radius. Real density profiles from PIC simulations show that width is actually less, so generally we can treat the width of the narrow sheath as a small fraction of the blowout radius. This will be a key approximation in the theoretical model for blowout regime given in the next section.

2.4 Wake Excitation in the Blowout Regime

In the previous sections, we have presented the basic theoretical framework for wake excitation and some physical insight for the blowout regime. In this section we use this framework and insight to develop a general model for wakefields in the blowout regime. The key approximation is based on the observation that the plasma density and current profile can be roughly divided into three distinct regions: an ion channel, a narrow plasma electron sheath and a linear response region where the perturbation of the plasma is very weak . The ion channel has a sharp boundary. That is at the blowout radius the electron density rises from 0 to a large value in an essentially infinitesimal distance. For much of the ion channel, the channel boundary, $r_b(\xi)$, is also the trajectory of most inner electron. The plasma electron density and axial current density profiles in the narrow electron sheath are rather narrow at $r_b(\xi)$ and the width $\Delta_s(\xi)$ is small compared with $r_b(\xi)$ for most part of the ion channel except where r_b is very close to zero. Indeed the profiles are more like exponential decay than constant. Beyond the narrow sheath, the perturbation of plasma density and current becomes very weak, so this region can be described by linear fluid model. From linear theory, we know this region has a typical width around one plasma skindepth c/ω_p . The contribution to the wakefield from the linear response region must be taken into account due to its rather large width. For small blowout radius the contribution from this outer linear response region is dominant.

At this point, we will assume the wake is excited by a bi-Gaussian electron driver with a density profile

$$n_b(r, \xi) = \frac{N}{(2\pi)^{3/2} \sigma_r^2 \sigma_z} e^{-r^2/2\sigma_r^2} e^{-\xi^2/2\sigma_z^2} \quad (2.29)$$

How the formalism is modified for a laser driver will be addressed later. In addition, for laser drivers the assumption that the sheath is narrow is not necessarily valid. By assuming azimuthal symmetry, we can rapidly obtain solutions for Eq.2.7 and Eq.2.13 because of their Poisson like form. Inside the ion channel, i.e., for $r \leq r_b$ and for $r \gg \sigma_r$,

$$\phi = \phi_0(\xi) - \frac{r^2}{4} + \lambda(\xi) \ln r \quad (2.30)$$

$$A_z = A_{z0}(\xi) + \lambda(\xi) \ln r \quad (2.31)$$

where $\lambda(\xi) = \int_0^{r \gg \sigma_r} rn_b dr$ and $\phi_0(\xi) \equiv \phi(r = 0, \xi)$ and $A_{z0}(\xi) \equiv A_z(r = 0, \xi)$.

In addition,

$$A_r = \sigma(\xi)r \quad (2.32)$$

where from the gauge condition,

$$\begin{aligned} \sigma(\xi) &= -\frac{1}{2} \frac{d}{d\xi} \psi_0(\xi) \\ &= -\frac{1}{2} E_{z0} \end{aligned} \quad (2.33)$$

$$\psi = \psi_0 - \frac{r^2}{4} \quad (2.34)$$

We have also assumed that the beam is highly relativistic, i.e., $\rho_b - J_b = \rho_b(1 - v_{zb}) \rightarrow 0$. The force on a plasma electron at $r = r_b(\xi)$ or for a beam electron can therefore be written as

$$\begin{aligned}
F_{\perp} &= -(E_r - V_z B_\theta) = \frac{\partial \phi}{\partial r} - V_z \frac{\partial A_z}{\partial r} + (1 - V_z) \frac{\partial A_r}{\partial \xi} \\
&= -\frac{1}{2}r + (1 - V_z) \frac{\lambda(\xi)}{r} + (1 - V_z) \frac{d\sigma}{d\xi} r
\end{aligned} \tag{2.35}$$

where the first term is due to the space charge of the unshielded ion channel, the second and the third terms are due to the electric and magnetic fields from the electron beam and to plasma radial currents respectively. Note that the focusing force on a beam electron with $V_z \sim 1$ is due solely due to the space charge of the ion channel because the electric and magnetic forces from the plasma currents and the beam's self-forces each cancel. On the other hand for plasma electrons for which $-1 < V_z \ll 1$ the force is due to the full electromagnetic character of the wake. In order to uniquely calculate the force on a plasma electron at $r = r_b(\xi)$, we next need to calculate $\sigma(\xi)$ or equivalently $\psi_0(\xi)$.

The source term for $\psi(r, \xi)$ is $\rho - J_z$. From the continuity equation it follows that

$$\frac{d}{d\xi} \int r(\rho - J_z) dr = 0 \tag{2.36}$$

Far in front of the electron beam where the plasma is unperturbed $\rho - J_z = 0$ so $\int r(\rho - J_z) dr = 0$ for all ξ . This is a critical condition because it grants ψ a global definition. At each ξ we assume

$$\rho - J_z = \rho_{ion} + \rho_e - J_{ze} \tag{2.37}$$

where $\rho_{ion} = 1$ for all r and $\rho_e - J_{ze}$ is zero for $r < r_b$, rises sharply within a sheath of thickness of Δ_s and gradually falls to unity in a width Δ_L . The region defined by Δ_L is where the plasma electrons respond nearly as they would have

in a linear wake. This is illustrated in Fig.2.4 where the profile $J_z/c - \rho$ vs. r is plotted for an arbitrary value of ξ from Fig.2.1. It does not appear possible to analytically determine the exact profiles of $\rho - J_z$ within the sheath and linear regions. However, the results are very insensitive to the forms of the profiles and we find that very accurate results can be obtained by assuming $J_z - \rho = -1$ for $r < r_b$ and is a constant

$$n_\Delta = \frac{r_b^2}{(r_b + \Delta)^2 - r_b^2} \quad (2.38)$$

for $r_b < r < r_b + \Delta$. This is illustrated in Fig.3.

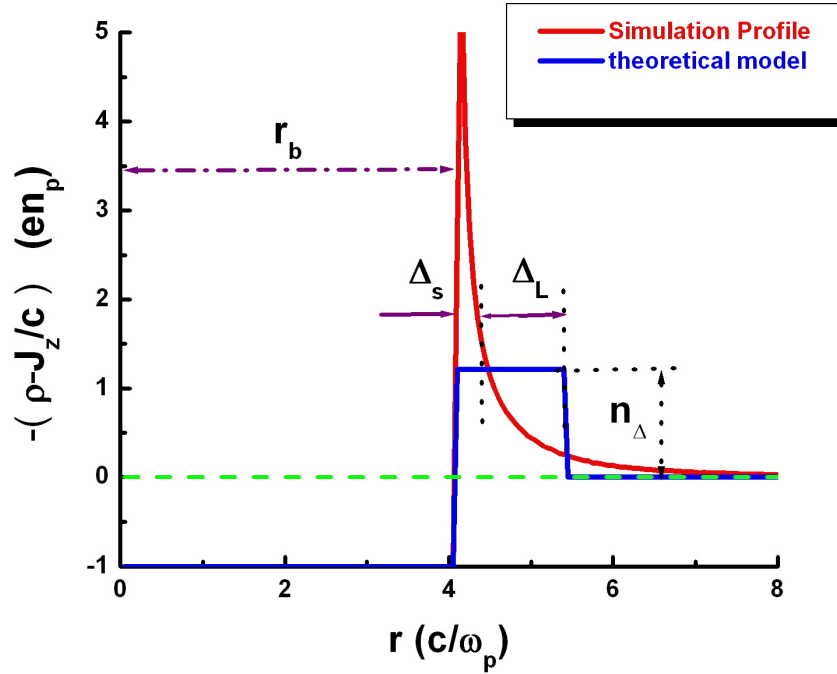


Figure 2.3: $J_z/c - \rho$ profile from a PIC simulation

Obviously, more refined profiles can be used. Under these assumptions

$$\psi = \frac{r_b^2(\xi)}{4}(1 + \beta(\xi)) - \frac{r^2}{4} \quad (2.39)$$

for $r \leq r_b$ where

$$\beta(\xi) = \frac{(1 + \alpha)^2 \ln(1 + \alpha)^2}{(1 + \alpha)^2 - 1} - 1 \quad (2.40)$$

$$\alpha \equiv \frac{\Delta}{r_b} = \frac{\Delta_L}{r_b} + \frac{\Delta_s}{r_b} \quad (2.41)$$

We assume $\frac{\Delta_s}{r_b} \equiv \epsilon \ll 1$ except at the back of the blowout region where $r_b \ll 1$. To complete the analysis, we use these results to derive a single equation for $r_b(\xi)$ by using the relativistic equation of motion for a plasma electron,

$$\frac{dP_\perp}{d\xi} = \frac{1}{1 - V_z} F_\perp \quad (2.42)$$

We can rewrite the left hand side as

$$\begin{aligned} \frac{dP_\perp}{d\xi} &= \frac{d\gamma V_\perp}{d\xi} \\ &= \frac{d}{d\xi} \gamma (1 - V_z) \frac{d}{d\xi} r_\perp \\ &= \frac{d}{d\xi} (1 + \psi) \frac{d}{d\xi} r_\perp \end{aligned} \quad (2.43)$$

and use the expression for $1 - V_z$ from Eq.2.12. The equation of motion for a plasma particle at r_b can now be written as

$$\begin{aligned}\frac{d}{d\xi}[(1+\psi)\frac{d}{d\xi}r_b] &= r_b\left\{-\frac{1}{4}[1+\frac{1}{(1+\psi)^2}+(\frac{dr_b}{d\xi})^2]\right. \\ &\quad \left. +(\frac{d\sigma}{d\xi})+\frac{\lambda(\xi)}{r_b^2}\right\}\end{aligned}\quad (2.44)$$

where $\psi(r_b(\xi))$ is given by Eq.2.39. This can be simplified further if we assume that the width, Δ , depends weakly on ξ , i.e.,

$$\frac{\partial\Delta}{\partial\xi}\approx 0\quad (2.45)$$

,

so that $\frac{d\beta}{d\xi}=\frac{dr_b}{d\xi}\frac{\partial\beta}{\partial r_b}$. Under this assumption Eq.2.44 reduces to

$$A(r_b)\frac{d^2r_b}{d\xi^2}+B(r_b)r_b(\frac{dr_b}{d\xi})^2+C(r_b)r_b=\frac{\lambda(\xi)}{r_b}\quad (2.46)$$

where

$$\begin{aligned}A(r_b) &= 1+\left[\frac{1}{4}+\frac{\beta}{2}+\frac{1}{8}r_b\frac{d\beta}{dr_b}\right]r_b^2 \\ B(r_b) &= \frac{1}{2}+\frac{3}{4}\beta+\frac{3}{4}r_b\frac{d\beta}{dr_b}+\frac{1}{8}r_b^2\frac{d^2\beta}{dr_b^2} \\ C(r_b) &= \frac{1}{4}\left[1+\frac{1}{(1+\frac{\beta}{4}r_b^2)^2}\right]\end{aligned}$$

Recall that once $r_b(\xi)$ is solved for then $\psi(r,\xi)$ is known (Eq.2.39) and

$$\begin{aligned}E_z(r,\xi) &= \frac{d}{d\xi}\psi(r=0,\xi) \\ &= \frac{d}{d\xi}\left[\frac{1}{4}r_b^2(1+\beta(\xi))\right]\end{aligned}\quad (2.47)$$

is known. We note here that for a laser driver $C(r_b) = \frac{1}{4}[1 + \frac{1+\frac{a^2}{2}}{(1+\frac{\beta}{4}r_b^2)^2}]$ and the right side of Eq.2.46 becomes $-\frac{\frac{d}{dr}\frac{|a|^2}{4}}{1+\frac{\beta}{4}r_b^2}$, which comes from the laser's ponderomotive force.

We show the accuracy of our model by directly integrating Eq.2.46 for a bi-Gaussian electron beam driver. We choose $k_p\sigma_r = 0.1$ and $k_p\sigma_z = \sqrt{2}$. In Fig.4, we plot the trajectories of $r_b(\xi)$ for different values of beam charge, i.e., eN , and hence different maximum blowout radius (r_m varies from 0.18 to 4) and compare these trajectories with the ion channel boundaries extracted from fully nonlinear PIC simulations. The theory and PIC simulation results for r_b are essentially identical for each case. We used $\Delta_s = 0.1r_b$ and $\Delta_L = 1$ for each case. Varying Δ_L from 0 to 3 leads to only a 20 percent deviation in both the blowout radius and the ion channel length. Fig.2.4 also compares the wakefields, E_z , calculated from the model with those from PIC simulations. The agreement is excellent until near the rear of the blowout region (large values of ξ). We have determined that much of the disagreement comes from assuming constant Δ_s/r_b and Δ_L , which is not exactly true near the rear of the first bucket where r_b becomes small. In Fig.4a, we also plot the wakefield, E_z , which is calculated using a Δ_L which depends on ξ . This gives better agreement near the rear of the ion column. Although this simple model cannot give exact predictions for E_z near the very rear of the ion channel, it provides the correct trajectory for r_b and hence the correct structure of the wakefield ,e.g., the peak decelerating field, the useful accelerating field, the useful transformer ratio and the wake's wavelength for arbitrary shaped bunches. It also describes quantitatively how the wakefield's structure changes as r_m increases. We also note that it is accurate enough to treat the beamloading problem. Fig.4b shows the agreement between the theory and simulation where a drive beam and a trailing beam are used. The agreement

is exact within the trailing beam.

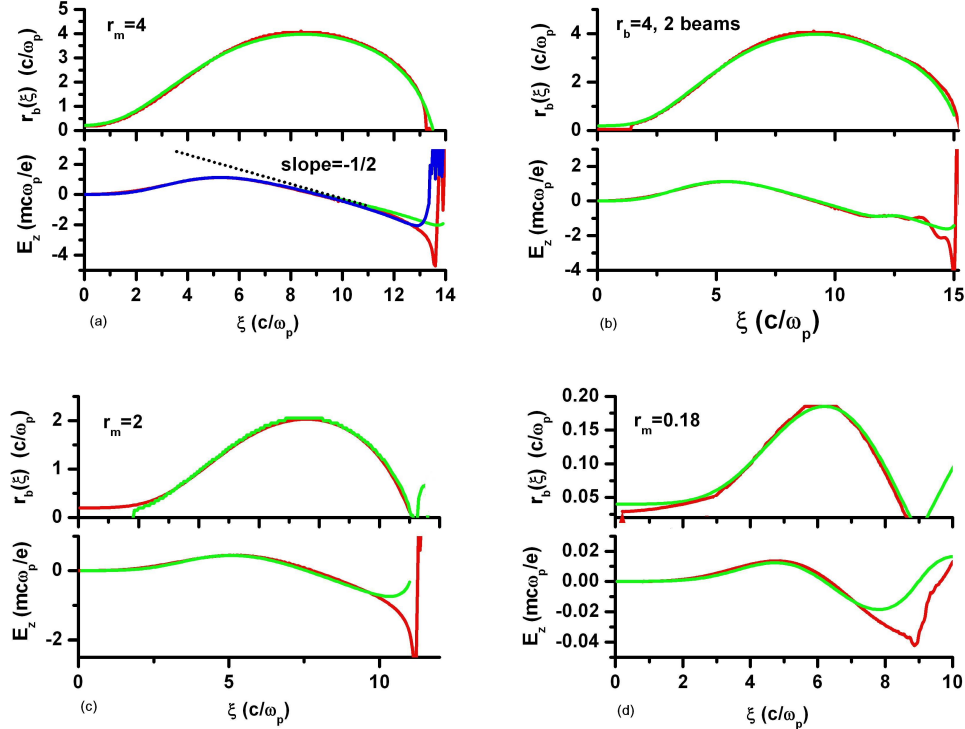


Figure 2.4: Comparison of the trajectories of $r_b(\xi)$ and the accelerating field $E_z(\xi)$ between theoretical calculations and PIC simulations: PIC simulation(red), calculation using a constant profile (green), and calculation using a varying profile (blue). The maximum blowout radius is (a) $r_m = 4$ (b) $r_m = 4$ with two beams (c) $r_m = 2$ (d) $r_m = 0.18$

Much can be learned by examining Eq.2.46 in two distinct limits; namely the non-relativistic blowout regime where $r_m \ll 1$ and the ultra-relativistic blowout regime where $r_m \gg 1$. Before providing details on these two distinct regimes in the following two sections, we summarize some key features.

In the ion channel, $r < r_b$, the wakefield $E_z(r, \xi)$ can be expressed as

$$E_z(r, \xi) = \frac{\partial}{\partial \xi} \psi(0, \xi) \quad (2.48)$$

All three plasma regions (ion channel, narrow electron sheath and the linear response region) contribute to $\psi(0, \xi)$,

$$\begin{aligned} \psi(0, \xi) &= \int_0^\infty \frac{dr}{r} \int_0^r (\rho - J_z/c) r' dr' \\ &= \left\{ \int_0^{r_b} + \int_{r_b}^{r_b + \Delta_s} + \int_{r_b + \Delta_s}^\infty \right\} \left[\frac{dr}{r} \int_0^r (\rho - J_z/c) r' dr' \right] \\ &= \psi_{ion} + \psi_s + \psi_{Linear} \end{aligned} \quad (2.49)$$

where $\psi_{ion} = \frac{r_b^2}{4}$ is the part contributed by ion channel and ψ_s is the part contributed by the narrow electron sheath. Because the width of the sheath is small compared with r_b for almost all values of ξ , ψ_s is a small fraction of ψ_{ion} . The third term, ψ_{Linear} , is the part contributed by the linear response region. This is a region of width around 1 (c/ω_p in unnormalized units), so its relevant importance depends on the blowout radius r_m . If $r_m \gg 1$ (the ultra-relativistic blowout), it will be much smaller than ψ_{ion} . If $r_m \ll 1$ (the non-relativistic blowout), it will be the dominating part.

We can estimate the form of $\beta(\xi)$ in these two limits:

When $r_m \gg 1$ the ratio $\alpha \ll 1$, providing

$$\beta(\xi) \approx \alpha \quad (2.50)$$

We can see that in this limit the ion channel is the dominant contribution to $\psi(0, \xi)$ because $\beta(\xi) \approx \alpha \ll 1$.

On the other hand, when $r_m \ll 1$ the ratio $\alpha \gg 1$, leading to

$$\beta(\xi) \approx 2 \ln \alpha \quad (2.51)$$

This logarithmic term provides a direct connection between linear fluid theory and the linear response region. In this limit, the contribution from the linear region is now much larger than that from the ion channel.

2.5 On the Transition between Linear Theory and the Breakdown of Fluid Theory

In this section we use the results in the previous section for $r_m \ll 1$ to make a connection between blowout theory and the results of linear fluid theory.

In the linear fluid theory [49] for a narrow short electron driver (e.g., $k_p \sigma_z = \sqrt{2}$ and $k_p \sigma_r \ll 1$), the maximum wakefield E_{zMax} can be written as

$$\frac{eE_{zMax}}{mc\omega_p} \approx 1.3 \frac{n_{b0}}{n_p} k_p^2 \sigma_r^2 \ln \frac{1}{k_p \sigma_r} \quad (2.52)$$

This formula has a logarithmically divergent term, $\ln \frac{1}{k_p \sigma_r}$. If we fix the charge per unit length $\Lambda \equiv \frac{n_{b0}}{n_p} k_p^2 \sigma_r^2$ and keep decreasing the beam spot size $k_p \sigma_r$, Eq.2.52 predicts the wakefield will blow up. Indeed this divergence inherently exists in the Green's function of the wakefield for a point charge.

This nonphysical infinity arises from the breakdown of linear fluid theory. When the spot size decreases, the beam density also increases, and eventually will become larger than the background plasma density. When the beam density is much larger than the plasma density, clear blowout will happen and the wakefield will saturate. Recently [49], we showed through PIC simulations that such a saturation happens at $n_{b0}/n_p \sim 10$ where a clear blowout occurs at the front of

the beam. We found [49] that an approximate formula for the wakefield after clear blowout has the following form:

$$\frac{eE_{zMax}}{mc\omega_p} \approx 1.3\Lambda \ln \frac{1}{\sqrt{\Lambda/10}} \quad (2.53)$$

Based on the present theory, it is easy to understand such a logarithmic dependence on Λ . Once the beam spot size has decreased to a value such that clear blowout occurs, decreasing the beam spot size further will not change the plasma response to the beam. The linear response region beyond the maximum blowout radius r_m ($k_p r_m \approx 2\sqrt{\Lambda}$, as shown in section III) will give a such a logarithmic dependence.

In the non-relativistic blowout regime ($r_m \ll 1$), the plasma current induced fields (e.g., $\frac{\partial A_r}{\partial \xi}$) are of 2nd order as compared with space charge fields (e.g., $\frac{\partial \phi}{\partial r}$). In the linear response region no trajectory crossing occurs so plasma electrons only feel the electric forces from the beam and the ions that they cross. Therefore, the plasma response in the region $r > r_m + \Delta_s$ is the same as it would be from a wider low density beam with the same Λ but with a width $r_m + \Delta_s$. Therefore, we can calculate an expression for ψ_{Linear} from linear theory.

For simplicity, we calculate this ψ_{Linear} for a bi-flat-top beam with spot size a , length L and density n_{b0} ($a \ll 1, L \approx 2\pi$).

From the linear theory [49], $E_z(r, \xi)$ for this beam profile is:

$$E_z(r, \xi) = n_{b0} R(r) \sin \xi \quad (2.54)$$

where $R(r) = \int_0^\infty n_b(r') I_0(r_<) K_0(r_>) r' dr'$ is the radial function of the linear wakefield.

Integrating this along ξ we get

$$\psi(r, \xi) = n_{b0}R(r)(1 - \cos \xi) \quad (2.55)$$

$R(r)$ can be expanded for $a \ll 1$ and $r \ll 1$,

$$R(r) \approx R(0) - \frac{1}{4}(1 - R(0))r^2 \quad (2.56)$$

where

$$R(0) \approx \frac{a^2}{2} \ln\left(\frac{1.85}{a}\right) \quad (2.57)$$

For $a = r_m + \Delta_s \approx r_m$ and $n_{b0} = 2\frac{\Lambda}{r_m^2}$, we get

$$\psi_{Linear}(\xi) \approx 2\Lambda \ln\left(\frac{1.12}{r_m}\right)\left(\frac{1 - \cos \xi}{2}\right) \quad (2.58)$$

This expression reaches its maximum of $2\Lambda \ln\left(\frac{1.12}{r_m}\right)$ at $\xi = \pi$, which is also where $r_b(\xi)$ reaches its maximum r_m . We can combine the three contributions to $\psi(0, \xi)$ and get $\psi(0, \xi)$ near the maximum blowout radius r_m ($\xi \approx \pi$),

$$\psi(0, \xi) \approx 2\Lambda \ln\left(\frac{1.12}{r_m}\right)\left(\frac{1 - \cos \xi}{2}\right) + (1 + \epsilon(\xi))\frac{r_b^2}{4} \quad (2.59)$$

where $\epsilon \equiv \frac{\Delta_s}{r_b}$. The wakefield E_z in the ion channel is therefore

$$E_z(r, \xi) \approx \frac{1 + \epsilon(\xi)}{2}r_b(\xi)\frac{d}{d\xi}r_b(\xi) + 2\Lambda \ln\left(\frac{1.12}{r_m}\right)\frac{\sin \xi}{2} \quad (2.60)$$

For small r_b , the equation of motion for $r_b(\xi)$, Eq.2.46, can be reduced to

$$\frac{d^2r_b}{d\xi^2} = -\frac{1}{2}r_b + \frac{\lambda(\xi)}{r_b} \quad (2.61)$$

which is identical to Eq.19. At the maximum blowout where $\xi = \xi_0 \approx \pi$, $\frac{dr_b}{d\xi} = 0$. Therefore, to 1st order in $(\xi - \xi_0)$,

$$r_b(\xi) \frac{d}{d\xi} r_b(\xi) \approx r_m \frac{d^2 r_b}{d^2 \xi}(\xi_0)(\xi - \xi_0) \quad (2.62)$$

It thus follows that to lowest order, $E_z(r, \xi)$ is

$$E_z(r, \xi) \approx -\left(\frac{1}{4}r_m^2(1+\epsilon)\left(1 - \frac{2c(\xi_0)}{r_m^2}\right) + \Lambda \ln\left(\frac{1.12}{r_m}\right)\right)(\xi - \xi_0) \quad (2.63)$$

Substituting $r_m \approx 2.58\Lambda^{1/2}$ into the above expression for E_z , and also noting that ϵ and $\frac{2c(\xi_0)}{r_m^2}$ are both small, we obtain

$$E_z(r, \xi) \approx -\left(\Lambda \ln\left(\frac{1}{\sqrt{\Lambda/5.3}}\right)\right)(\xi - \xi_0) \quad (2.64)$$

For very small blowout radius, the wakefield structure is close to a sinusoidal form, so the slope at the point where $E_z = 0$ can be used to roughly determine the maximum wake amplitude. This gives

$$E_{zmax} \approx \Lambda \ln\left(\frac{1}{\sqrt{\Lambda/5.3}}\right) \quad (2.65)$$

Although this is calculated for a bi-flat-top beam, we can see it is very close to the formula given in Eq.2.53 which was deduced from simulations [49].

2.6 The Ultra-relativistic Blowout Regime

In the ultra-relativistic limit where $r_m \gg 1$, $\beta \ll 1$ and $\beta r_m^2 \gtrsim 4$, Eq.2.46 reduces to:

$$r_b \frac{d^2 r_b}{d\xi^2} + 2\left[\frac{dr_b}{d\xi}\right]^2 + 1 = \frac{4\lambda(\xi)}{r_b^2} \quad (2.66)$$

The bunch length is typically much shorter than the nonlinear ion channel length, so we can ignore the driving term on the right hand side for much of the trajectory. The equation for a circle is

$$r_b \frac{d^2 r_b}{d\xi^2} + \left[\frac{dr_b}{d\xi} \right]^2 + 1 = 0 \quad (2.67)$$

while Eq.2.66 gives

$$r_b \frac{d^2 r_b}{d\xi^2} + 2 \left[\frac{dr_b}{d\xi} \right]^2 + 1 = 0 \quad (2.68)$$

with the right hand side set to zero. Near the top of a circle $dr_b/d\xi \rightarrow 0$, so the trajectory $r_b(\xi)$ maps out a circle until the rear of the blowout region. The effect of the “extra” $\left[\frac{dr_b}{d\xi} \right]^2$ term is to bend the trajectory downward more quickly as $\frac{dr_b}{d\xi}$ becomes large. This is indeed what is observed in Fig.4.a. We can rewrite the left hand side of Eq.2.66 as

$$\frac{d}{d\xi} \left[\frac{1}{2} r_b \frac{dr_b}{d\xi} \right] = -\frac{1}{2} - \frac{1}{2} \left[\frac{dr_b}{d\xi} \right]^2 \quad (2.69)$$

,

and since it follows from Eq.2.47 that $E_z(\xi) \approx \frac{1}{2} r_b \frac{dr_b}{d\xi}$ when $\beta(\xi)$ can be neglected for $r_b \gg 1$, we see that E_z has a slope $\frac{\partial E}{\partial \xi} = -\frac{1}{2}$ at the top of the channel and the slope increases as $\frac{dr_b}{d\xi}$ increases leading to the characteristic spike. This is seen in Fig.4.a where a line with a slope of $-1/2$ is shown for convenience.

For most situations of interest, the driver is sufficiently short that the right hand side of eqs.2.46 and 2.66 can be neglected at the point where $r_b(\xi_0) = r_m$. For $\xi > \xi_0$ and for $r_m \gtrsim 4$ the trajectory for r_b maps out a circle and the ion column is a sphere, i.e., a bubble. The value of $E_z = 0$ at $\xi = \xi_0$, and E_z decreases linearly from 0 to $-r_m/2$ in a distance $L_c = r_m$. Therefore the

nonlinear frequency (or wave number) is $\omega_{NL} = \frac{\pi}{r_m} \omega_p$ and in terms of the amplitude $E_{zmax} = r_m/2$, $\omega_{NL} = \frac{\pi}{2E_{zmax}} \omega_p$. Interestingly the same relationship holds for nonlinear one-dimensional plasma oscillations [65] although the physics is completely different. In these 3D wakes the wakefields are electromagnetic in character. Besides the accelerating axial electric field, E_z , there are transverse electric, E_r , and magnetic fields, B_θ . The E_r fields come from the ion column, $E_{rion} = \frac{1}{2}r$, and the radial plasma current, $E_{rEM} = -\frac{1}{4}r$ while B_θ comes from the radial plasma current, $B_{\theta EM} = -\frac{1}{4}r$. The total focusing field on a beam electron is $E_r - B_\theta = \frac{1}{2}r = E_{rion}$.

2.7 Formulas for Arbitrary Blowout Radius

We can also get expressions for arbitrary blowout radius by taking into account all the terms in the equation of motion. First we can get the slope of the wakefield near the top of the ion channel by expanding the equation of motion near the maximum blowout radius. From Eq.2.45 the wakefield inside the ion channel is:

$$E_z(\xi) = \frac{d}{d\xi} \psi(0, \xi) = \left(\frac{1}{2} + \frac{1}{2}\beta + \frac{1}{4}r_b \frac{d\beta}{dr_b} \right) r_b \frac{dr_b}{d\xi} \quad (2.70)$$

At the maximum blowout radius $\xi = \xi_m$, $r_b = r_m$ and $\frac{dr_b}{d\xi} = 0$. The blowout radius $r_b(\xi)$ can then be expanded about $\xi = \xi_m$:

$$r_b(\xi) \approx r_m + \frac{1}{2} \frac{d^2 r_b}{d\xi^2} (\xi_m)(\xi - \xi_m)^2 \quad (2.71)$$

This leads to

$$\frac{dr_b}{d\xi} \approx \frac{d^2 r_b}{d\xi^2} (\xi_m)(\xi - \xi_m) \quad (2.72)$$

and

$$E_z(\xi) \approx [\frac{1}{2} + \frac{1}{2}\beta(r_m) + \frac{1}{4}r_m \frac{d\beta}{dr_b}(r_m)]r_m \frac{d^2r_b}{d\xi^2}(\xi_m)(\xi - \xi_m) \quad (2.73)$$

From the equation of motion for r_b ,

$$\frac{d^2r_b}{d\xi^2}(r_m) = -\frac{[C(r_m) - \frac{\lambda(\xi_m)}{r_m^2}]}{A(r_m)}r_m \quad (2.74)$$

So the slope of E_z at $\xi = \xi_m$ can be written as:

$$\frac{dE_z}{d\xi}(\xi_m) = -[\frac{1}{2} + \frac{1}{2}\beta(r_m) + \frac{1}{4}r_m \frac{d\beta}{dr_b}(r_m)]r_m^2 \frac{[\frac{1}{4}[1 + \frac{1}{(1+\beta r_m^2)^2}] - \frac{\lambda(\xi_m)}{r_m^2}]}{1 + [\frac{1}{4} + \frac{1}{2}\beta + \frac{1}{8}r_m \frac{d\beta}{dr_b}]r_m^2} \quad (2.75)$$

We can easily check this formula for the two limits. For non-relativistic blowout where $r_m \ll 1$, $\beta(r_m) \gg 1$, $\beta(r_m)r_m^2 \ll 1$ and $\frac{1}{4}r_m \frac{d\beta}{dr_b}(r_m) \sim -\frac{1}{2}$, resulting in

$$\frac{dE_z}{d\xi}(\xi_m) \approx -\frac{1}{4}\beta(r_m)r_m^2 \quad (2.76)$$

By substituting $r_m \sim 2\sqrt{\Lambda}$ and $\beta(r_m) \sim \ln \frac{1}{r_m^2}$, we can roughly recover the scaling $\Lambda \ln \frac{1}{\Lambda}$. The wakefield also scales the same way because the wavelength in this limit is a constant. So we can roughly say that in the non-relativistic blowout regime the accelerating field scales as r_m^2 .

On the other hand for ultra-relativistic blowout where $r_m \gg 1$, $\beta(r_m) \ll 1$, $\beta(r_m)r_m^2 \gg 1$ and $\frac{1}{4}r_m \frac{d\beta}{dr_b}(r_m) \sim \beta(r_m)$, leading to

$$\frac{dE_z}{d\xi}(\xi_m) \approx -\frac{1}{2} \quad (2.77)$$

In this limit, the slope is a constant, and the ion channel has a spherical shape, so the accelerating field scales as r_m .

We can also get estimates for the ion channel length for arbitrary blowout radius. For small blowout radius, the half length of the ion channel is fixed at $\pi/\sqrt{2}$. For large blowout radius ($r_m \gtrsim 4$), half of the ion channel length is almost the same as the blowout radius. For a blowout radius between ($1 < r_m < 4$), the ion channel is close to an ellipse, and the half length of this channel can be calculated by assuming a constant wakefield slope.

$$E_z \approx \frac{1}{2}(1 + \beta(r_m))r_b \frac{dr_b}{d\xi} \approx -k_s \xi \quad (2.78)$$

Integrating once gives an equation for an ellipse,

$$r_b^2 + \frac{2k_s}{1 + \beta} \xi^2 \approx r_m^2 \quad (2.79)$$

Evaluating ξ for $r_b = 0$ provides the half length of the ion channel, $L_h \approx \sqrt{\frac{1+\beta}{2k_s}} r_m$.

2.8 Differences between Laser Driver and Electron Beam Driver

In previous sections, we treated both laser drivers and the beam drivers on the same footing. We used the same sheath model for each and the analysis indicated that the wake structure is basically dictated by the maximum blowout radius, r_m , so long as the laser or particle beam driver is sufficiently short.

In this section we will discuss the differences between the laser and the beam drivers in several important aspects: driver spot size, blowout radius and the matching condition.

For the electron driver case, the bunch is typically narrow, $\sigma_r \ll r_m$, and

the ultra-relativistic limit is generally not reached, $r_m \sim 2$. For example, in the E164X experiments [48], $N = 1.8 \times 10^{10}$, $\sigma_z = 30\mu m$, $\sigma_r = 10\mu m$ and the plasma density was $5 \times 10^{16} cm^{-3}$. Therefore $n_b/n_p \approx 7$ and $\Lambda \approx 1$. For these parameters, $k_p r_m \approx 2$. For such an r_m , both the ion channel and linear response regions contribute significantly to the wake excitation.

For the laser driver case, narrow lasers ($W_0 \frac{\omega_p}{c} \ll 1$) cannot be guided because even a fully evacuated channel can not provide an index of refraction with enough depth to compensate the laser diffraction. This can be seen from the linear guiding condition. For a transverse Gaussian laser profile with spot size W_0 , the normalized channel depth $\Delta n_c/n_p$ needed to guide the laser is[85]

$$\frac{\Delta n_c}{n_p} = \frac{4}{(k_p W_0)^2} \quad (2.80)$$

Complete blowout occurs when $\frac{\Delta n_c}{n_p} \sim 1$ and $k_p W_0 > 2$ is the requirement for optical guiding. In order for a laser with such a spot size to cause blowout, the normalized vector potential a_0 also needs to be larger than 1. Therefore, laser powers larger than P_c (the critical power for relativistic self focusing [55]) are needed to generate blowout. Since the blowout radius will exceed the laser spot size, when using laser drivers, one is often in the ultra-relativistic blowout regime or bubble regime.

Unlike the space charge force of an electron beam, the ponderomotive force of the laser only extends out to the edge of the laser. For a given laser power P and plasma density n_p , there is a matched spot size which produces well defined sheaths and good guiding properties for the laser. If the spot size is much larger than this matched size, the normalized vector potential a_0 will be too small to cause blowout initially. However, relativistic self focusing will also result in the back of the pulse focusing down to a spot size $\sim c/\omega_p$ which will then lead to

blowout [55]. Conversely, if the laser is focused to a spot size smaller than the matched size, the normalized vector potential is so large that electrons near the axis will be blown out very rapidly while the electrons at the laser edge will feel a very small ponderomotive force so they move very little. This leads to a very wide sheath. In addition, the laser will diffract because its spot size is too small to be guided. To form a well defined narrow sheath which is a key assumption of our model, one needs the laser spot size to roughly be the same as the blowout radius, $W_0 \sim r_m$. Under this condition, electrons at an initial radius near W_0 will experience an impulse before the ion channel forces have fully developed. These electrons then move outward until the ion channel force brings them to rest. This suggests the blowout radius can be estimated by balancing the laser ponderomotive force on a single electron and the ion channel force. Typically, we also choose a laser pulse length around r_m , which is short enough that the impulse approximation is reasonable. Balancing the two forces to get an estimate of the matched spot size gives

$$\frac{a_0^2}{\bar{\gamma} k_p r_m} \sim k_p r_m \quad (2.81)$$

and by substituting $\bar{\gamma} \sim a_0$, we get

$$k_p r_m \sim 2\sqrt{a_0} \quad (2.82)$$

where the factor of 2 is deduced from full PIC simulations. Estimating the blowout radius in this manner was also done in references [79] and [80]. In these references give an estimate a factor of two smaller. In addition, it is also how the requirement for electron cavitation was determined in Ref.[55].

The need to use a matched laser spot size is illustrated in Fig.2.5 where the

plasma density is plotted from simulations with matched and unmatched spot sizes for the same laser power and plasma density. In Fig.5a $k_p W_0 = 4$ while in Fig.5b $k_p W_0 = 3$.

Our simple sheath model only works well for the matched case (Fig.2.5a), therefore for the other value of W_0 our model(Fig.2.5.b) does not work as well. From the formula for r_m , Eq.2.82, we can see that the ultra-relativistic limit, $r_m \gtrsim 4$, can be reached when $a_0 \gtrsim 4$ and $W_0 \sim r_m \sim 2\sqrt{a_0}$. Reaching this limit requires a laser power $a_0^2 W_0^2 \sim 8P_c$ where P_c is the critical power for relativistic self-focusing [84]. For current stat-of-the-art lasers [60, 61, 62, 59], $15 \lesssim P \lesssim 100TW$, reaching the ultra-relativistic blowout (bubble) regime therefore requires the use of plasma densities between $2 \times 10^{19} \gtrsim n_p \gtrsim \times 10^{18} cm^{-3}$ respectively.

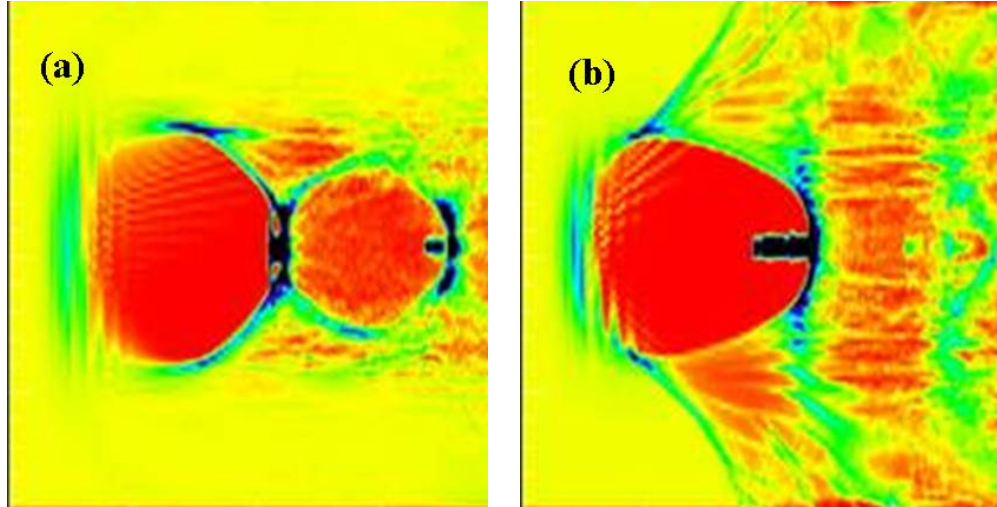


Figure 2.5: Plasma density plots from PIC simulations with matched and unmatched spot sizes for the same laser power P and plasma density n_p , $P/P_c = 8$
(a) matched case with $k_p W_0 = 4$ and $a_0 = 4$ (b) unmatched case with $k_p W_0 = 3$ and $a_0 = 5.3$

2.9 Summary

We have described a nonlinear, kinetic (non-fluid) theory for describing multi-dimensional plasma wave wakefields generated by relativistic electron beams or intense short lasers with matched spot sizes propagating in plasmas. These wake fields are generated when all electrons within a radius r_b are expelled leaving behind an ion channel. The expelled electrons form a narrow sheath. The theory permits the derivation of an equation of motion for an electron at the blowout radius. Integrating this equation directly for electron beam drivers provides accurate agreement with fully nonlinear particle-in-cell simulation results. For laser drivers, the maximum blowout radius is determined from force balance and the equation of motion can then be used to determine the shape of the ion channel behind the laser. We have examined the consequences of this equation in the limit that $r_b \ll c/\omega_p$ and when $r_b \gg c/\omega_p$. For the small r_b limit we show how linear fluid theory breaks down and how the logarithmic divergence in the linear Green's function saturates for small radii. For the large r_b limit we show that the trajectory for r_b maps out a circle. We also discuss the differences between lasers and electron beam drivers. For e-beam drivers the spot size is typically much less than c/ω_p and for typical parameters the maximum blowout radius is $\lesssim 2c/\omega_p$. On the other hand, for lasers a matched spot size is required, $k_p W_0 \approx 2\sqrt{a_0}$, and the maximum blowout radius is typically $\gtrsim 4$.

CHAPTER 3

Some Applications of the Nonlinear Wakefield Theory

3.1 Introduction

The nonlinear theoretical framework presented in last chapter can be used to understand many physical problems that occur in the blowout regime. This chapter will describe several such examples in several short sections. These examples include determining the plasma density which optimizes the wake amplitude for given beam parameters, calculating the number of electrons that can be accelerated (nonlinear beam loading), calculating the transformer ratio for a ramped electron driver, and developing the proper equation for describing the electron hosing instability of short, intense bunches.

3.2 The optimum Plasma Density for Plasma Wakefield Excitation in the Blowout Regime

Experimentalists always want to get useful information from theorists in terms of formulas which are easy to use. One can then plug in the numbers to get what he needs without going through a maze of symbols. In plasma based acceleration, one simple but very important question an experimentalist may ask is the

following: If one has an electron beam driver with given parameters (e.g., total charge N , energy γ , spot size σ_r and duration σ_z), what will be the optimum plasma density to obtain the largest wakefield? Is it possible we have a simple engineering formula for it?

It should be noted determining the optimum density can be obtained via laboratory and simulation experiments. However, the parameter scan needed could be formidable. Therefore, even a theoretical model which is not exact but that catches the key physical effects is always useful and even needed. For such a highly nonlinear problem the interplay between the insight obtained through experiments and simulations and through a theoretical model are crucial. The idea is to use the theoretical model to identify a limited parameter space for which experiments and simulations are carried to precisely answer the question.

Let's get back to our special question here. We can first look at this question about the optimum plasma density in the linear plasma wakefield case. Linear theory is based on the assumption that the beam density n_b is assumed to be much smaller than the plasma density n_p so the density perturbation δn is small comparing with n_p . For narrow bunches this must still be true otherwise complete blowout (trajectory crossing) will occur. We can get the expression for wakefield amplitude for a bi-Gaussian beam as:

$$E_{zMax} = \left[\frac{mc\omega_p}{e} \right] \sqrt{\frac{\pi}{2}} \frac{n_b}{n_p} k_p \sigma_z (k_p \sigma_r)^2 [e^{-k_p^2 \sigma_z^2 / 2 + k_p^2 \sigma_r^2 / 2} \Gamma(0, k_p^2 \sigma_r^2 / 2)] \quad (3.1)$$

where $\Gamma(x, y) = \int_y^\infty t^{x-1} e^{-t} dt$. Recently Lu et. al showed that for a beam with a small aspect ratio ($\sigma_r/\sigma_z \ll 1$), the maximum wakefield is achieved when $k_p \sigma_z \approx \sqrt{2}$.

This is the generally accepted condition for the optimum plasma density. How

different will the prediction of nonlinear theory be compared with the above linear result?

From the previous chapter we know that the total charge per unit length Λ is an important parameter in wakefield theory as long as $f k_p \sigma_z \gtrsim 1$. We can rewrite Λ for a bi-Gaussian electron driver as:

$$\begin{aligned}\Lambda &= \frac{n_b}{n_p} (k_p \sigma_r)^2 \\ &= [(2\pi)^{3/2} n_b \sigma_r^2 \sigma_z] [(2\pi)^{-3/2} k_p^2 n_p^{-1} \sigma_z^{-1}] \\ &= \sqrt{\frac{2}{\pi}} \left[\frac{r_e}{\sigma_z} \right] N\end{aligned}\tag{3.2}$$

Where $N = (2\pi)^{3/2} n_b \sigma_r^2 \sigma_z$ is the total electron number and $r_e = mc^2/e^2$ is the classical electron radius. This formula suggests that for a constant N , Λ is independent of plasma density n_p and the beam spot size σ_r although both appear in its definition. As we know from the previous chapter, for Λ to be a meaningful parameter, two implicit assumptions are made: one is that the beam is not much shorter than a plasma skin depth k_p^{-1} , otherwise blowout does not occur within the bunch and plasma electrons simply receive an impulse; the other is that the beam density n_b should be comparable or larger than the plasma density n_p so that the condition for blowout is satisfied. For given beam parameters (N, σ_r, σ_z) , the first condition gives a lower limit for the plasma density, e.g., $k_p \sigma_z \gtrsim 0.2$; The second gives an upper limit for the plasma density, e.g., $n_b \gtrsim n_p$ or $k_p \sigma_r \lesssim \sqrt{\Lambda}$.

For a plasma density much lower than the lower limit (e.g., $k_p \sigma_z \lesssim 0.2$), the meaningful parameter for the beam plasma interaction should be the normalized total charge $Q \equiv \Lambda k_p \sigma_z$ because it is only impulse that matters. The parameter Q increases when the plasma density increases from zero to the lower limit, therefore both the normalized and the absolute wakefield amplitudes increase.

When the plasma density is in the intermediate range (e.g., $k_p\sigma_z \gtrsim 0.2$ and $k_p\sigma_r \lesssim \sqrt{\Lambda}$, typically $\sigma_r < \sigma_z$), the normalized wakefield amplitude is mainly determined by the normalized blowout radius $k_p r_m$, which for this density range is roughly given by $k_p r_m \approx 2\sqrt{\Lambda}$. Since for fixed beam parameter (N , σ_z , σ_r) Λ does not depend on the plasma density, the normalized wakefield amplitude is insensitive to the density. Therefore, the absolute wakefield amplitude will increase with the plasma density in this density range.

For a plasma density above the upper limit (e.g., $n_b/n_p \lesssim 1$ or $k_p\sigma_r \gtrsim \sqrt{\Lambda}$), the beam plasma interaction is close to linear. Therefore, linear theory is valid for this density range. If $k_p\sigma_z < \sqrt{2}$, the absolute wakefield amplitude will get its maximum value at $k_p\sigma_z \approx \sqrt{2}$. If $k_p\sigma_z > \sqrt{2}$, the absolute wakefield amplitude will decrease with plasma density; therefore, the maximum wakefield amplitude is reached for $n_b/n_p \sim 1$.

As noted in chapter 2, there are two different regimes for blowout: non-relativistic blowout where $\Lambda \ll 1$ and relativistic blowout where $\Lambda \gtrsim 1$. In the non-relativistic blowout regime, the field amplitude scales as $\Lambda \log \frac{1}{\Lambda}$, which is close to the prediction of linear theory. Therefore, based on the above analysis, for $\Lambda \ll 1$ the optimum plasma density for which the wakefield amplitude is maximum close to the results from linear theory, i.e., $k_p\sigma_z \approx \sqrt{2}$. However from the arguments in the preceding paragraph, for the relativistic blowout regime, $\Lambda \gtrsim 1$, the optimum plasma density for which the absolute wakefield amplitude is maximum is approximately $n_p \sim n_b$. When $n_p \sim n_b$ and $\Lambda \gtrsim 1$ then $k_p\sigma_r > \gtrsim 1$.

To see the implications of the simple arguments given above, we consider the beam at SLAC. A typical bunch has, $N \sim 10^{10}$, or $\sim nC$ of charge (interestingly, this is also similar to the value of N for a bunch of the proposed ILC). At SLAC the value of N can not be increased. Therefore, Λ is mainly determined by the

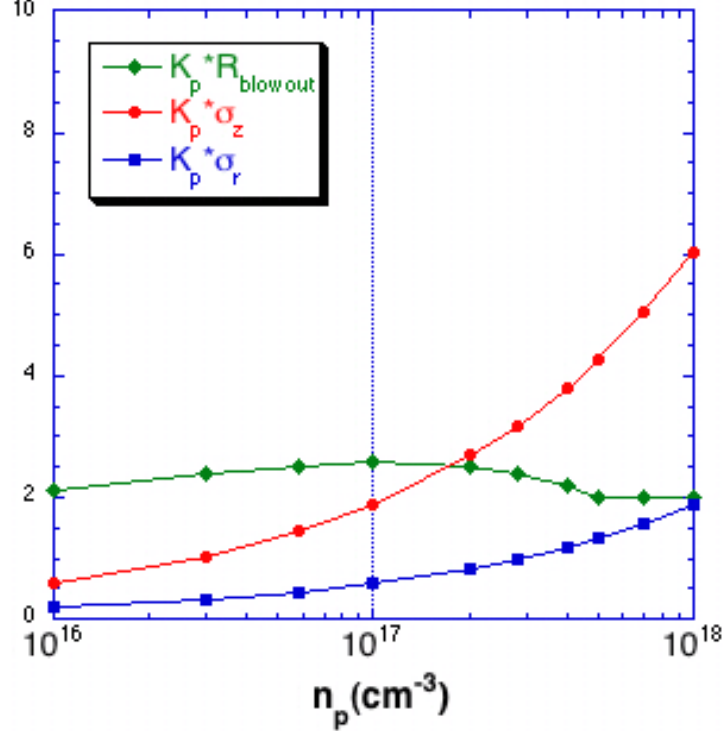


Figure 3.1: The normalized beam dimensions $k_p\sigma_r$, $k_p\sigma_z$ and the normalized blowout radius $k_p r_m$ (the driver is a bi-Gaussian beam with $N = 1.8 \times 10^{19}$, $\sigma_z = 32\mu\text{m}$ and $\sigma_r = 10\mu\text{m}$)

beam duration ($c\tau$ or σ_z). For $N \sim 10^{10}$ and pulse durations on the order of picosecond, the beam plasma interaction is in the non-relativistic blowout regime, $\Lambda \ll 1$. For example, in the original E157 experiment carried out at SLAC, $N = 1.9 \times 10^{10}$, $\sigma_z = 700\mu\text{m}$ ($c\tau \sim 2\text{ps}$) and $\sigma_r = 30\mu\text{m}$, these parameters give $\Lambda = 0.06$. Experiments and simulations both showed that the optimum plasma density for this beam is around $n_p = 1.4 \times 10^{14}\text{cm}^{-3}$, which is close to the linear prediction $n_p = 1.2 \times 10^{14}\text{cm}^{-3}$ for a bi-Gaussian beam.

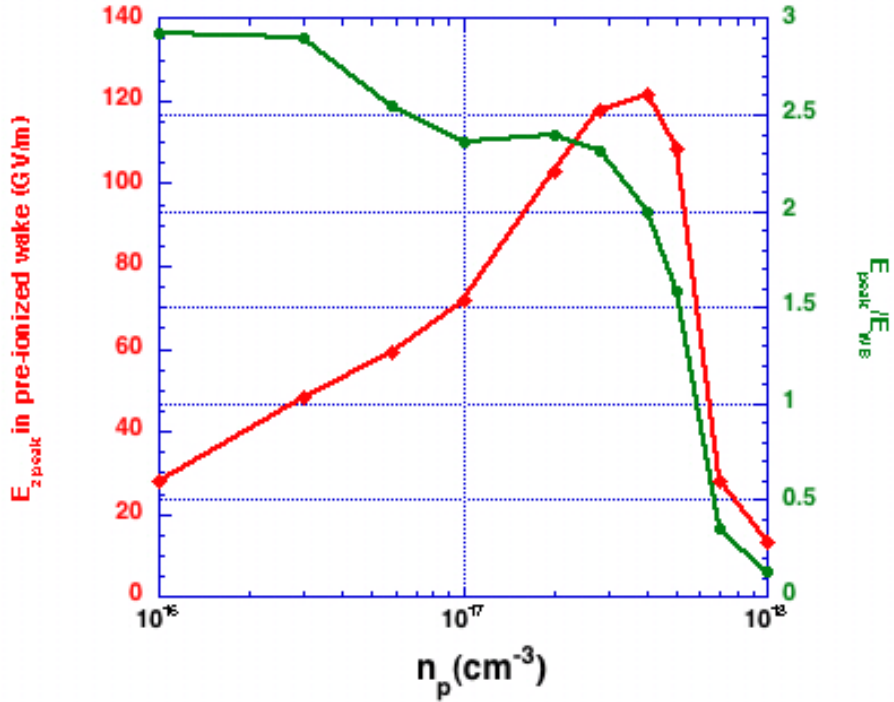


Figure 3.2: The normalized and absolute peak wakefield amplitudes (the driver is a bi-Gaussian beam with $N = 1.8 \times 10^{19}$, $\sigma_z = 32\mu m$ and $\sigma_r = 10\mu m$)

Recently, the bunch duration was shortened to $\lesssim 100fs$, and when $\tau = 100fs$, $\Lambda \sim 1$. Several experiments were carried out using the shorter bunches. In one set of experiment, E164/E164x, the beam parameters were $N = 1.8 \times 10^{19}$, $\sigma_z = 32\mu m$ and $\sigma_r = 10\mu m$, which give $\Lambda = 1.27$ and $n_b = 3.6 \times 10^{17} cm^{-3}$. Our analysis suggests that the optimum plasma density is near n_b for this case. This is nearly ten times larger than the optimum plasma density obtained from linear theory ($n_p = 3.5 \times 10^{16} cm^{-3}$ when the fully linear expression is used). To verify the nonlinear prediction, we show the results of a plasma density scan using PIC simulation in Fig.3.2 and Fig.3.2. In Fig.3.2, the normalized beam

dimensions, $k_p\sigma_r$, $k_p\sigma_z$, and the normalized blowout radius $k_p r_m$ are shown. In Fig.3.2, the normalized and absolute peak wakefield amplitudes are shown. In these simulations, the plasma densities range over two orders of magnitude (from $1 \times 10^{16} cm^{-3}$ to $1 \times 10^{18} cm^{-3}$). Several points are worth noting. First, the normalized blowout radius $k_p r_m$ changes very little over the full density range (the average is about 2.2, very close to our estimate of $2\sqrt{\Lambda} \approx 2.25$, and after $n_p \gtrsim 2n_b$, the blowout is not complete so the value of $k_p r_m$ is very rough). Second, the trend of the absolute wake amplitude increasing with density agrees with our analysis and the optimum density, $n_p \approx 4 \times 10^{17} cm^{-3}$, is close to the prediction of $3.5 \times 10^{17} cm^{-3}$. In light of the factor of ten difference of the plasma density between the linear and nonlinear predictions, this agreement clearly shows the usefulness of the nonlinear analysis.

For even short electron bunches, e.g., sub 30 fs ($\sigma_z \lesssim 10 \mu m$), the beam plasma interaction is in the ultra-relativistic blowout regime ($\Lambda \gg 1$). For example, if the beam duration in the E164 experiment was shorten by a factor of 3 (to $10 \mu m$ or 30 fs), we get $\Lambda \approx 4$ and $k_p r_m \approx 4$. In this case, the ion channel will have a spherical or bubble shape behind the driver.

From the above discussions, one can see that the parameter Λ has a very important meaning in the blowout regime. The optimum plasma density for maximizing the wakefield amplitude, predicted by linear theory ($k_p\sigma_z = \sqrt{2}$) is only useful in non-relativistic blowout regime, i.e., for $\Lambda \ll 1$. In the relativistic blowout regime ($\Lambda \gtrsim 1$), linear prediction can be too low by one order of magnitude for certain beam parameters and the nonlinear analysis indicates that the optimum plasma density is roughly equal to the peak beam density. When $\Lambda \gtrsim 1$ and $n_b \sim n_p$ then the spot size is $k_p\sigma_r = \sqrt{\Lambda} \sim k_p r_m/2$. Therefore, the absolute wake is maximized when the spot size is roughly matched to the blowout radius.

3.3 Beam Loading in the Blowout Regime

In plasma based acceleration, a charged particle beam of sufficient charge must be loaded into a plasma wakefield. Determining how much charge can and should be loaded into the wake while achieving high beam loading efficiency and beam quality (i.e., the energy spread and emittance) is a key question. If both the plasma wake excitation and the beam loading are in the linear regime, linear plasma wakefield theory can be used to address these problems. The beam loading and relevant issues in the linear regime were comprehensively discussed in the seminal work of Kasouleas et al. in 1986. Much has changed and much has been learned since 1986. The main topic of this dissertation is nonlinear wake in the blowout regime. Clearly, analysis based on linear theory will not work. There has been little to no analysis on beam loading of nonlinear wakes because of the lack of a general theory for wake excitation in the blowout regime. The theoretical framework introduced in chapter 2 can be used to analyze wake excitation by shaped electron bunches and to explore beam loading in the blowout regime. In this short section, we will use the blowout theory to simply estimate the number of particles that can be loaded into the wake driven by a sufficiently short driver in the ultra-relativistic blowout regime. A direction for future research is to use eqn.2.46 to determine the best shape for the electron beam profiles and how to choose the relative phase between these bunches to achieve better beam loading efficiency and more uniform acceleration. However, much insight into beam loading in the blowout regime can be immediately seen from eqn.2.46 and 2.47. When a trailing beam is placed in the rear of the bubble, its space charge forces (it corresponding to λ on the RHS of eq.2.46) will slow down the rate at which $r_b\xi$ is decreasing. If $\frac{dr_b}{d\xi}$ is smaller then from eqn.27 E_z is reduced. One way to determine the maximum number of particles that can be loaded is to see how

large a Λ is needed to have $\frac{dr_b}{d\xi} \rightarrow 0$ at the back of the beam. Another, which we employ here is to calculate the total energy in the wake and use energy balance.

In the ultra-relativistic blowout regime driven by a sufficiently short driver (either electron beam or laser pulse), the ion channel has a spherical shape and the wake fields inside the channel have a special form. If we normalize the fields to $mc\omega_p/e$ and the length to c/ω_p , we have $E_z = -\frac{\xi}{2}$, $B_\theta = \frac{r}{4}$, $E_r = -\frac{r}{4}$.

The total energy of the electromagnetic fields inside the ion channel E_t can be decomposed as the sum of the energy of the longitudinal field (E_z) and the energy of the transverse focusing fields (B_θ and E_r):

$$\begin{aligned} E_t &= \int \frac{E_z^2 + E_r^2 + B_\theta^2}{8\pi} dV \\ &= \int \frac{E_z^2}{8\pi} dV + \int \frac{E_r^2 + B_\theta^2}{8\pi} dV \\ &= E_w + E_f \end{aligned} \quad (3.3)$$

By carrying out the integration, we get

$$\begin{aligned} E_w &= \int \frac{E_z^2}{8\pi} dV \\ &= \int \frac{\bar{E}_z^2}{8\pi} d\bar{V} \left(\frac{m^2 c^5}{e^2 \omega_p} \right) \\ &= \int_{-k_p R_m}^{k_p R_m} d\xi \int_0^{\sqrt{(k_p R_m)^2 - \xi^2}} \frac{1}{8\pi} \frac{\xi^2}{4} 2\pi r dr \left(\frac{m^2 c^5}{e^2 \omega_p} \right) \\ &= \frac{1}{120} (k_p R_m)^5 \left(\frac{m^2 c^5}{e^2 \omega_p} \right) \end{aligned} \quad (3.4)$$

$$\begin{aligned}
E_f &= \int \frac{E_r^2 + B_\theta^2}{8\pi} dV \\
&= \int \frac{\bar{E}_r^2 + \bar{B}_\theta^2}{8\pi} d\bar{V} \left(\frac{m^2 c^5}{e^2 \omega_p} \right) \\
&= \int_{-k_p R_m}^{k_p R_m} d\xi \int_0^{\sqrt{(k_p R_m)^2 - \xi^2}} \frac{1}{8\pi} \frac{r^2}{8} 2\pi r dr \left(\frac{m^2 c^5}{e^2 \omega_p} \right) \\
&= \frac{1}{120} (k_p R_m)^5 \left(\frac{m^2 c^5}{e^2 \omega_p} \right)
\end{aligned} \tag{3.5}$$

The above calculations show that the wakefield energy equals the focusing field energy, therefore the total field energy is:

$$E_t = \frac{1}{60} (k_p R_m)^5 \left(\frac{m^2 c^5}{e^2 \omega_p} \right) \tag{3.6}$$

The field energy scales as $k_p R_m$ to the 5th power. Therefore, a variation of about 15% in $k_p R_m$ will lead to 100% variation in E_t . It is also worth noting that the real field energy inside the ion channel will be larger than this estimate because the real fields have larger field amplitudes near the tail of the ion channel.

Next we can get an approximate estimate for the number of electrons N that can absorb all the energy in the ion channel. We can balance the energy gained by N electrons as by the longitudinal field in a distance of $2R_m$ with the energy of the wake in one bucket, $eNE_z 2R_m = E_t$. with the energy loss for a distance of $2R_m$ (the length of the full ion channel). It is worth noting that the energy absorbed by the beam should also include a fraction of the plasma kinetic energy because the beam can reduce the plasma kinetic energy by changing the motion of the plasma boundary. The kinetic energy also scales as $(k_p R_m)^5$. If we assume that the kinetic energy absorbed by the beam is about the same amount as the field energy, we can write

$$eN \times E_{ave} \times 2R_m \approx \frac{1}{30} (k_p R_m)^5 \left(\frac{m^2 c^5}{e^2 \omega_p} \right) \quad (3.7)$$

Where E_{ave} is the average accelerating field the beam experiences. We chose E_{ave} as half of the maximal E_z ($E_{zmax} = (k_p R_m / 2)(mc\omega_p/e)$). This gives

$$N \approx \frac{1}{30} (k_p R_m)^3 \left(\frac{1}{k_p r_e} \right) \quad (3.8)$$

where $r_e = e^2/mc^2$ is the classical electron radius. To compare with the beam loading formula obtained from linear wake field theory, we rewrite this formula as

$$N \approx 1.4 \times 10^5 \sqrt{n_p} A_{eff} \epsilon \quad (3.9)$$

here $A_{eff} = \pi R_m^2$ is the effective area of the wake and $\epsilon = k_p R_m / 2$ is the normalized field amplitude in the wake. Preliminary simulations have verified this estimate.

The result from linear theory also has a similar form:

$$N_{linear} \approx 5 \times 10^5 \sqrt{n_p} A_{linear} \epsilon_{linear} \quad (3.10)$$

Where A_{linear} is the effective area of the beam. For a wide beam with $k_p a \gg 1$, it is just πa^2 , for a narrow beam with $k_p a \ll 1$, it is on the order of c^2/ω_p^2 ($A_{linear} \approx \pi c^2/\omega_p^2 [-2/(0.577 + \ln k_p a/2)]$), where $A_{linear} = (0.6 \text{ to } 2) c^2/\omega_p^2$ for $k_p a = 10^{-4} \text{ to } 10^{-1}$. ϵ_{linear} is the normalized wave amplitude $\delta n/n_p$. Therefore, for narrow beams the maximum beam loading efficiency is between $(.6 \text{ to } 2) / \pi = 20\% \text{ to } 60\%$ for $k_p a = 10^{-4} \text{ to } 10^{-1}$.

From these similar formulas, we can see that the total charge obtained for a narrow beam in the blowout regime can be much larger than that obtained from the linear formula. This is because the wakes in the relativistic blowout regime have both larger effective area, i.e., $R_m \gg c/\omega_p$, and large amplitude. For example, in linear theory for $\epsilon_{linear} \sim 1/2$ and $k_p a = 10^{-4}$ one gets $N \sim .6 \times 10^9 / \sqrt{n_p} (10^{16} cm^{-3})$. While for $k_p R_m = 4$ we get $N \sim 3.5 \times 10^{10} / \sqrt{n_p} (10^{16} cm^{-3})$.

3.4 The Transformer Ratio for a Ramped Electron Beam

As mentioned in last section, our nonlinear theoretical framework can be used to address the problem of how wake excitation depends on the pulse shape in the blowout regime. In particular, determining the bunch shape that optimizing the transformer ratio of the wakefield is of much interest. It can be shown using 1D linear theory of beam driven plasma wakefield, that the transformer ratio of the wakefield E_+/E_- from a symmetric longitudinal profile is always less than two. To increase the transformer ratio, an asymmetric profile can be used. A particularly interesting example to achieve large transformer ratio is to use a linearly ramped beam profile with a sharp termination. It was also shown that in 1D larger transformer ratios can be obtained in the nonlinear regime. However, it is now well established that the 1D nonlinear regime is inaccessible because blowout will occur instead. It is natural to ask what bunch shapes lead to constant decelerating field in the blowout regime. For a linear ramped drive beam in the blowout regime, we can think about the transition from the 1D linear regime to the 3D nonlinear blowout regime as follows. We assume a fixed longitudinal beam profile and the total beam charge. Initially, we choose a very large spot size such that $n_b/n_p \ll 1$. In this case linear theory predicts a nearly uniform decelerating field within the beam and a large transformer ratio. If we keep decrease the spot

size, eventually it will reach the blowout regime. So will these special properties based on predictions from linear theory still hold when blowout is reached?

It will be helpful to gain some insight from a PIC simulation. In fig.3.4 , a linearly ramped electron beam driver is used to excite the plasma wake in the relativistic blowout regime. This beam has a normalized length $k_p L_0 \approx 22$ and a flat top transverse profile ($n_{b0} = 100$ for $k_p r < 0.5$ and drop to zero linearly at $k_p r = 0.6$). These parameters give $\Lambda_0 \approx 15$. In this simulation, the maximum blowout radius is about 7.5, which is very close to $2\sqrt{\Lambda_0} = 7.75$. We can see that the decelerating field within the driver is still close to uniform as in the linear case and has an amplitude near 0.7. It turns out that the fact that the decelerating field within a wedge shaped driver remains constant can be explained by simple arguments from the nonlinear theory of chapter 2.

In the relativistic blowout regime, approximately we have,

$$\psi(0, \xi) \approx \frac{r_b^2(\xi)}{4} \quad (3.11)$$

for $r_b \gtrsim 1$. For a long electron beam with an adiabatically increasing current profile $\Lambda(\xi) = \frac{\xi}{L_0} \Lambda_0$, where Λ_0 is calculated at the maximum beam density, the blowout radius $r_b(\xi)$ also increases adiabatically, so

$$r_b(\xi) \approx 2\sqrt{\Lambda(\xi)} \quad (3.12)$$

It is worth discussing the origin of the factor of two in the above expression. In the non-relativistic blowout regime, the adiabatic blowout radius for a long beam driver is $r_b \approx \sqrt{2\Lambda}$ because the dominate force on the plasma electrons is the transverse electric force from the beam. In the relativistic blowout regime, the plasma electrons in the narrow sheath move backward in the longitudinal

direction with speed comparable to the speed of light. Therefore they also feel the magnetic field from the driver. Since the electric and magnetic fields from an ultra-relativistic electron bunch are nearly the same amplitude (for cgs units), the total force on a plasma electron is doubled when it moves backwards with the speed of light. As a result, the adiabatic blowout radius , which scales as the \sqrt{Force} , will increase by $\sqrt{2}$. Therefore $r_b \approx 2\sqrt{\Lambda}$. It is interesting to note that this expression is also very accurate for the non-adiabatic case for either a large or small blowout radius for a short driver.

With this expression of r_b , we get

$$\psi(0, \xi) \approx \frac{\xi}{L_0} \Lambda_0 \quad (3.13)$$

and hence

$$\begin{aligned} E_z(\xi) &= \frac{d\psi}{d\xi} \\ &\approx \frac{\Lambda_0}{L_0} \end{aligned} \quad (3.14)$$

Therefore, the decelerating field is roughly a constant that is mainly determined by the peak beam current Λ_0 and the beam length L_0 . To see the accuracy of this result we substitute in the simulation parameters, $\Lambda_0 = 15$ and $L_0 = 22$, giving $E_z \approx 0.68$, which is very close to the simulation result.

We can also get an estimate of the transformer ratio if we assume that the beam current is terminated sharply at $\xi = L_0$, then the wake field behind the beam is mainly determined by the maximum blowout radius r_m , so the maximum useful accelerating field $E_{max} \approx \frac{1}{2}r_m \approx \sqrt{\Lambda_0}$ (the peak field is roughly two times larger than the useful field). Therefore, the transformer ratio for this beam driver is

$$E_+/E_- \approx \sqrt{\Lambda_0}/\left(\frac{\Lambda_0}{L_0}\right) = \frac{L_0}{\sqrt{\Lambda_0}} \quad (3.15)$$

It is worth noting that in the linear case it was necessary to use a precursor to get a constant decelerating field. In the nonlinear blowout regime, this is not necessary.

3.5 The Electron Hosing Instability in the Blowout Regime

The three examples in sections 3.2, 3.3 and 3.4 are solely based on our nonlinear theory of wake excitation in the blowout regime. It is obvious that this theory of wake excitation can not give direct answers for any beam plasma instabilities in the blowout regime because the beam evolution and the coupling between the beam and the plasma must be taken into account. However, we will show in this section that significant understanding of arguably the most important beam plasma instability in the blowout regime, the electron hosing instability, can be achieved if we combine our nonlinear wake excitation framework with a linear perturbation method on the blowout boundary. We will clarify how the linear hosing growth is affected by the blowout radius, the relativistic mass and the longitudinal velocity and the self-force from the plasma sheath. In this short section, only the main ideas to obtain this hosing theory will be given. More detail on the derivation and the simulation verification can be found elsewhere (see C. Huang's thesis, several plots are copied from there for convenience).

3.5.1 What is the Electron Hosing Instability?

In the blowout regime, plasma electrons are completely evacuated by the space charge force from an intense electron beam or the ponderomotive force from a

short laser pulse forming an ion channel with a narrow laminar layer of electrons at its boundary. How does this electron sheath interact with a self-injected or externally injected electron beam on the time scale of the beam evolution is of fundamental importance for plasma based acceleration. In early 1990's, a fast growing instability was found by Whittum et al. from a fluid model for an equilibrium geometry, where the ion channel is either pre-formed or adiabatically formed by an electron beam with long bunch length, i.e., $L \gg k_p^{-1}$. This instability will cause the oscillation of beam centroid to grow, therefore degrading the beam quality. They called it the electron hosing instability. The central result from their analysis is the following coupled equations:

$$\frac{\partial^2 x_c}{\partial \xi^2} + \omega_0^2 x_c = \omega_0^2 x_b \quad (3.16)$$

$$\frac{\partial^2 x_b}{\partial s^2} + \omega_\beta^2 x_b = \omega_\beta^2 x_c \quad (3.17)$$

where $x_c(s, \xi)$ and $x_b(s, \xi)$ are the centroids of the ion channel and the electron beam respectively, $\omega_\beta = \omega_p/\sqrt{2\gamma}$ is the betatron frequency of the beam and $\omega_0 = \omega_p/\sqrt{2}$. A moving window in $(x, y, s = z, \xi = ct - z)$ coordinates is used with s being the propagation distance and ξ being the position in the beam.

For the above equations to be valid, three conditions are assumed. First, the bunch length L should be long compared with the plasma wavelength, i.e., $L \gg k_p^{-1}$, such that the channel is balanced by the force from the electron beam and the force from the ion channel. Therefore the channel radius r_c is equal to the charge neutralization radius $r_{neu} \equiv \sqrt{n_b \sigma_b^2 / n_p}$, where n_b and n_p are the density of the beam and the plasma density and σ_b is the radius of the beam. Second, the channel radius r_c should be much smaller than a plasma skin depth c/ω_p such that the return current of the plasma sheath is negligible , or equivalently the

parallel velocity of the electrons in the sheath is much smaller than the speed of light. Third, the radius of the electron beam σ_b should be much smaller than the channel radius r_c such that the electron beam can be treated as a point charge in each slice.

However, under the current or future experiment conditions, most of these assumptions are not valid. First, the channels are generally non-adabatically formed by relatively short bunches, i.e., $L \sim k_p^{-1}$, so the channel boundary is highly curved. Second, the blowout radiiuses are generally comparable or larger than the skin depth so the parallel motion of the plasma electrons and the effect of magnetic field are important. Third, the beam width can be comparable with the channel width. For example, as mentioned in section 3.2, for relativistic blowout, the maximum wakefield amplitude is reached when the beam width is comparable to the channel width.

How these conditions can change the hosing instability is of much interests. In ref , the hosing instability in the non-adiabatic blowout regime was investigated using fully explicit 3D Particle-In-Cell(PIC) simulation. It was shown that the hosing is much less severe than the adiabatic theory predicts. However, the reasons for this reduced growth were not clearly identified and related to the beam parameters. Furthermore, there is no applicable theory for relevant parameters of current or future PWFA and LWFA experiments, such as the proposed “afterburner” parameters. These are the motivations for our theoretical analysis in this section.

Before touching the detail of our analysis, it may be helpful to see what hosing looks like in a simulation. Fig. 3.4 shows a real space plot of the beam when hosing occurs and saturates for the nominal parameters used in Fig. 5 of Ref. . Three regions along the beam which exhibit different behavior can be

identified from this plot. The first is the region near the head of the beam, i.e., the yellow box in Fig. 3.4. The lack of hosing in this region is observed in many simulations. Instead a self-aligning effect that the latter part of the head aligns with the former part happens gradually. It is difficult to quantify this behavior exactly. However, some qualitative explanations can be provided. At the very front of beam where $\Lambda \ll 1$, the analysis of transverse two stream instability may apply and the growth rate is generally orders of magnitudes smaller than the hosing instability. Further back in the beam where Λ increases, the electrons begin to blow-out yet there are a lot of trajectory crossing and phase mixing. The ion channel is not completely formed in this situation, thus reducing the focusing force on the beam. The combination of these effects will certainly leads to a much smaller growth rate. In addition, this region is too short for any hosing instability to grow significantly. Therefore, for practical reason we may assume there is no hosing in this region.

The second region is around the area indicated by the blue arrow. In this region, the ion channel is clearly formed and the electron motion in the plasma sheath is highly laminar. Consequently the shape of the ion channel can be represented by a single particle's trajectory. Hosing causes the beam centroid to oscillate with a spatiotemporal growth. The growth rate is linear for small amplitudes and begins to saturate for large amplitudes. Fig. 3.5 shows the linear and the saturation stages for the ξ point indicated by the blue arrow in Fig. 3.4 with the comparison to the asymptotic solution from the fluid hosing theory for the same parameters.

Further back in the beam a third region of the hosing behavior exists where the beam centroid oscillation amplitude becomes comparable to the channel radius. The beam hits the boundary of the ion channel and particles are lost when they

get out of the channel. Therefore the maximum centroid oscillation amplitude is limited by the width of the ion channel. This region is indicated by the green arrow in Fig. 3.4.

For a narrow electron beam ($\sigma_b \ll r_c$), we can simply divid the hosing instability into four different regimes , namely non-relativistic adiabatic blowout ($k_p r_c \ll 1$ and $r_c = constant$), non-relativistic non-adiabatic blowout ($k_p r_c \ll 1$ and $r_c \neq constant$) , relativistic adiabatic blowout ($k_p r_c \gtrsim 1$ and $r_c = constant$)and relativistic non-adiabatic blowout ($k_p r_c \gtrsim 1$ and $r_c \neq constant$).

3.5.2 Toward a more General Hosing Theory for a Narrow Electron Beam

In many problems in physics, the following two statements are often true. One is that a more general theory should be able to easily reproduce a theory for a specific regime. Another is that some parts from a special theory can still be valid in a more general one.

By carefully checking the assumptions of the existing hosing theory, we have the following observations. There are two distinct time scales in these two coupled equations. The beam centroid evolves on the betatron period ω_β^{-1} and the channel centroid is determined on the plasma response period ω_0^{-1} . Since $\omega_0^{-1} \ll \omega_\beta^{-1}$, one can determine the channel centroid by assuming the beam centroid is still fixed. No surprise, this is just the quasi-static approximation. If the change of the channel shape is negligible, which is very reasonable when the oscillation amplitudes of x_c and x_b both are small, the transverse force on the beam centroid is still linearly depending on the relative displacement between the beam centroid and the channel centroid. Therefore, the equation for the beam centroid in existing theory will still be valid even when the channel is non-adabatically formed

or the plasma responses are relativistic.

With this key observation, the search for a new hosing theory is reduced to find out how the channel centroid responds to the beam centroid on a short time scale. This is just what our nonlinear framework of the blowout regime can do!

The first try following this line is to reproduce the old theory, or a little bit better, to get a theory for non-relativistic blowout ($k_p r_b \ll 1$) including both adiabatically and non-adiabatically formed channels. This is the simplest case because in non-relativistic regime the motion equation of the channel is

$$\frac{d^2 r_b}{d\xi^2} + \frac{1}{2} r_b = \frac{\lambda(\xi)}{r_b} \quad (3.18)$$

which is solely determined by the beam parameter $\lambda(\xi)$ due to that the self-generated plasma fields are negligibly small in this case. Indeed, the theory for this case is our first result . It reproduced exactly the old theory in the non-relativistic adiabatic regime, therefore give us the confidence that we are on the right track.

However, for simplicity we will not give the derivation for this case alone. Instead, we will directly perform a derivation for the most general case (relativistic non-adabatic blowout) since the essential steps are very similar in all cases.

We start from the motion equation of the ion channel boundary obtained in chapter 2.

$$2 \frac{d}{d\xi} \left[(1 + \psi) \frac{dr}{d\xi} \right] = -(E_r - V_z B_\theta) \left[1 + \left(\frac{dr}{d\xi} \right)^2 + \frac{1}{(1 + \psi)^2} \right]. \quad (3.19)$$

To calculate the small deviation from a cylindrically symmetric blowout, we can linearly perturb the motion equation for both the upper boundary r_+ and

lower boundary r_- . The center of the channel can be defined as $x_c(\xi) = (r_+(\xi) - r_-(\xi))/2$. $(r_+ + r_-)$ is the diameter of the channel, the change of this quantity is assumed to be a higher order effect and is consequently dropped in our analysis.

When the beam is straight, i.e., there is no perturbation, the solution of the motion equation is $r_0(\xi)$ and the fields and potential are E_0 , B_0 and ψ_0 . The longitudinal velocity and the Lorentz factor are denoted as $V_0(\xi)$ and $\gamma_0(\xi)$ respectively. Here we drop the subscript denoting the direction of the fields and velocity. Next we perturb this solution by a small amount and the perturbation variables are denoted by subscript “1” in the following equations.

$$\begin{aligned} r &= r_0 + r_1, V = V_0 + V_1, \\ E &= E_0 + E_1, B = B_0 + B_1, \end{aligned} \quad (3.20)$$

$$\psi(r_0 + r_1) = \psi_0(r_0). \quad (3.21)$$

Relationship in Eq. (3.21) follows from the assumption that the channel shape does not change and the channel is simply displaced by r_1 . By substituting the above expressions into Eq. (3.19) and ordering the resulting terms, we obtain the 0th order equation which has the same form as Eq. (3.19). It is rewritten into the following form for the Lorentz force. Here we adopt the convention $' \equiv d/d\xi$.

$$-(E_0 - V_0 B_0) = \frac{1 + \psi_0}{\gamma_0} [(1 + \psi_0) r_0'' + \psi_0' r_0']. \quad (3.22)$$

The 1st order equation is,

$$\begin{aligned} &2\psi_0' r_1' + 2(1 + \psi_0) r_1'' + 2(E_0 - V_0 B_0) r_0' r_1' \\ &= -2(E_1 - V_0 B_1 - V_1 B_0) \frac{\gamma_0}{(1 + \psi_0)}. \end{aligned} \quad (3.23)$$

One can further simplify Eq. (3.23) by substituting the 0th order Lorentz

force from Eq. (3.22), then Eq. (3.23) becomes,

$$\begin{aligned} r_1'' + \left\{ \frac{\psi'_0}{1 + \psi_0} - \frac{1}{\gamma_0} [(1 + \psi_0)r_0'' + \psi'_0 r_0'] r_0' \right\} r_1' \\ = -\frac{\gamma_0}{(1 + \psi_0)^2} (E_1 - V_0 B_1 - V_1 B_0). \end{aligned} \quad (3.24)$$

Eq. (3.24) is a second order ODE for r_1 . The coefficients depend on the 0th order quantities and their ξ derivatives which are both determined by the current profile of the drive beam. One can obtain the exact values of all these coefficients in a simulation or approximate them using our simple model in chapter 2 as we will do later. The perturbation $-(E_1 - V_0 B_1 - V_1 B_0)$ is the sum of the perturbation from the beam and the change in the plasma self-force. However, it is difficult to calculate the charge and current profiles of the plasma response and their changes. We express this sum in terms of the perturbation from the beam with a numerical factor $c_l(\xi)$ in Eq. (3.25) (For simplicity, $c_l(\xi)$ is assumed to be independent of the hosing amplitude.),

$$-(E_1 - V_0 B_1 - V_1 B_0) = F_{b1} + F_{e1} = F_{b1} c_l(\xi), \quad (3.25)$$

where $F_{b1} = -(E_{b1} - V_0 B_{b1})$ is the perturbation to the Lorentz force from the beam, and $F_{e1} = F_{b1}(c_l(\xi) - 1)$ is the change in the force from the plasma response. E_{b1} and B_{b1} are the change of the electric and magnetic fields from the beam when the centroid is shifted by x_b ,

$$E_{b1} = B_{b1} = -2\pi n_b \sigma_b^2 \left[\frac{1}{r_0 + r_1 - x_b} - \frac{1}{r_0} \right]. \quad (3.26)$$

Therefore, when $|r_1 - x_b| \ll r_0$,

$$F_{b1} \approx \frac{2\pi n_b \sigma_b^2 (1 - V_0)}{r_0^2} (x_b - r_1). \quad (3.27)$$

Finally, Eq. (3.24) is written as,

$$\begin{aligned} r_1'' + \left\{ \frac{\psi'_0}{1 + \psi_0} - \frac{1}{\gamma_0} [(1 + \psi_0)r_0'' + \psi'_0 r_0'] r_0' \right\} r_1' \\ = c_r c_\psi c_l \omega_0^2 (x_b - r_1), \end{aligned} \quad (3.28)$$

where $\omega_0^2 = 2\pi n_p^2$, $c_\psi(\xi) = 1/(1 + \psi_0)$ and $c_r(\xi) = n_b \sigma_b^2 / (n_p r_0^2)$.

Eq. (3.28) is for the upper trajectory $r_+ = r_0 + r_1$. For the lower trajectory $-r_- = -r_0 - r_2$, r_2 can be solved from a similar equation. So the channel centroid $x_c = (r_+ - r_-)/2 = (r_1 - r_2)/2$ satisfies,

$$\begin{aligned} x_c'' &+ \left\{ \frac{\psi'_0}{1 + \psi_0} - \frac{1}{\gamma_0} [(1 + \psi_0)r_0'' + \psi'_0 r_0'] r_0' \right\} x_c' \\ &= c_r c_\psi c_l \omega_0^2 (x_b - x_c). \end{aligned} \quad (3.29)$$

If we ignore ψ'_0 and r_0' , this result can be cast into a form comparable to the channel centroid equation from the fluid theory.

$$x_c'' + c_r c_\psi c_l \omega_0^2 x_c = c_r c_\psi c_l \omega_0^2 x_b. \quad (3.30)$$

For adiabatically formed channel with small blow-out radius, plasma electrons are pushed to the charge neutralization radius slowly with $V_r \ll 1$ and $V_{z0} \ll 1$. The fields from the plasma sheath is weak, so are the changes in the fields when there is a perturbation. In this case, $c_r \approx c_\psi \approx c_l \approx 1$, therefore we recover the result of whittum. If the beam-plasma interaction becomes more intense, the following effects need to be taken into account: 1) The blow-out radius varies along the blow-out trajectory; 2) The relativistic mass will change the resonant frequency and the plasma electrons may also gain substantial longitudinal velocity so the magnetic field becomes important; 3)The plasma sheath generates strong electric and magnetic fields which tend to reduce the perturbation from the beam. These effects change the coupling coefficients c_r , c_ψ and c_l , therefore changing the hosing growth. The fluid analysis does take into account of effects 1 and 3, however they are included in an inconsistent manner, e.g. the effect of c_r only appears in the RHS of Eq. (3.30) not the LHS. Generally, for a relativistic non-adiabatic ion channel, $c_r c_\psi c_l < 1$, therefore the hosing growth is reduced by the combination of all these effects.

To see how well this simple theory can be in describing the hosing instability, a lot of 3D PIC simulations using QuickPIC have been done by C. Huang. Very good agreements between theory and simulations have been achieved. Here I will not go into the detail of these simulations. Instead I will just show two plots of the comparisons between simulations and theory.

Fig.3.6 show the density plots of the beam and the plasma for these four different regimes. In the simulations for the adiabatic regime, two beams are used to create an equilibrium channel. The first one is short and narrow to blow out a channel. The second beam follows the first beam and its density is chosen to keep the channel radius constant. In Fig.3.7, hosing growth for four different regimes are shown.

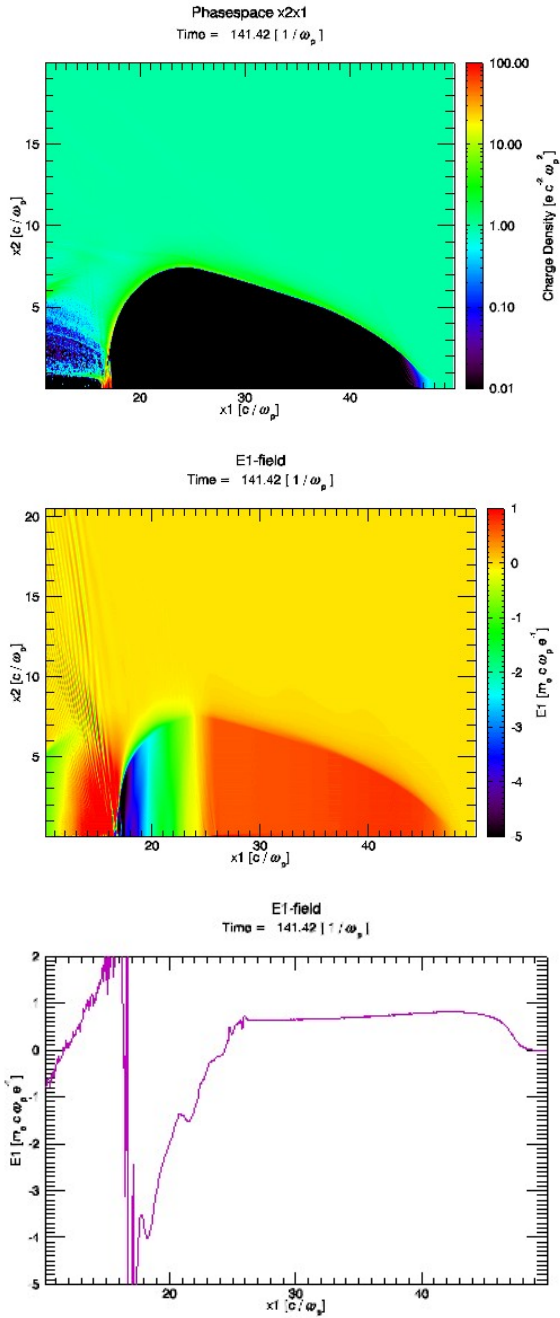


Figure 3.3: Plasma wake driven by an electron beam with a linearly ramped current profile $n_b/n_p = 100$, $k_p a = 0.5$, $L_0 = 22$ (a) plasma phase space x2x1 (b) color plot of E1 (c) lineout of E1

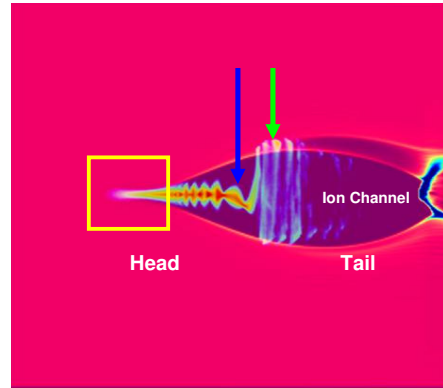


Figure 3.4: A plot of the beam on top of the plot of the ion channel in the nominal “afterburner” simulation.

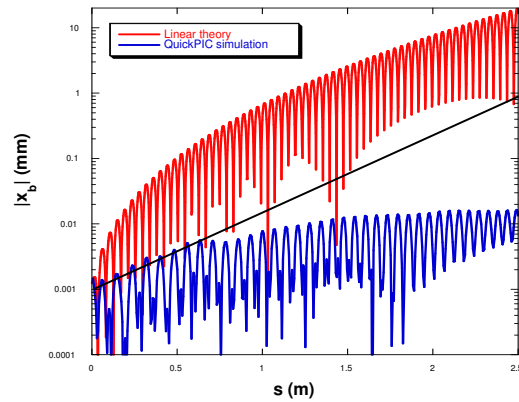


Figure 3.5: The centroid oscillation $|x_b|$ (blue curve) in a self-generated channel and the prediction (red curve) from the fluid theory for an equilibrium channel. The black line is a linear fit for the initial growth in the simulation before the nonlinearity occurs. This initial growth is one order of magnitude smaller than the result for a equilibrium channel.

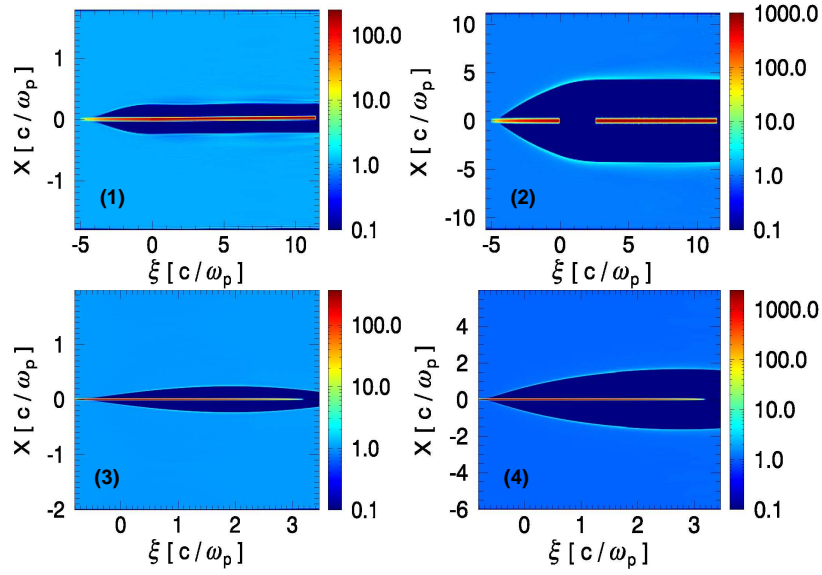


Figure 3.6: Density plots of the beams (red) and plasma (blue) in (a) the adiabatic non-relativistic regime; (b) the adiabatic relativistic regime; (c) the non-adiabatic non-relativistic regime; (d) the non-adiabatic relativistic regime. The beams move to the left in these plots.

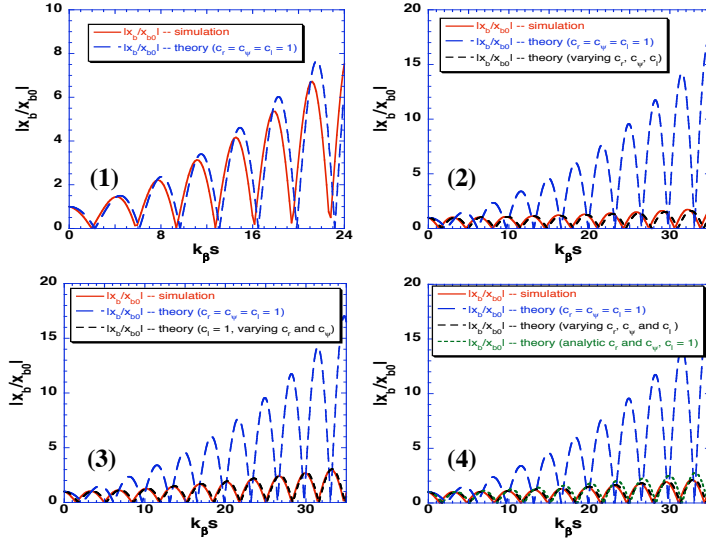


Figure 3.7: Hosing growth in four regimes.

CHAPTER 4

On Wave Breaking and Particle Trapping in Plasma Waves

4.1 Introduction

A fundamental question in plasma physics is what is the maximum possible amplitude of a nonlinear plasma wave? And a related question is what limits the amplitude? The literature is filled with papers that address these questions. In the 1D limit, these questions have essentially been answered for non-relativistic phase velocity / cold plasmas [65, 66], for non-relativistic phase velocity / warm plasmas [67], for relativistic phase velocity / cold plasmas [65] , and for relativistic phase velocity / warm plasmas [68, 69, 70, 71, 72, 73]. For multi-dimensional plasma waves, there has been much recent work[79, 80], however, in our opinion there is no unified understanding yet. With this extensive literature, it might appear that for 1D waves, this topic may be solved. Because this appearance, the 1D theoretical limits are often used as a guide for the multi-dimensional waves. However, there has been recent work that purports to offer new results for 1D relativistic wave in warm plasmas. However, in multi-dimensional waves trajectory crossing, wave steepening, and particle trapping are not equivalent, so there is no clear definition for wave breaking in this case. Furthermore, in 1D or multi-dimensional simulations, field amplitudes near the 1D expressions are mere

obtained for high γ_ϕ . In this chapter will resolve some of these issues.

For any physical problem, it is always attractive to have some kind of unified picture if possible. It is thus interesting to ask the following question: Can we give an unified physical picture on wave breaking for both 1D and multi-dimensional plasma waves with constant phase velocities?

Indeed, before answering this question, one at least needs to know what “wave breaking” exactly means. Unfortunately there is no clear definition. The term is loosely used whenever phenomena like wave incoherence, particle trapping, or particle trajectory crossing occurs.

It seems that it is therefore imperative to “wave breaking” a clear definition. It should be broad enough to include interesting physics but also narrow enough to avoid ambiguity. To obtain such a definition we approach the issue as follows. First, we need to clearly understand how the concept of “wave breaking” originally arose when the 1D limits were derived. Second, we need to clearly understand the similarities and differences between 1D and multi-dimensinal waves. Lastly, we discuss its meaning for driven plasma wave in both 1D and multidimensional cases .

4.1.1 What Does “Wave Breaking ” Mean in One-dimensional Plasma Waves

The concept of “wave breaking” in plasma waves originates from an interesting discovery: A cold non-relativistic plasma can only support a self-sustained traveling wave with constant phase velocity up to a maximum electric field amplitude given by , $E = mv_\phi\omega_p/e$.

This was first shown as a fact of mathematics, e.g., the nonexistence of traveling wave solution of the cold fluid equation for amplitudes beyond a limit. Later

it was shown that the breakdown of fluid equation is directly due to the particle trajectory crossing, i.e., sheet crossing. It is worth noting that in 1D cold fluid model, that particle trapping and complete wave steepening (of the electric field) occur simultaneously with sheet crossing. Based on the analogy of an ocean wave breaking when it steepens, this limit for plasma wave was called the wave breaking limit.

For 1D plasma wave with relativistic phase velocity, i.e., $v_\phi \sim 1$ or $\gamma_\phi \gg 1$, the same reasoning can be directly applied to a cold 1D relativistic fluid model and a new limit can be derived: $\sqrt{2(\gamma_\phi - 1)}mc\omega_p/e$. In fact the relativistic formula was derived first but the physical picture of sheet crossing, particle trapping, and wave breaking came later. The wave breaking limit for 1D planar self-sustained cold plasma oscillations is well defined. However, possible confusion comes into play if a warm plasma is considered or a driver is used to excite such a large amplitude wave. First, let's look at how wave breaking limits for warm plasmas were derived in literature.

To get these limits, one still uses a fluid description of plasma and follows the logic for deriving cold limits. The fluid equations are closed by choosing a proper equation of state, i.e., one finds an expression for pressure which is a function of the plasma density. As we know, for a fluid model to be valid for describing plasma waves, one requirement is that the main body of the velocity (momentum) distribution function is far below the phase velocity of the wave. If this is not so, the details of velocity distribution become important and the fluid model is not adequate for describing the plasma. For such cases, a nonlinear kinetic model (e.g., BGK modes) must be used. Indeed, it is well known that one can construct a BGK mode with arbitrarily large amplitudes by choosing a self-consistent distribution function. So the concept of wave breaking, which

originated from waves in a cold plasma, can not be properly defined if the main body of the velocity distribution function does not start well below the phase velocity of the wave, i.e., $v_{th} \ll v_\phi$.

For a plasma with velocity distribution below the phase velocity of a periodic traveling wave, a reasonable description on how wave breaking occurs may be as follows. First, assume a small amplitude wave with a given phase velocity has been excited everywhere. For a sufficiently small amplitude, all the particles in the plasma travel through the wave without getting trapped. For such periodic traveling waves, the total energy in the fields and the kinetic energy of the plasma are constant. If the wave amplitude is slowly increased everywhere then this remains true until the wave amplitude is larger than some critical value. When the wave gets sufficiently large a significant number of the plasma particles start to get trapped in the wave. When enough particles get trapped they damp or beam load the wave so that a traveling wave structure can not necessarily be sustained.

The waterbag model can describe the above picture accurately. Historically, the wave breaking limit for both non-relativistic and relativistic phase velocities in a warm plasma were all first derived using a waterbag model. The waterbag models allow one to rigorously close the fluid equation and still have some physical intuition regarding when the fluid description breaks down. The fluid equations are then used to derive an equation for a wave potential assuming periodic wave-like solutions. For large enough amplitudes, the fluid model breaks down. This can be seen by divergences of $\partial\pi/\partial v$ or by when a particle at the upper boundary of the waterbag velocity distribution gets trapped. While these two conditions look different, it can be shown that they give identical results.

It is worth noting that a warm fluid model can break down before any particle

gets trapped if an ill-behaved equation of state is chosen. Different equations of state used in literature are the major source for the disagreements and confusions on the warm wave breaking limits. For example, there are different results in the literature on the wavebreaking limit for relativistic warm plasma in the regime $\gamma_\phi^2 \beta \gg 1$, where β is the plasma temperature. The waterbag model predicts that the wavebreaking limit goes to infinity if the phase velocity of the wave goes to the speed of light. However, some authors got finite results by using different equations of state derived from certain warm plasma models. The reason for this is that the assumptions of these models for the above mentioned regime are not valid, leading to incorrect equations of state.

4.1.2 What Does “Wave Breaking ” Mean in Multi-dimensional Plasma Waves

The structure of multidimensional plasma waves can be very different than those in 1D. As discussed in chapter 2, generally it is not possible to get periodic traveling wave solutions over full space with a 3D structure. This is mainly due to the reason that particles tend to have different oscillation frequency depending on their positions and their trajectories will cross each other over time, leading to the damping of the wave amplitude due to phase mixing. However, it is possible to excite multi-dimensional wakes which are not periodic through a driver that moves through the plasma. The phase velocity of the wake is equal to the velocity of the driver. So for multidimensional waves, we directly face the existence of a driver. In front of the driver, the plasma is not disturbed yet, and behind the driver, a plasma wave with 3D structure is excited. Far behind the driver, the wave amplitude decreases due to the effect of trajectory mixing. Of course, a fluid model can not be used when trajectory mixing occurs.

We will show shortly that even in 1D there are some profound differences between the periodic traveling wave solutions to the fluid equations and the wakes excited by a driver.

How can we define “wave breaking” for these multidimensional driven plasma waves? If we define it as the occurrence of trajectory crossing and the subsequent breakdown of the fluid model, (which is what we used in chapter 2 following Dawson’s work), then we will conclude that plasma wakes in 2D or 3D always break, even for very small amplitudes. In order to make closer connection to the 1D wave breaking limit, another possible definition for wave breaking of multidimensional wakes is the occurrence of particle trapping. For driven plasma waves, a non-evolving wake in the driver’s frame is still possible until particle trapping occurs. Continuous particle trapping will also reduce the wake amplitude behind the driver. For these reasons we prefer to view wavebreaking and particle trapping as equivalent.

4.1.3 “Periodic ” vs. “Driven” Waves

We will show that even if particle trapping is used as the definition for wave breaking of multi-dimensional driven wake, there is no a unique wave breaking amplitude for driven wakes. This is because different drivers can produce different wake structures, which will affect how particles get trapped in the first bucket. Indeed this is also true for 1D driven waves. This fact has not been recognized until now. This is most likely due to the existence of periodic traveling wave solutions in 1D. It appears that researchers believed that waves with amplitudes up to the 1D wave breaking limits (derived by assuming no driver) can be excited when a driver is used.

In fact, this is not true. For example, in last subsection we discussed the

finiteness of wave breaking limit of a warm plasma in the limit that $\gamma_\phi^2 \beta \gg 1$. As γ_ϕ tends to infinity, the wave breaking limit also tends to infinity. However, amplitudes near $2\sqrt{\gamma_\phi - 1}$ for large γ_ϕ have never been observed in simulations of wakefields. In published results from Vlasov simulations in which a non-evolving electron beam driver was used to excite the plasma wave, it was found that changing the γ of the driver does not increase the wake amplitude at which the wave starts to break, i.e., trap electrons. They believed that this finite result was due to the thermal effects. To our knowledge the observation of trapping at wake amplitudes substantially below the accepted wave breaking amplitudes has been observed by many others using PIC simulations. This was sometimes believed to be due to resolution issues.

It turns out that the finite limit of the wave amplitude in these simulations is not the result of a warm plasma or resolution. Instead it is due to the fact that particle trapping can occur at much lower wake amplitudes when a driver is used to excite the wave. In all the calculations on 1D wave breaking limit, the plasma waves were assumed to be periodic oscillations over full space. Later we will show how this finite limit is the result of a driver by showing simulation results for a cold plasma. It is kind of interesting that despite over 50 years of research no one has recognized that the periodic traveling wave solutions can not be excited by a driver. Therefore, it is difficult to see how they could be excited in a laboratory.

As we can see from above discussions, particle trapping is important to understand wave breaking. In 1D, it occurs when the fluid models break down. In 2D and 3D, the break down of fluid models is only a necessary condition for trapping. When a wake is excited by a driver, the trapping condition is very different. Therefore, it will be very useful to provide a general analysis for trapping that is valid in arbitrary traveling wave fields. This is the topic of next section.

4.2 General Formalism for Particle Motion in Fields with Translational Symmetry

Within the framework of classical physics (electromagnetic field theory and special relativity), the motion of a charged particle in a general electromagnetic field is described by the Lorentz force equation:

$$\frac{d\bar{\mathbf{p}}}{d\bar{t}} = \bar{q}(\bar{\mathbf{E}} + \bar{\mathbf{v}} \times \bar{\mathbf{B}}) \quad (4.1)$$

Here normalized units are used for convenience. Time is normalized to ω_0^{-1} (arbitrary frequency), length is normalized to $c\omega_0^{-1}$, momentum is normalized to mc (m, particle rest mass), energy is normalized to mc^2 , velocity is normalized to the speed of light c , charge is normalized to e (electron charge), electromagnetic fields are normalized to $mc\omega_0/e$ and potentials are normalized to mc^2/e .

In the Hamiltonian formalism, the canonical momentum $\bar{\mathbf{P}}$ is defined as

$$\bar{\mathbf{P}} = \bar{\mathbf{p}} + \bar{q}\bar{\mathbf{A}} \quad (4.2)$$

and the Hamiltonian H then is defined as:

$$\bar{H} = \sqrt{1 + |\bar{\mathbf{P}} - \bar{q}\bar{\mathbf{A}}|^2} + \bar{q}\bar{\phi} \quad (4.3)$$

The equation of the motion are then

$$\begin{aligned} \frac{d\bar{\mathbf{r}}}{d\bar{t}} &= \frac{\partial \bar{H}}{\partial \bar{\mathbf{P}}} \\ \frac{d\bar{\mathbf{P}}}{d\bar{t}} &= -\frac{\partial \bar{H}}{\partial \bar{\mathbf{r}}} \end{aligned} \quad (4.4)$$

If we write them out explicitly, they become,

$$\begin{aligned}\frac{d\bar{\mathbf{r}}}{d\bar{t}} &= \bar{\mathbf{v}} \\ \frac{d(\bar{\mathbf{p}} + \bar{q}\bar{\mathbf{A}})}{d\bar{t}} &= \bar{q}(\nabla\bar{\mathbf{A}} \cdot \bar{\mathbf{v}} - \nabla\bar{\phi})\end{aligned}\quad (4.5)$$

The fields can be written in terms of the potentials as

$$\begin{aligned}\bar{\mathbf{E}} &= -\nabla\bar{\phi} - \frac{\partial\bar{\mathbf{A}}}{\partial\bar{t}} \\ \bar{\mathbf{B}} &= \nabla \times \bar{\mathbf{A}}\end{aligned}\quad (4.6)$$

and the total change in time of the vector potential $\frac{d\bar{\mathbf{A}}}{d\bar{t}}$, can be rewritten as $(\frac{\partial}{dt} + \bar{\mathbf{v}} \cdot \nabla)\bar{\mathbf{A}}$. By using the following vector identity

$$\bar{\mathbf{v}} \times \nabla \times \bar{\mathbf{A}} = \nabla\bar{\mathbf{A}} \cdot \bar{\mathbf{v}} - \bar{\mathbf{v}} \cdot \nabla\bar{\mathbf{A}} \quad (4.7)$$

the original equation of motion is reproduced readily.

If we are interested in the change of some quantity $\bar{Q}(\bar{\mathbf{P}}, \bar{\mathbf{r}}, t)$, we can write the change in time of \bar{Q} as:

$$\frac{d\bar{Q}}{dt} = \left\{ \frac{\partial\bar{H}}{\partial\bar{\mathbf{P}}} \cdot \frac{\partial\bar{Q}}{\partial\bar{\mathbf{r}}} - \frac{\partial\bar{Q}}{\partial\bar{\mathbf{P}}} \cdot \frac{\partial\bar{H}}{\partial\bar{\mathbf{r}}} \right\} + \frac{\partial\bar{Q}}{\partial\bar{t}} \quad (4.8)$$

For example, when we replace \bar{H} for \bar{Q} , we will get $\frac{d\bar{H}}{dt} = \frac{\partial\bar{H}}{\partial\bar{t}}$, or when written explicitly,

$$\frac{d\bar{H}}{dt} = \bar{q}\left(\frac{\partial\bar{\phi}}{\partial\bar{t}} - \bar{\mathbf{v}} \cdot \frac{\partial\bar{\mathbf{A}}}{\partial\bar{t}}\right) \quad (4.9)$$

One obvious conclusion is that if the electromagnetic fields are static (they do not explicitly depend on time), the total energy, \bar{H} , is conserved. But a static field in one frame is not a static field in a moving frame (Lorentz transform); as a consequence, in the moving frame, \bar{H} is not conserved. For electromagnetic fields in a wake which moves with a constant velocity (depending on time and space only by the combination of $x - v_\phi t$, e.g., $\bar{\mathbf{E}}(\bar{\mathbf{r}}_\perp, x - v_\phi t)$), we can make a Lorentz transformation to the moving frame, in which the fields are static. A natural question is what is the conserved quantity in the lab frame?

The answer is $\bar{H} - \bar{v}_\phi \bar{P}_x$. Let's look at how can we show this.

If a field, e.g, ϕ , has the form $\phi(\bar{\mathbf{r}}_\perp, x - v_\phi t)$, then it satisfies the equation:

$$\left(\frac{\partial}{\partial \bar{t}} + v_\phi \frac{\partial}{\partial \bar{x}} \right) \phi = 0 \quad (4.10)$$

For fields with the above form, i.e., wake fields, we have

$$\frac{d\bar{H}}{d\bar{t}} = -\bar{q}v_\phi \left(\frac{\partial \bar{\phi}}{\partial \bar{x}} - \bar{\mathbf{v}} \cdot \frac{\partial \bar{\mathbf{A}}}{\partial \bar{x}} \right) \quad (4.11)$$

It can then readily be shown that

$$\frac{d\bar{H} - \bar{v}_\phi \bar{P}_x}{d\bar{t}} = 0 \quad (4.12)$$

which can be rewritten explicitly as:

$$\gamma - v_\phi p_x + q(\phi - v_\phi A_x) = Const \quad (4.13)$$

For convenience, we define $\psi \equiv -q(\phi - v_\phi A_x)$. If the initial condition for a particle is known, e.g., $\lambda \equiv \gamma_0 - v_\phi p_{x0}$ and ψ_0 are known, eq.(4.13) becomes

$$\gamma - v_\phi p_x = \lambda + \delta\psi \quad (4.14)$$

where $\delta\psi \equiv \psi - \psi_0$. It is obvious to see that $\lambda + \delta\psi > 0$. By using this algebraic equation, we can express γ , p_x and v_x in terms of $\delta\psi$ and \mathbf{p}_\perp .

Moving $v_\phi p_x$ in eq.(4.14) to the right side and squaring both sides, we get an equation for p_x (we used $\gamma^2 = 1 + p_\perp^2 + p_x^2$):

$$[1 - v_\phi^2]p_x^2 - 2v_\phi[\lambda + \delta\psi]p_x + [1 + p_\perp^2 - (\lambda + \delta\psi)^2] = 0 \quad (4.15)$$

This is a second order algebra equation (i.e., $ax^2 + bx + c = 0$). To see if this equation has real roots, we check the sign of $\Delta \equiv [b^2 - 4ac]/4$:

$$\begin{aligned} \Delta &= (\lambda + \delta\psi)^2 - (1 - v_\phi^2)(1 + p_\perp^2) \\ &= \gamma^2(1 - v_\phi v_x)^2 - (1 - v_\phi^2)(\gamma^2 - \gamma^2 v_x^2) \\ &= \gamma^2(v_x - v_\phi)^2 \geq 0 \end{aligned} \quad (4.16)$$

This implies that eq.(4.15) has two real roots. They can be solved directly as:

$$\begin{aligned} p_x &= \frac{v_\phi(\lambda + \delta\psi) \pm \sqrt{\Delta}}{1 - v_\phi^2} \\ &= \frac{1 + p_\perp^2 - (\lambda + \delta\psi)^2}{v_\phi(\lambda + \delta\psi) \mp \sqrt{\Delta}} \\ &= \frac{1 + p_\perp^2 - (\lambda + \delta\psi)^2}{v_\phi(\lambda + \delta\psi) \mp \sqrt{(\lambda + \delta\psi)^2 - (1 - v_\phi^2)(1 + p_\perp^2)}} \end{aligned} \quad (4.17)$$

We can also solve for γ and v_x ,

$$\begin{aligned}
\gamma &= (\lambda + \delta\psi) + v_\phi p_x & (4.18) \\
&= \frac{v_\phi(1 + p_\perp^2) \mp (\lambda + \delta\psi)\sqrt{\Delta}}{v_\phi(\lambda + \delta\psi) \mp \sqrt{\Delta}} \\
&= \frac{v_\phi(1 + p_\perp^2) \mp (\lambda + \delta\psi)\sqrt{(\lambda + \delta\psi)^2 - (1 - v_\phi^2)(1 + p_\perp^2)}}{v_\phi(\lambda + \delta\psi) \mp \sqrt{(\lambda + \delta\psi)^2 - (1 - v_\phi^2)(1 + p_\perp^2)}}
\end{aligned}$$

$$\begin{aligned}
v_x &= \frac{p_x}{\gamma} & (4.19) \\
&= \frac{1 + p_\perp^2 - (\lambda + \delta\psi)^2}{v_\phi(1 + p_\perp^2) \mp (\lambda + \delta\psi)\sqrt{\Delta}} \\
&= \frac{1 + p_\perp^2 - (\lambda + \delta\psi)^2}{v_\phi(1 + p_\perp^2) \mp (\lambda + \delta\psi)\sqrt{(\lambda + \delta\psi)^2 - (1 - v_\phi^2)(1 + p_\perp^2)}}
\end{aligned}$$

To see the meaning of the two branches, we check $v_x - v_\phi$:

$$\begin{aligned}
v_x - v_\phi &= \frac{-\Delta \pm v_\phi(\lambda + \delta\psi)\sqrt{\Delta}}{v_\phi(1 + p_\perp^2) \mp (\lambda + \delta\psi)\sqrt{\Delta}} & (4.20) \\
&= \frac{-\gamma^2(v_x - v_\phi)^2 \pm \gamma^2 v_\phi(1 - v_x v_\phi)|v_x - v_\phi|}{v_\phi(\gamma^2 - \gamma^2 v_x^2) \mp \gamma^2(1 - v_x v_\phi)|v_x - v_\phi|} \\
&= |v_x - v_\phi| \left\{ \frac{-|v_x - v_\phi| \pm v_\phi(1 - v_x v_\phi)}{v_\phi(1 - v_x^2) \mp (1 - v_x v_\phi)|v_x - v_\phi|} \right\} \\
&= |v_x - v_\phi| \cdot T
\end{aligned}$$

This equation implies that T must be ± 1 and its sign depends on the sign of $v_x - v_\phi$. It is now possible to see the difference of the two branches. If we choose $-/+$ ($-$ sign in numerator and $+$ sign in the denominator), then $T < 0$ can be seen immediately. This means that $T = -1$ and $v_x < v_\phi$. (note: if $v_\phi = 1$, we only have this branch). It can also be easily verified that if $v_x < v_\phi$, $T = -1$.

For the other branch (+/−), we have $T = 1$ so that $v_x > v_\phi$. The fact that $T = 1$ can be directly checked by assuming $v_x > v_\phi$. If instead we assume $v_x < v_\phi$ (so $T = -1$), the T calculated from the equation is $\frac{1-v_\phi^2}{(1-v_x^2)+(v_\phi-v_x)^2} > 0$, which contradicts the assumption.

The above discussion indicates that if \mathbf{p}_\perp and $\delta\psi$ are known, one can directly get expressions for γ , p_x and v_x as functions of \mathbf{p}_\perp , λ , and $\delta\psi$. If $v_x > v_\phi$, the +/− branch should be used, otherwise the −/+ branch should be used. For $v_x = v_\phi$, both branches give the same result.

4.2.1 The General Trapping Condition

In order for a particle to get trapped it starts with a $v_x < v_\phi$ and it then has a $v_x > v_\phi$. The occurrence of trapping arises when $v_x = v_\phi$. So let us see what the above expressions give when $v_x = v_\phi$. Notice that $\Delta = 0$ with this equation occurs and we can get the following relationships:

$$p_x = \frac{1 + p_\perp^2 - (\lambda + \delta\psi)^2}{v_\phi(\lambda + \delta\psi)} \quad (4.21)$$

$$\gamma = \frac{1 + p_\perp^2}{\lambda + \delta\psi} \quad (4.22)$$

Eq.(4.22) can therefore be viewed as the condition for trapping to happen. We can rewrite it as:

$$\begin{aligned}
\lambda + \delta\psi &= \frac{1 + p_\perp^2}{\gamma} \\
&= \frac{\gamma^2 - \gamma^2 v_\phi^2}{\gamma} \\
&= \frac{\gamma}{\gamma_\phi^2} \\
&= \left\{ \frac{\gamma}{\gamma_\phi} \right\} \frac{1}{\gamma_\phi}
\end{aligned} \tag{4.23}$$

Here $\gamma/\gamma_\phi = \sqrt{\frac{1-v_\phi^2}{1-v_\phi^2-v_\perp^2}}$. For 1D motion, $v_\perp = 0$ so $\gamma = \gamma_\phi$ when $v_x = v_\phi$, and we recover the well known 1D condition for trapping. Consider 2D or 3D motion and $\gamma_\phi \gg 1$, then if γ/γ_ϕ is bounded and the bound is much smaller than γ_ϕ , we can see that for 2D or 3D motion the trapping condition is close to the 1D result. If γ/γ_ϕ is not bounded (e.g., the surfatron), this condition can be very different to the 1D result.

4.2.2 The General Particle Energy Bounds

We can rewrite the particle energy γ (eq.4.2) as the following:

$$\begin{aligned}
\gamma &= \frac{v_\phi(1 + p_\perp^2) \mp (\lambda + \delta\psi)\sqrt{\Delta}}{v_\phi(\lambda + \delta\psi) \mp \sqrt{\Delta}} \\
&= \lambda + \delta\psi + \frac{v_\phi[1 + p_\perp^2 - (\lambda + \delta\psi)^2]}{v_\phi(\lambda + \delta\psi) \mp \sqrt{\Delta}} \\
&= \lambda + \delta\psi + \gamma_\phi^2 v_\phi [v_\phi(\lambda + \delta\psi) \pm \sqrt{\Delta}] \\
&= \lambda + \delta\psi + \gamma_\phi^2 v_\phi [v_\phi(\lambda + \delta\psi) \pm \sqrt{(\lambda + \delta\psi)^2 - (1 - v_\phi^2)(1 + p_\perp^2)}]
\end{aligned} \tag{4.24}$$

where $\gamma_\phi = 1/\sqrt{1 - v_\phi^2}$. For $v_x < v_\phi$, “-” is chosen and for $v_x > v_\phi$, “+” is chosen.

We can now check the particle energy for the two different branches. For $v_x < v_\phi$, we have

$$\begin{aligned}
\gamma &= \lambda + \delta\psi + \gamma_\phi^2 v_\phi [v_\phi(\lambda + \delta\psi) - \sqrt{(\lambda + \delta\psi)^2 - (1 - v_\phi^2)(1 + p_\perp^2)}] \\
&= \lambda + \delta\psi + \gamma_\phi^2 v_\phi [v_\phi(\lambda + \delta\psi) - (\lambda + \delta\psi) \sqrt{1 - \frac{(1 + p_\perp^2)}{\gamma_\phi^2(\lambda + \delta\psi)^2}}] \\
&= \frac{\lambda + \delta\psi}{1 + v_\phi} + \frac{v_\phi(1 + p_\perp^2)}{2(\lambda + \delta\psi)} + O\left(\frac{v_\phi(1 + p_\perp^2)^2}{8\gamma_\phi^2(\lambda + \delta\psi)^3}\right)
\end{aligned} \tag{4.25}$$

In the limit $\gamma_\phi \gg 1$, we have $v_\phi \approx 1$ and the first two terms in the expansion reduce to the familiar form used in chapter 2:

$$\gamma = \frac{1 + p_\perp^2 + (\lambda + \delta\psi)^2}{2(\lambda + \delta\psi)} \tag{4.26}$$

As long as $|p_\perp| < \frac{\gamma_\phi(\lambda + \delta\psi)}{\sqrt{2}}$ is satisfied, the above expression is very accurate (it gives a value slight larger than the exact value, with an error less than 5%).

For $v_x > v_\phi$, we have

$$\begin{aligned}
\gamma &= \lambda + \delta\psi + \gamma_\phi^2 v_\phi [v_\phi(\lambda + \delta\psi) + \sqrt{(\lambda + \delta\psi)^2 - (1 - v_\phi^2)(1 + p_\perp^2)}] \\
&= \lambda + \delta\psi + \gamma_\phi^2 v_\phi [v_\phi(\lambda + \delta\psi) + (\lambda + \delta\psi) \sqrt{1 - \frac{(1 + p_\perp^2)}{\gamma_\phi^2(\lambda + \delta\psi)^2}}] \\
&= \gamma_\phi^2 v_\phi (\lambda + \delta\psi) [v_\phi + \sqrt{1 - \frac{(1 + p_\perp^2)}{\gamma_\phi^2(\lambda + \delta\psi)^2}}]
\end{aligned} \tag{4.27}$$

This formula clearly shows the upper and low bounds for γ for $v_x > v_\phi$

$$\gamma_\phi^2 v_\phi^2 (\lambda + \delta\phi) < \gamma < \gamma_\phi^2 v_\phi (v_\phi + 1) (\lambda + \delta\psi) \tag{4.28}$$

because the term in the square root is between 0 and 1.

We can check the validity of this expression for some well known special cases. For example, for the 1D linear wakefield case ($\gamma_\phi \gg 1$, $E_x = E_0 \sin(v_\phi t - x) \theta(v_\phi t - x)$ and $E_0 \ll 1$). In this case, $\psi = [E_0 - E_0 \cos(v_\phi t - x)] \theta(v_\phi t - x)$. Supposing a particle is injected with $v_x = v_\phi$ at the tail of the accelerating field ($v_\phi t - x = 2\pi$) where $\psi = 0$, this particle will be accelerated along x direction until it runs into decelerating region ($v_\phi t - x = \pi$ where $\psi = 2E_0$). At this time, the upper bound will be achieved since $p_\perp \ll 1$ so we get $\gamma = \gamma_\phi^2 v_\phi (v_\phi + 1)(\lambda + \delta\phi) \approx 2\gamma_\phi^2 (\frac{1}{\gamma_\phi} + 2E_0)$. If $\gamma_\phi E_0 \gg 1$, it reduces to the well known 1D result $\gamma \approx 4\gamma_\phi^2 E_0$.

One interesting use of this formula is for getting the particle energy when an intense laser pulse ($a_0 \gg 1$) interacts with a very underdense plasma ($\omega_p/\omega_0 \ll 1$). In next chapter, we will use it to show that when $a_0 \lesssim \omega_0/\omega_p$, the energy gain of the particles scales as a_0^2 which leads to a constant etching back velocity of the laser front.

One simple conclusion one can draw from the about energy bound is that the energy gain is bounded if the potential ψ is bounded. In the case of plasma wake field driven by a laser pulse or a charged particle beam in a non-magnetized plasma, the driver only has a finite spot size and so does the wake field. Far away from the driver (in the transverse dimensions), ψ is zero so ψ is bounded.

In some very special cases, unlimited acceleration is possible. For example, in the Surfatron concept there is a uniform magnetic field aligned in a transverse dimension. The vector potential associated with such a field (A_x) is not bounded in the y direction so ψ is not bounded.

4.3 Wave Breaking of Driven Plasma Waves

In previous subsections, we defined wave breaking condition for plasma wave wakes driven by a non-evolving driver as when a plasma electron initially at rest (before the driver) gets trapped at the back of the first wavelength. We also provided a general particle trapping condition in arbitrary traveling waves. Based on these definitions and conditions, we can now discuss wave breaking for driven plasma waves in both 1D and 3D.

For a relativistic driven plasma wake ($\gamma_\phi \gg 1$) in a cold plasma, the electrons initially have $\lambda_0 = 0$ and $\psi_0 = 0$ before the driver. An exception is when electrons are born inside the wake due to ionization. Electrons born this way can be more easily trapped. The trapping condition for electrons beginning in front of the driver is therefore

$$1 + \psi = \left\{ \frac{\gamma}{\gamma_\phi} \right\} \frac{1}{\gamma_\phi} \quad (4.29)$$

or $1 + \psi_{min} < \gamma/\gamma_\phi^2$.

In the 1D limit, this reduces to

$$1 + \psi = \frac{1}{\gamma_\phi} \quad (4.30)$$

We can see that the trapping condition in 1D only depends on ψ and γ_ϕ . In both 1D and 3D, when ψ approaching -1 , particles can get large forward momenta and keep in phase with the accelerating field until they get trapped. For $\gamma_\phi \gg 1$, the potential ψ is determined by the accelerating field E_{\parallel} .

$$E_{\parallel} = \frac{\partial \psi}{\partial \xi} \quad (4.31)$$

or

$$\psi(\xi) = \int_{-\infty}^{\xi} E_{\parallel}(\xi') d\xi' \quad (4.32)$$

Since the the wake's structure (E_{\parallel}) within the first wavelength just behind the driver generally depends on the profile and intensity of the driver, the wake's amplitude at wave breaking also depends on the driver (although the value of ψ is the same). If one fixes the profile of the driver and increases the intensity of the driver (beam charge for beam driver, laser intensity for laser driver) from very small to very large, the wake behind the driver will change from weakly nonlinear sinusoidal structure to highly nonlinear triangle like structure. At a certain intensity (wake amplitude), particle trapping occurs. The wake amplitude at this point can be defined as the wave breaking amplitude for this specific driver profile. As we will show the critical amplitude derived from this point of view is profoundly different than the well accepted 1D cold wave breaking limits derived for infinitely long wave trains.

A better way to make this point clear is to show some PIC simulation results for plasma wakes driven by ultra-relativistic electron beam drivers. In these simulations, $\gamma_{\phi} \sim \gamma_b = 60000$. The cold wave breaking limit, $E = 2\sqrt{2\gamma_{\phi} - 1}$, for this γ_{ϕ} is about $346mc\omega_p/e$. In fig.4.3, a weakly nonlinear wakefield driven by a 1D electron beam driver is shown. We can see the coherent wave structure far behind the driver and see that there are no trapped particles in phase space. In fig.4.3, the very nonlinear wakefield is driven by a 1D beam with much more charge. From the phase space plot and the lineout of the wakefield, one can see large number of particles get trapped near the tail of the field spike causing the wave to lose coherence immediately behind the first peak. The plot of potential ψ clearly show that $\psi \approx -1$ near the spike. The maximum amplitude of the

wakefield in this case is less than $15mc\omega_p/e$, which is more than 20 times smaller than the theoretical limit. This significant difference between waves with and without a driver is due to the fact that a driver changes the symmetry between decelerating field and accelerating field so that ψ can reach -1 at much lower wave amplitude.

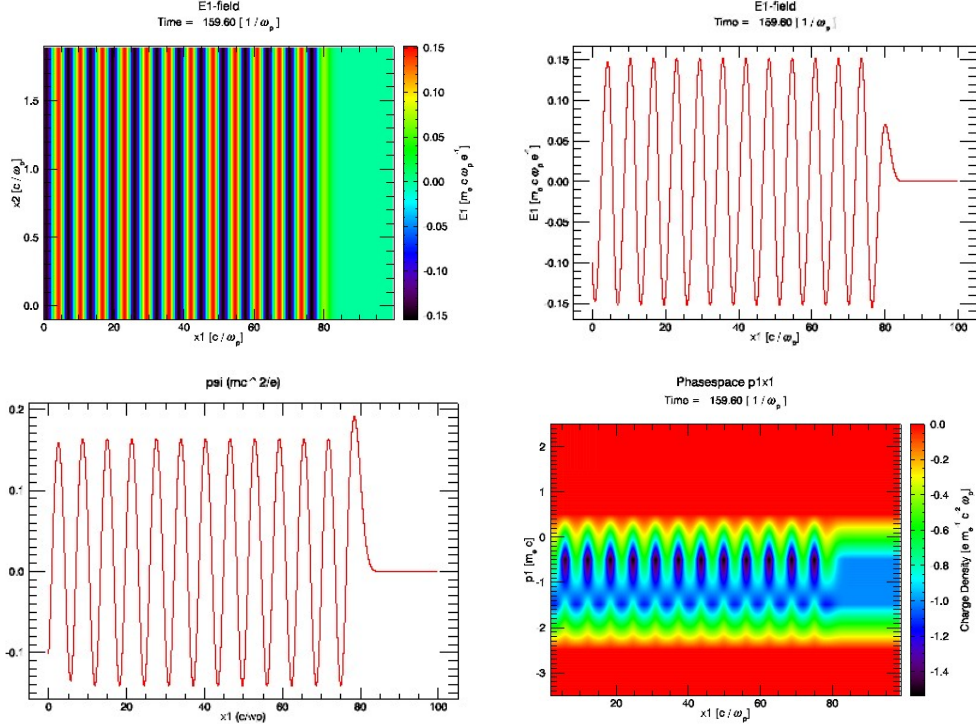


Figure 4.1: A weakly nonlinear coherent wake field driven by an 1D electron driver: $n_b/n_p = 0.1$, $k_p\sigma_z = 1.5$ (a) color plot of E1 (b) lineout of E1 (c) lineout of ψ (d) phase space p1x1

Not surprisingly, similar physics occurs in wakes excited in the blowout regime (3D). Fig.4.3 shows a very nonlinear wake driven by a 3D electron beam driver in the blowout regime. We can see large amounts of trapped particles and a broken wave behind the first bucket. We can also see that ψ approaches -1 near the tail of the ion channel.

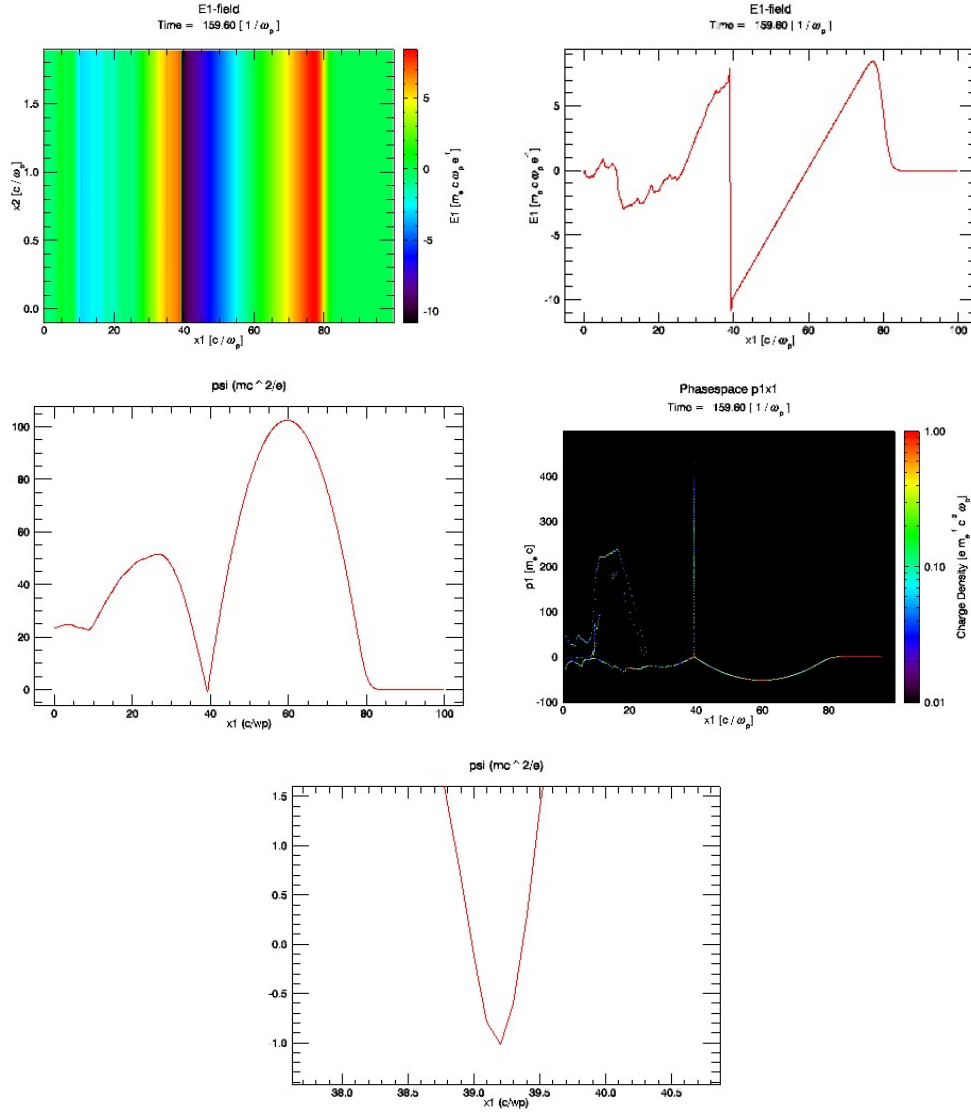


Figure 4.2: A strongly nonlinear wake field driven by an 1D electron driver: $n_b/n_p = 0.1$, $k_p\sigma_z = 1.5$ (a) color plot of E1 (b) lineout of E1 (c) lineout of ψ (d) phase space p1x1 (e) ψ near -1

An interesting difference between the nonlinear 1D and 3D wakefields is that for 1D wakes the slope of the wake is constant until very close to the spike, while for 3D wakes slope rapidly increases at a finite distance in front of the spike. This

difference make the particle trapping easier in 3D than in 1D because it cause ψ to increase.

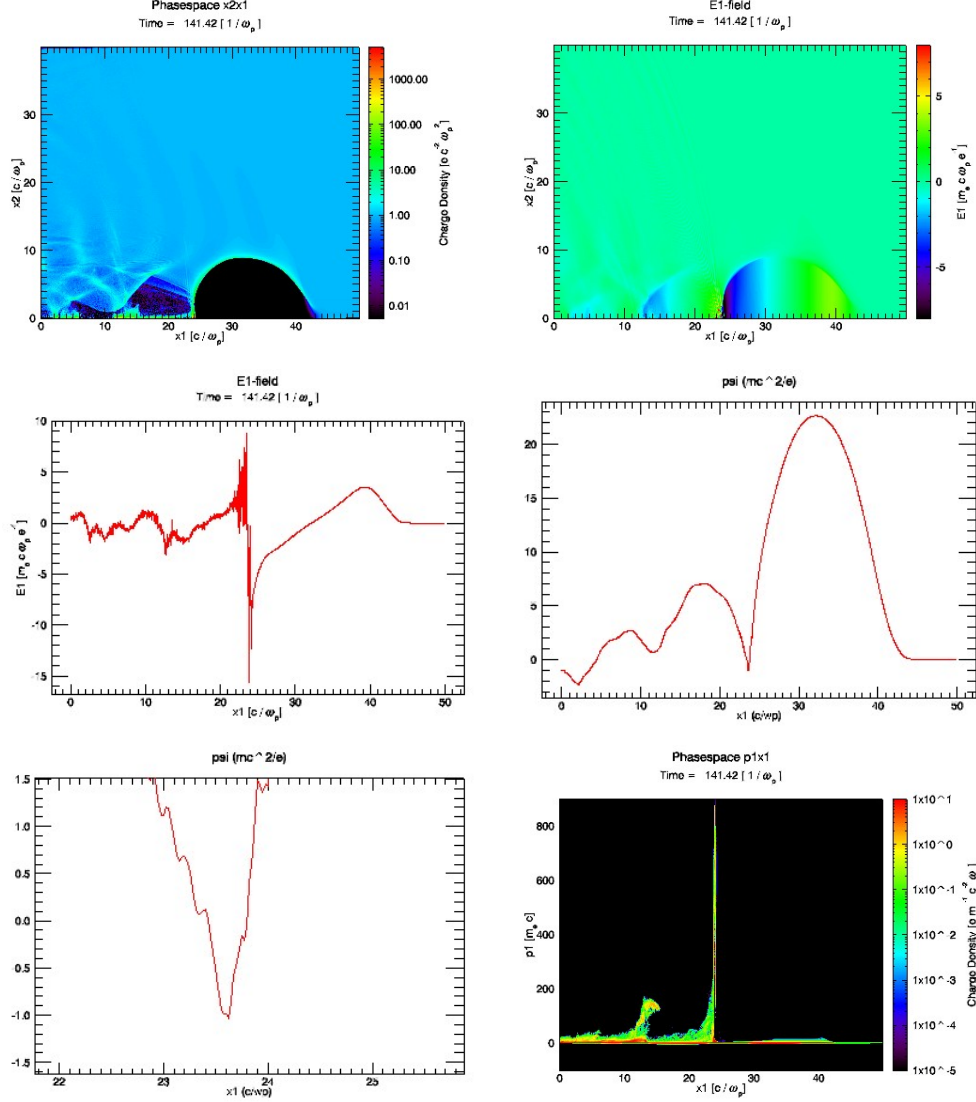


Figure 4.3: A strongly nonlinear wake field driven by an 3D electron driver: $n_b/n_p = 100$, $k_p\sigma_z = \sqrt{2}$, $k_p\sigma_r = 0.5$ (a) color plot of phase space x2x1 (b) color plot of E1(c) lineout of E1 (d) lineout of ψ (e) ψ near -1 (f) phase space p1x1

From the above analysis and simulations, we can see clearly that the theoretical wavebreaking limit for 1D periodic (infinitely long) plasma oscillations is of

little use for wakefields driven by a typical driver. For a periodic 1D oscillation, the symmetry of the field structure (only the part within the very high density spike is asymmetrical), makes the field amplitude necessary for reaching trapping ($\Delta\psi \approx -1$) strongly dependent on γ_ϕ such that very high field amplitudes , $E = \sqrt{2(\gamma_\phi - 1)}mc\omega_p/e$ are needed for trapping to occur. On the other hand for the driven waves, the symmetry between accelerating and decelerating field is broken by the driver. For typical drivers, wave amplitudes only a few times larger than the non-relativistic wavebreaking limit, $mc\omega_p/e$, are needed in order for ψ to be very close to -1 near the tail of the first wavelength. Therefore, large amounts of particles can keep in phase with the wave spike and keep gaining energy from the wave, leading to a heavily damped wake behind the first bucket.

CHAPTER 5

LWFA Scaling in the Blowout Regime

5.1 Introduction

In plasma based acceleration a short laser pulse or ultra-relativistic particle beam creates a plasma wave wakefield with a phase velocity close to the speed of light, c. [27, 35]. The acceleration gradients in these wakefields can easily approach 50 GeV/m which is three orders of magnitude larger than that achieved in conventional RF technology. A particle injected in such a wave with sufficient initial energy can interact, i.e., stay in phase, with the longitudinal component of the electric field for a time long enough that its energy gain is significant.

Although this idea seems very simple, in reality it is highly nonlinear and hence difficult to describe theoretically and to simulate numerically. Furthermore, it pushes laser and particle beam technology to the limit so it is very hard to realize it experimentally. To do full scale three-dimensional PIC simulations on LWFA requires huge computing power, which has only been available for the past five years. To experimentally demonstrate LWFA, one needs three different types of equipment or technology, namely a high power laser, a uniform plasma and an injector such as a RF accelerator. Furthermore, each must work together and be synchronized. Due to the lack of a sufficiently short-pulse, high-power laser, longer pulses were used to excite wakes in the 1980's and 1990's. Despite all these technological difficulties, steady progress was still made in the early age

of this field (middle 80s to middle 90s) through beat wave excitation or Raman forward scattering type instabilities. The first milestone was the demonstration that relativistic plasma waves could be excited. This was accomplished by the UCLA group in middle 80s. The second milestone was to prove that such waves can be used to accelerate a electron beam. This was also done by the UCLA group after nearly a ten years struggle. Both milestones were achieved using PBWA (Plasma Beat Wave Acceleration), in which two long pulses with a frequency difference equal to the plasma frequency are used to form a beat pattern. In 1990's, advances in short-pulse high-power laser, especially the invention of chirped pulse amplification (CPA) and of the development of Ti:Sapphire laser systems led to steady progress in SMLWFA results, including what is called the forced LWFA regime. These results include the observation of 100 MeV electrons and gradient $\sim 1TeV/m$. However, there was 100% energy spread and the acceleration distance was limited to $100\mu m - 1mm$. A recent important development in the LWFA concept was the simulation and experimental observations of highly-nonlinear 3D wakefield structures and the formation of quasi-monoenergetic self-trapped electrons [58, 59, 60, 61, 62, 48]. In these experiments quasi-monoenergetic beams of electrons with energies on the order of 100 MeV and charge about nC were generated by shooting $10 \sim 30TW$ $30 \sim 50fs$ laser pulses into mm scale target (some with channels) with plasma density between $6 \times 10^{18} \sim 2 \times 10^{19} cm^{-3}$ [60, 61, 62].

These new results are exciting, at same time they also raise many questions: Can these results be scaled to higher energy with better beam quality? Can the results be more reproducible? Can LWFA be the basis of a real high energy physics accelerator? Full scale 3D PIC simulations of these experiments show that the energetic electron generation mechanism involves an interplay of many complex phenomena , e.g., significant evolution of the laser excitation of three

dimensional wake fields, self-trapping of electrons and significant beam loading on the wake. In light of the complexities involved in these experiments, it is clear that these questions can not be fully answered before we have a clear understanding of the underlying physics.

Luckily, after more than 25 years' of progress, our abilities to get answers have been expanded significantly. In the early days the understanding of the underlying physics were quite limited. The theory was most one dimensional and/or weakly nonlinear, simulations were limited to one or two dimensional and as alluded to earlier, experiments were limited by laser technology. To put things in perspective, even 10 years ago a 1D PIC simulation for a 1GeV stage could not be done easily. Now we have the ability to simulate such a stage in 3D. Ten year ago, 1TW Ti:Sapphire laser systems were not widely available. Now many 10TW to 100TW systems exist in small labs around the world. With all these new capabilities, this field is rapidly progressing and the basic understanding of the underlying physics is improving. It is therefore now the time to carefully consider the path towards a real LWFA stage.

In this chapter, we will give one possible path to a real accelerator. We will first define some important conditions for a real accelerator. Then after analysis based on weakly nonlinear theory, we will demonstrate that the highly nonlinear blowout regime is preferred. After that, we will present the relevant physics in detail and provide a phenomenological theory for it. This theory leads to a group of scaling laws which we then use to design parameters for future experiments.

5.2 What Do We Need for a LWFA as an Useful Accelerator?

Accelerators based on traditional technology are very robust machines. They can be operated continuously with just regular maintenance. In most applications for accelerators, it is critical that a accelerator operate robustly. Although the technology for building accelerator will evolve, this basic requirement of robustness will always be an essential part of a future workhorse accelerator. Besides this general requirement for all accelerators, different applications need different beam parameters and overall efficiency, e.g., a large facility needs a high wall plug efficiency to reduce the operating costs. The most important parameters are beam energy, beam current, beam emittance and repetition rate.

Experiments on LWFA have already demonstrated huge accelerating gradients. But a critical question still remains: Is there parameter space for LWFA such that it can satisfy all the requirements for a real accelerator?

To answer this question to some extent, we need to be more specific on the requirements for a useful accelerator. We assume the following four requirements are essential:

1. The accelerating structure must remain stable over long propagation distances. In particular, the amplitude and phase velocity of the wake need to be relatively constant. This requires that the laser be guided with a constant, i.e., match, spot size and with little group velocity dispersion.
2. The conversion efficiency from the laser energy into the accelerating structure must be high. This requires that the effective acceleration length, e.g., the dephasing length be close to the pump depletion length.
3. The conversion efficiency from the plasma wake into the accelerated beam

must be high while at the same time the quality of the beam, i.e., its energy spread and emittance, must remain high. This requires that the wake amplitude vary little across and along the beam, and that the focusing force be linear in the transverse coordinate.

4. The repetition rate of the accelerator must be high. This requires that high rep rate lasers be used. And in order to keep the overall efficiency of the accelerator high, the laser must have a high wall-plug efficiency.

We next see what can be concluded from linear theory if one tries to meet the above requirements.

5.3 What Does Linear Theory Tell Us?

The simplest and most well developed theoretical framework for the plasma based acceleration is the linear and weakly nonlinear theory. This framework assumes that the laser vector potential a_0 is much smaller than unity (the beam density $n_b \ll n_p$ for charge particle drivers) and the plasma density perturbation δn from the laser or beam driver is much smaller than the ambient plasma density n_p . Under these conditions, well developed mathematic tools (e.g., small parameter perturbation expansions, variational principles) can be used to construct theoretical models. Indeed, most theoretical work to date in the plasma based acceleration belong to this category. One can think these theories as natural extensions of traditional nonlinear optics theories for crystals to a richer and more complex situation, namely, the weakly nonlinear laser plasma or beam plasma interaction. Within this framework, many important aspects of plasma based acceleration have been addressed theoretically, e.g., the wakefield excitation, the beam loading, the laser guiding by plasma density channel , and growth rates

for numerous laser plasma or beam plasma instabilities. Although for situations of interest, e.g., highly nonlinear 3D wake structures, non laminar plasma flow, and cavitation blowout, linear theory is not appropriate, it can still serve as a knowledge base for understanding the field of plasma based acceleration.

As a starting point, it is useful to know what kind of parameter regime should be chosen based on the well developed linear and weakly nonlinear theory. Following the requirements raised in last section, we will discuss separately the issue of the stability of the wake, the laser guiding, the laser to wake efficiency, the beam loading efficiency and beam quality in the following subsections.

5.3.1 Stability Consideration

Stability is the most important issue for any accelerator design. In traditional accelerators, many instabilities arise when the beam current is too high and collective coupling between beam and accelerating cavity becomes strong. They are limiting factors for the performance of accelerators. The typical mechanism for these instabilities is the coupling between the beam current and its wakefield in a metallic cavity. A real cavity has a finite conductivity and some resistance. When a charge particle moves through a cavity, it produces a wakefield by inducing surface currents in the walls. In a non-ideal cavity, the charged particles in the wall get out of phase with the beam. This leads to an instability via the coupling between the beam and the surface current in the cavity wall. This interaction is detrimental to the beam quality, and it puts a limit in the beam current. So generally speaking, in traditional accelerators, the wakefields due to collective motion of charges in the accelerator need to be avoided.

For plasma based acceleration (LWFA and PWFA), the situation is totally different. We are trying to utilize a wakefield to accelerate a beam of particles.

To be useful the wakefield must be stable and change little as the laser driver propagate long distances. Since the wake is driven by the laser this requires that the laser evolve in a well controlled, i.e., stable, manner. A plasma with its many degrees of freedom can support numerous instabilities. In fact during the early days in plasma based acceleration research, there were many critics for just this reason. Significant effort was made in the early years to identify and understand the numerous instabilities for short-pulse lasers and particle beams propagating through plasma. Not surprisingly it was found that most of the growth rates for laser plasma instabilities increase from the head of the pulse to the tail, so the longer the pulse, the more likely it is unstable. These theoretical analyses based on weakly nonlinear theory suggest that only pulses with pulse length smaller than plasma wavelength may be able to support stable propagation over long distances. These theories also demand a plasma density channel to guide the laser over distances that greatly exceed the laser Rayleigh length Z_r .

In the early experimental work in plasma based acceleration, very long pulses compared to the wake's wavelength were used to driven large wakefields due to the lack of sufficiently short-pulse lasers. As noted earlier, this was done using the beat wave or self-modulated LWFA methods. While both of these methods, PBWA and SMLWFA, produced large gradients and high energy electrons, they are not attractive for a real accelerator due to the fact that the wakefields are excited by an instability (SMLWFA) or the plasma wave is susceptible to instabilities or degradation to its phase velocity (PBWA). Therefore, we are of the option that the LWFA scheme is desirable. This has also been verified in fully nonlinear simulations. As we will show, there are still issues regarding the stability of the wake for LWFA. In particular the spot size of the laser and the frequency content of the laser should remain relatively constant.

5.3.2 Efficiency Consideration: Pump to Wake

We next consider the constraints imposed by requiring that there must be high conversion efficiency from the driver (laser) to the wake. The basic idea is that in order to obtain high efficiency the acceleration length, typically the dephasing length, must be a large fraction of the pump depletion length. We will define a laser to wake (LW) efficiency $\eta_{lw} \equiv L_{dp}/L_{pd}$ where L_{dp} is the dephasing length and L_{pd} is the pump depletion length. We will use approximate expressions for L_{dp} and L_{pd} obtained from linear theory.

$$\begin{aligned} L_{dp} &\cong \frac{\omega_0^2}{\omega_p^2} \lambda_p \\ L_{pd} &\cong 2 \frac{\omega_0^2}{\omega_p^2} \lambda_p a_0^{-2} \end{aligned} \quad (5.1)$$

Note we assume a linearly polarized laser. These formulas suggest that η_{lw} scales as $a_0^2/2$ for $a_0^2 < 1$, therefore, in order to achieve enough efficiency $a_0 \sim 1$ should be used. However, it should be stressed that the expression for η_{lw} obtained above is probably an upper bound (there has been little or no research on how to optimize the efficiency by shaping the pulse and tailoring the frequency chirp). The true efficiency is several times smaller. There are two main reasons for this. First, in a 3D linear wake, half of the accelerating region of the buck also has defocusing fields. Therefore, the dephasing length is actually a factor of 2 smaller. Second, the central frequency of the laser will decrease due to photon deceleration as the laser pump depletes. This means that unless one is clever in choosing the correct frequency chirp the laser will distort significantly before all of its energy is deposited in the wake. Once it distorts the quality of the wake will degrade.

To quantify the best case efficiency in the linear and/or weakly nonlinear

regime we performed PIC simulations. We use a_0 's of unity or slightly higher. In Fig. we show the results from two simulations with different a_0 (1 and 2) and fixed plasma and laser parameters ($k_p c \tau = \pi(FWHM)$). In both cases, the laser propagates into the plasma for a 3D linear dephasing length ($L_{dp} = \frac{\omega_0^2}{\omega_p^2} \lambda_p / 2$). Using this “3D” L_{dp} we get $\eta_{lw} = a_0^2/4$. We then compare the pulse at this propagation distance to the original one to determine the energy that remains.

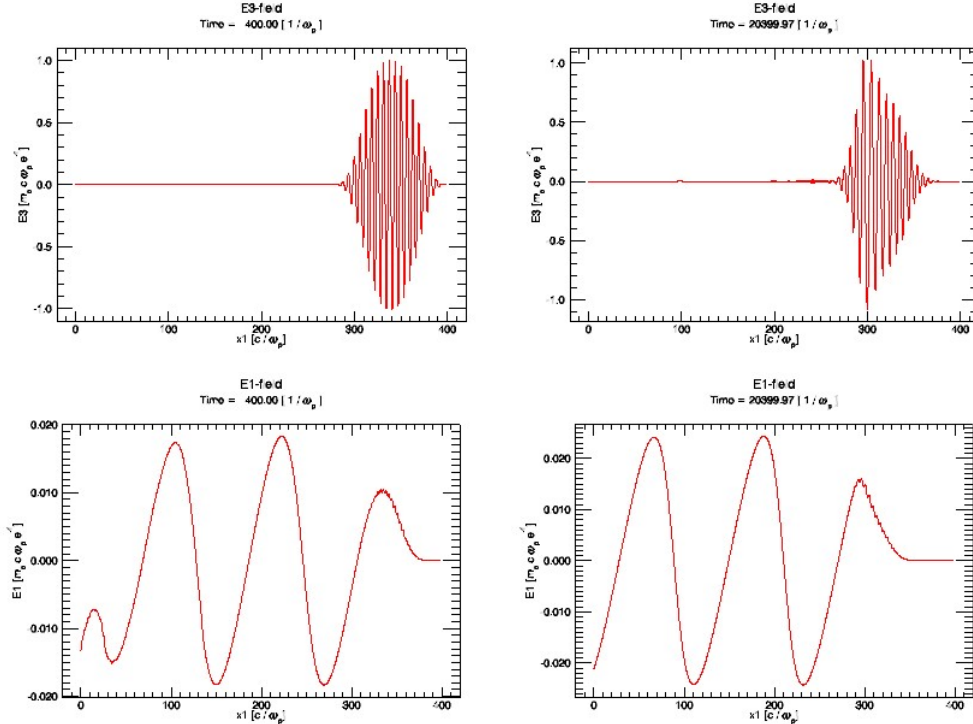


Figure 5.1: A laser pulse with $a_0 = 1$, $k_p c \tau = \pi$ propagating through a plasma with $n_p/n_c = 0.00287$, (a) E3 at time $t = 400\omega_0^{-1}$ (b) E3 at time $t = 20400\omega_0^{-1}$ (c) E1 at time $t = 400\omega_0^{-1}$ (d) E1 at time $t = 20400\omega_0^{-1}$

For the $a_0 = 1$ case, Fig.5.1, the simulation shows that more than 80% of the laser energy remains after one linear dephasing length. This agrees reasonably well with $\eta_{lw} = a_0^2/4$. After two linear dephasing lengths, there is still more than 50% of the laser energy remaining. These results agree very well with our

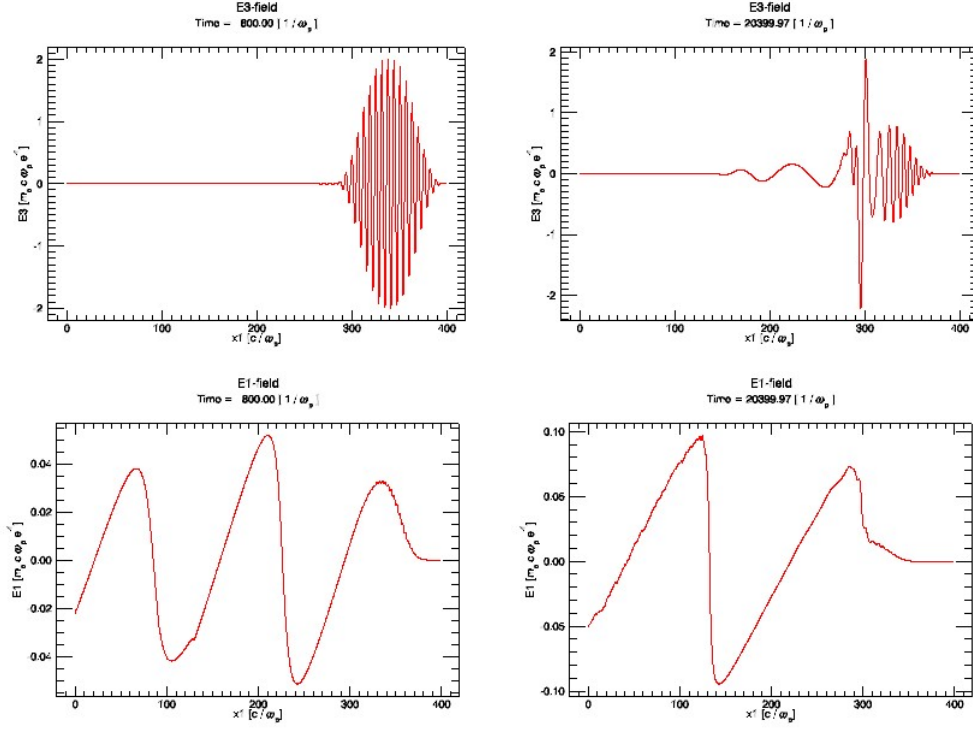


Figure 5.2: A laser pulse with $a_0 = 2$, $k_p c \tau = \pi$ propagating through a plasma with $n_p/n_c = 0.00287$, (a) E3 at time $t = 800\omega_0^{-1}$ (b) E3 at time $t = 20400\omega_0^{-1}$ (c) E1 at time $t = 800\omega_0^{-1}$ (d) E1 at time $t = 20400\omega_0^{-1}$

discussions above. For the case $a_0 = 2$, Fig.5.2, about 40% remains after one linear dephasing length.

The main point of the discussion is that to obtain high efficiency it is necessary for a_0 to be larger than unity (one way around this would be to increase the dephasing distance using a density ramp, an asymmetrically shaped laser pulse or a laser with a frequency chirp. However, each of these options also leads to additional issues). This a_0 corresponds to a laser intensity $I \sim 10^{19}W/cm^2$.

Supposing we fixed the laser intensity I around $10^{19}W/cm^2$, then what determines the other parameters like plasma density n_p , laser spot size W_0 and laser

pulse length $c\tau$?

To answer these questions , we first check the energy gain for given laser intensity and plasma density. From weakly nonlinear theory, it scales as $a_0^2 \frac{k_0^2}{k_p^2}$ for $a_0 \lesssim 1$. This suggests that for a given plasma density, higher intensities give higher energy gain. It also suggests that for a given intensity lower plasma density gives higher energy gain. The efficiency arguments indicate that $a_0 \sim 1$ and now from this well known expression for the energy gain, we can choose the proper plasma density n_p and the pulse length $c\tau$ (which is half the plasma wavelength for maximizing the wakefield) to provide the desired energy.

To chose the laser spot size W_0 , and hence the spot size of the wake, we need to consider how this choice impacts the evolution of the laser (e.g., laser guiding through the effective accelerating length) and the transverse plasma wakefield structure (relevant to beam loading efficiency and beam quality). We discuss these two issues separately.

5.3.3 Laser Guiding

A laser with a finite spot size W_0 will diffract in vacuum. The characteristic length for such diffraction is the Rayleigh length $Z_r = \frac{1}{2}k_0 W_0^2$. The ratio between the dephasing length L_{dp} and the Rayleigh length Z_r is $\frac{4\pi}{k_p^2 W_0^2} \frac{k_0}{k_p}$. This implies that 3D diffraction may only be omitted when very large spot sizes are chosen, e.g., $k_p W_0 > (4\pi k_0 / k_p)^{1/2}$, so that the laser does not evolve much transversely within the effective accelerating distance. large spot size with the fact that $a_0 \sim 1$ implies very large laser power, e.g., $P(TW) > 15(\frac{10^{19} cm^{-3}}{n_p})^{3/2}$. For example, if one need a density of $10^{17} cm^{-3}$ then the necessary power would be $15PW$ and the spot size would be 1mm. Such large power and spot size are unpractical for a variety of reasons. Most importantly, as we will argue shortly, such large spot

sizes lead to very inefficient beam loading. These beam loading arguments provide the condition that W_0 needs to be \sim of a few plasma skin depths. This needs a method to optically guide the laser through many Rayleigh lengths needed for LWFA. For the short-pulses ($c\tau \sim \lambda_p/2$), weakly nonlinear theory suggests that the only viable method to guide the pulse is to a plasma density channel. Such channels have the lowest plasma density on axis and can be approximated with a parabolic density profile like $n(r) = n_p(1 + \frac{r^2}{W_0^2}\Delta n)$. To guide a laser with spot size W_0 without significant spot size oscillation, the channel depth Δn should be chosen as $\Delta n_c = \frac{4}{(k_p W_0)^2} n_p$. However, the channel depths are usually a small fraction of the plasma density n_p because of limitations for the technologies used to form plasma channels and because substantial phase mixing can occur. For $\Delta n_c/n_p \ll 1$, then $k_p W_0$ must be larger than $\sim \pi$ for the matched channel condition to be met. If $a_0 \sim 1$ and $k_p W_0 > \pi$ then the laser will have a power near or exceeding the critical power for relativistic self-focusing. This will cause the tail of the laser to distort significantly.

5.3.4 Beam Loading and Beam Quality

The constraints imposed by linear theory on beam loading and beam quality were addressed in detail in the work of Katsouleas et al.. In this paper it was shown the maximum number of particles that could be accelerated in a linear wake of amplitude $eE/mc\omega_p \equiv \epsilon$ was

$$N = k_p n_p A \epsilon \approx 5 \times 10^5 \sqrt{n_p} A \epsilon \quad (5.2)$$

Where A is the cross sectional area of the wake. Furthermore, it was shown that in order that the emittance remain sufficiently small that the radius of the loading bunch, σ_r , be much smaller than the spot size of the wake, W . In

particular,

$$\frac{\sigma_r}{W} \sim \left(\frac{\epsilon_N}{W}\right)^{1/2} \left(\frac{1}{\gamma\epsilon}\right)^{1/4} \quad (5.3)$$

Where $\epsilon_N \equiv \gamma\sigma_r v_r/c$ is the normalized emittance of the electron beam. Kat-souleas et al. also showed that high beam loading efficiency (transfer of wake energy to accelerated particles) could only be achieved if $W \sim c/\omega_p$ and $\sigma_r \ll W$. This can be accomplished because linear theory predicts that a very narrow particle bunch excites a wake that is $\sim c/\omega_p$ wide because it takes a c/ω_p to shield the electromagnetic fields of the beam particle. For a narrow bunch the maximum number of particles that can be accelerated are

$$N \approx 5 \times 10^5 \sqrt{n_p} A_{eff} \epsilon \quad (5.4)$$

Where $A_{eff} = 2\pi\sigma_r^2/[1 - \sqrt{2}k_p\sigma_r K_1(\sqrt{2}k_p\sigma_r)]$. In reality N is less such that the loaded wake does not vanish. When $k_p\sigma_r \ll 1$, then $A_{eff} \sim .6$ to 2 times c^2/ω_p^2 for $\sqrt{2}k_p\sigma_r = 10^{-4}$ to 10^{-1} . Therefore, for narrow trailing bunches

$$N \approx \epsilon n_p (c/\omega_p)^3 \approx \frac{1.4 \times 10^8}{\sqrt{n_p(10^{18} cm^{-3})}} \epsilon \quad (5.5)$$

For plasma densities in the range of $10^{16} \sim 10^{18} cm^{-3}$ and for $\epsilon \sim 1$, the above expression gives a total amount of charge between $200pC$ and $20pC$, which are much smaller than the typical numbers in existing colliders.

There are additional restrictions when constraints on energy spread are imposed. In order that the energy spread remains small the trailing bunch can only fill a small phase of the bucket, e.g., $k_p\sigma_z \equiv \Delta\phi \lesssim 1$. Therefore, constraints on

the beam density, n_b , and charge per unit length, Λ , can be estimated. The beam density is

$$n_b = \frac{N}{(2\pi)^{3/2}\sigma_r^2\sigma_z} = \frac{\epsilon n_p}{(2\pi)^{3/2}k_p^2\sigma_r^2\Delta\phi} \quad (5.6)$$

which is much larger than n_p when $k_p^2\sigma_r^2 \ll 1$ and $\Delta\phi \lesssim 1$. Furthermore, the charge/unit length is

$$\Lambda = \frac{\epsilon}{(2\pi)^{3/2}\Delta\phi} \quad (5.7)$$

Which is much smaller than unit (about 0.06 for $\epsilon \sim 1$ and $\Delta\phi \sim 1$).

Recently, Lu et al. showed that for a narrow electron beam with $n_b/n_p \gg 1$ and $\Lambda \ll 1$, a non-relativistic blow occurs within the bunch and an channel is formed. However, the normalized field amplitude ϵ is still close to the linear prediction except a slowly changing logarithmic term. This suggests that the charged particle number obtained from the linear analysis is still valid in this case.

If more charge is needed, i.e., nC, the linear analysis suggests that it can not be supported by a linear wake. Indeed, if one calculates the charge/unit length for this amount of charge (assuming $\Delta\phi \lesssim 1$), Λ is about 0.3 for $n_p = 10^{16} cm^{-3}$ and 3 for $n_p = 10^{18} cm^{-3}$. In both cases, the electron bunch will generate an ion channel with radius larger than the plasma skin depth. So we may draw the conclusion that weakly nonlinear regime is not able to support sufficient charge (nC).

5.3.5 Summary

We can summarize our conclusions on how to choose parameters based on weakly nonlinear theory from above discussions. First, stable operation needs short pulse about a plasma wavelength long. Second, high laser to wake efficiency needs the intensity to be larger than $10^{18}W/cm^{-2}$ ($a_0 > 1$, as shown in PIC simulation, $a_0 \sim 2$ is better). To satisfy this condition, one needs the laser to be tightly focused. Third, the requirement for guiding over many Rayleigh length by shallow plasma channel needs the spot size of the laser to be at least half plasma wavelength wide. Fourth, the conservation of the emittance needs the spot size of a loaded electron beam to be much smaller than the laser spot size. Last, the driver can also not be much wider than plasma skin depth because the focusing field will be small and the beam loading efficiency for a narrow beam will be small.

We can also notice that even all the above requirements are satisfied, the overall efficiency is still very small (a few percents) if we choose to operate in this weakly nonlinear regime. The total charge that can be accelerated is around $10 \sim 100pC$. Other than these, for high energy gain like GeV or beyond, the accelerating distances are typically tens or hundreds of Rayleigh length. In these cases, the very weak instabilities for short pulse may still grow enough to play significant roles.

If we stop now and with all the above in mind, we may draw the conclusion that the plasma based accelerator is not interesting to pursue. Indeed, the real situation is not that bad. We can notice that the regime suggested by the above parameters is already not quite weakly nonlinear, some new physics may happen to rescue. This will be the topic of next section.

5.4 Does Nature Force Us to the Blowout Regime?

As we can see from last section, the possible optimum regime suggested by the weakly nonlinear theory is not weakly nonlinear at all. The laser vector potential a_0 is about $1 \sim 2$ (The weakly nonlinear assuming at least $a_0 < 1$), the laser spot size is about half to one plasma wavelength ($k_p W_0 \approx \pi \sim 2\pi$). In 1D theory it is known that when $a_0 \approx 1 \sim 2$, the density perturbation δn is on the order of plasma density n_p . Since it is 1D, the density perturbation only exists longitudinally. In the 2D or 3D geometry and with laser spot size around the plasma wavelength, the transverse laser ponderomotive force is almost as large as the longitudinal part, therefore the transverse plasma motion becomes very important. In this case the plasma electrons will move outward radially and a low electron density region will be formed inside. Furthermore, if the intensity is high enough ($a_0 \approx 2$), the electrons initially inside will move faster than those initially outside such that their trajectories cross each other (the plasma can not be treated as a single fluid any more). This results in a nearly pure ion region (called "ion column", "bubble") surrounded by a narrow electron sheath with high density and high flow velocity (on the order of speed of light).

As we already mentioned many times in this dissertation, this remarkable strongly nonlinear phenomena was first predicted by Sun et al. in 1987. In his work, the equilibrium profiles for both laser and plasma density are calculated for a self-guided short laser pulse (the pulses are much longer than electron plasma wavelength but much shorter than ion plasma wavelength, so the ions are treated as immobile). This is the first work trying to treat this problems self-consistently. Previous works on relativistic self-focusing all assumed the plasma density is uniform across the transverse dimensions so only the relativistic mass increase contributes to the self-focusing. As pointed out by Sun et al., this assumption

indeed is only valid for very large laser spot size and for the laser power near the threshold for relativistic self-focusing, P_c . For power slightly larger than P_c , the equilibrium electron density profile becomes highly non-uniform near the laser axis (nearly evacuated up to some radius) and this density channel contributes equally to the self-focusing as relativistic mass increase. This hollow structure is called "cavitation" by Sun et al. due to its similarity to some fluid phenomena. The radius of the channel is on the order of plasma skin depth and increases slowly as the laser power increases. In fact, it is simply estimated by the balancing between the laser ponderomotive force and the electric force of the pure ion column. It is also interesting to note that the equilibrium laser profile inside the channel is not Gaussian but more close to a zeroth order Bessel function. This simply implies that the Gaussian profile assumed in most of the works for laser propagation in plasma may not be good enough. Since this work is for relatively long pulses where the wakefield effect is negligible, its implication for acceleration was not discovered until a few years later.

In 1991, Rosenzweig et al. found an interesting regime for electron beam driven plasma wakefield through 2D PIC simulations. In this regime, a short (about plasma wavelength) and narrow (spot size smaller than plasma skin depth) electron bunch with sufficient charge can blow the plasma electrons away from its path and form a pure ion region around and behind it. This phenomena is totally similar to what Sun et al. found for laser case. The difference is just that in the laser case it is the ponderomotive force pushing electrons while in the beam case it is the electromagnetic force from the beam. Since the beam is short, the wakefield is significant. Rosenzweig et al. pointed out that the accelerating field inside the channel is uniform across the transverse dimensions and the focusing force inside a cylindrical symmetric channel depends linearly on the radius. Both properties are very attractive comparing with the weakly nonlinear wakefield (

as we can see from last section, the linear wake suffers significantly from the non-uniformity accelerating field and nonlinear focusing fields). This highly nonlinear multidimensional wakefield regime was later called the "blowout" regime.

At the same year (maybe even a little bit earlier), Mori et al. showed similar regime can be reached for a laser driver by 2D PIC simulations and they also pointed out the advantage of uniform accelerating field and linear focusing force. But at that time, the laser power was too low and the pulse length too long to reach this regime.

Now let's come back from the history and observe the consequence of parameters based on weakly nonlinear theory. Let's calculate the peak power for a linearly polarized laser in terms of the power for relativistic self-focusing P_c ($P_c = 17(GW) \frac{k_0^2}{k_p^2}$). The formula is:

$$\frac{P}{P_c} = \frac{1}{32}(k_p W_0)^2 a_0^2 \quad (5.8)$$

For those parameters suggested by weakly nonlinear theory ($a_0 \approx 1 \sim 2$ and $k_p W_0 \approx \pi \sim 2\pi$), this gives $P/P_c \approx 0.3 \sim 5$. We can see that for reasonable pump to wake efficiency (40%), P/P_c is larger than two. According to Sun et al. (although their results are for longer pulses), this will lead to cavitation or blowout. This can be confirmed by 3D PIC simulations. In Fig.5.3, a 30fs, 6TW short laser pulse propagates through a plasma channel with a minimum density on axis $n_p = 5 \times 10^{18} cm^{-3}$. The laser spot size W_0 is chosen as $6.7 \mu m$ and the plasma channel depth is chosen to match the laser spot size. For these parameters, we have $P/P_c \approx 1$, $a_0 \approx 2$, $k_p c \tau \approx \pi$ and $k_p W_0 \approx 2.83$. We can see that the blowout occurs immediately after the laser going into the plasma.

We would like to know what is the advantage for operating in such a regime. Indeed there are many. For example, it has better laser to wake efficiency, much

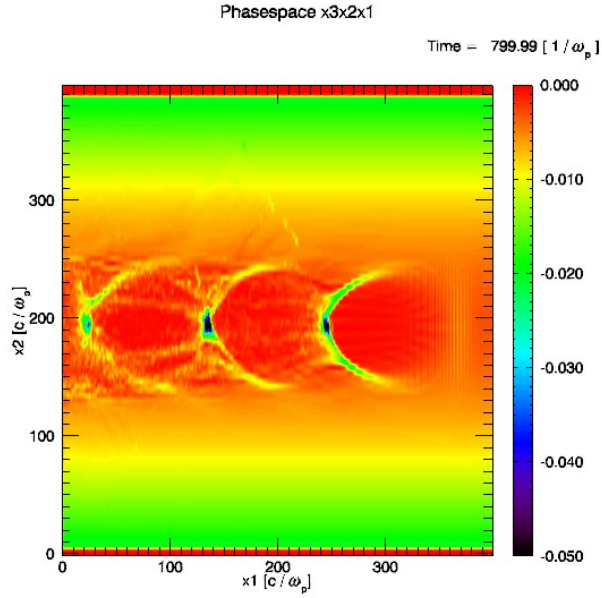


Figure 5.3: A 30fs, 6TW short laser pulse with $a_0 = 2$, $k_p c \tau = \pi$ and $k_p W_0 \approx 2.83$ propagating through a plasma channel with $n_p/n_c = 0.00287$ on axis, note that $k_p c \tau_{rise}/\pi = 0.7$ and $k_p c \tau_{fall}/\pi = 1.3$

better beam loading efficiency and beam quality, it also reduce various instabilities not avoidable in linear setups. In the next section, the details of many aspects in the blowout regime will be provided. Here we just point out briefly what leads to these good properties of this regime. Two major points are the following: The first one is , as pointed out by Rosenzweig et al. and Mori et al., the uniform accelerating field along the transverse dimensions and the linear focusing force. These can significantly improve the beam loading efficiency without degrading the beam quality (energy spread and emittance growth). The second is that this regime is more stable comparing with weakly nonlinear regime. one of the major reasons is that the tail part of the laser pulse is inside a region with very low plasma density (the ion channel) so that the coupling between laser and plasma

is significantly reduced.

As you can see from the discussions in this and the previous sections, we started from the weakly nonlinear theory and ended with the conclusion that weakly nonlinear regime is not the choice for LWFA. We then found that the hints we got from weakly nonlinear theory lead us to a new regime where even the fully nonlinear fluid theory is not applicable. Just like many other fields in the nature science, new physics shows up when the old model breaks down. And it seems that this is not avoidable if the requirements for a real accelerator are considered. Instead of asking question in the title of this section, we conclude by the end of this section that nature does force us to the blowout regime although if it will work eventually is not fully answered yet.

5.5 Physics in the Blowout Regime

As shown in previous sections, the blowout regime has many advantages for laser wakefield acceleration. Therefore it is important to understand the relevant physics for plasma based acceleration. In this section, we will carefully look at each relevant topic in some detail, and hopefully an integrated physical picture can be presented. These topics include: under what condition does the trajectory crossing and clear blowout happen? For given laser power and plasma density (also the laser profiles) , what is the matching condition for stable propagation? What is the structure of the wakefield, including both longitudinal and transverse fields? How does laser lose energy to the wake and how fast can it moves ? Is self-guiding possible and under what conditions? the mechanism of self-injection or external injection and how the loaded beam changes the wake? What kind of instabilities are there and how severe they can be?

5.5.1 Blowout and Matching Condition

For laser driven plasma wakefield, the blowout process and the matched laser propagation are two different but closely related concepts. The major distinction between these two concepts are the time scales during which these processes occur: the blowout process occurs on the plasma response time scale (ω_p^{-1}), while the laser intensity profile evolves on a much longer time scale, e.g., the time for laser to propagate one Rayleigh length Z_r (which is much larger than ω_p^{-1} if the plasma is very underdense ($\omega_p \ll \omega_0$) and the laser spot size is on the order of plasma skin depth c/ω_p). These two processes are closely coupled: on one hand, the fast time scale blowout process determines the slow time scale laser profile evolution by its induced channel of index of refraction, on the other hand, the changed laser profile also changes the blowout process. In order for the matched propagation to occur in the blowout regime (the laser is guided either by self-guiding or by plasma density channel guiding), the laser profiles are needed to be properly chosen such that both the laser profile and the shape of the plasma blowout channel change very little during the evolution.

We first look at the characteristics of the channel shape formed by the laser on the fast time scale. As already mentioned in chapter one, there are significant differences between the blowout for laser drivers and that for the electron beam drivers: in the electron beam driver case, the beam spot sizes are typically small than plasma skin depth, c/ω_p , and very nice electron sheath can always be formed no matter how the beam spot size evolves as long as it is much smaller than the blowout radius. These nice features are mainly due to the long range form of the electromagnetic force from the beam charge and current because these sheath electrons always feel nearly the same force when they are outside of the electron driver. For the laser driver, the ponderomotive force responsible for the electron

blowout is short range in nature, which only exists where there is laser intensity gradient. For the same laser power, what the sheath looks like depends strongly on how large the spot size is chosen. If the laser spot size is very large so that the intensity is very small, there is very small ponderomotive force, it then follows that on the short time scale the laser plasma interaction can be well described by weakly nonlinear theory, so on this time scale no electron trajectory crossing and blowout will happen. On the contrary, if the laser spot size is initially chosen very small so that the laser intensity is large, the plasma electrons within the laser intensity profile will feel very strong transverse ponderomotive force so that they will move outwards transversely. But the electrons initially outside the laser intensity profile will not feel any ponderomotive force so they do not move transversely at all. This different behavior of electrons inside and outside the laser profile generally leads to a wide sheath and an irregular ion channel : electrons inside the laser profile move strongly in the transverse dimension and reach position far beyond the laser intensity profile; electrons outside the laser profile just go through the laser without any motion. Due to these features, a nice narrow sheath can be formed for a laser driver only when the laser spot size is within a narrow range where the laser spot size W_0 roughly matches the blowout radius R_m : $W_0 \sim R_m$. In this case, the transverse ponderomotive force of the laser $k_p \nabla a_0^2 / \gamma \sim a_0 / (k_p W_0)$, is roughly balanced by the force of the ion channel $E_r \sim k_p R_m$, which pulls back the ponderomotively expelled electrons. Equating these two expressions yields :

$$\frac{1}{\gamma_0} \frac{a_0^2}{k_p W_0} \sim k_p W_0 \rightarrow k_p W_0 \sim \sqrt{a_0} \quad (5.9)$$

Such force balance argument was first used by Sun et al. [55] for matched propagation of a long laser pulse in underdense plasma (although it assumed the

ions were fixed). He showed that for intense and narrow lasers the transverse ponderomotive force can lead to complete electron blowout (cavitation) when the laser power slightly exceeds the critical power for relativistic self-focusing P_c and the laser is focused tightly. In the large radius limit ($k_p R_m \gg 1$ and $P/P_c \gg 1$), his result gives the same scaling as the above equation. When using ultra-short pulses as in the laser wakefield acceleration, e.g., $c\tau \lesssim w_0$, a rigorous derivation for the coefficient of the above matched spot size is not currently available. Through simulations we have found that a more refined condition in the spot size is:

$$k_p R_m \simeq k_p w_0 = 2\sqrt{a_0} \quad (5.10)$$

We can use eq.5.10 to reformulate the matched beam spot size condition as:

$$a_0 \simeq 2(P/P_c)^{1/3} \quad (5.11)$$

and

$$k_p R_m \simeq k_p w_0 \simeq 2\sqrt{2}(P/P_c)^{1/6} \quad (5.12)$$

The above matching condition originates from the requirement for a nice electron sheath to be formed, so it is a concept on the fast time scale. It turns out that such condition is also the requirement for the matched propagation on the slow time scale. This close relation between the condition for the forming of a narrow sheath and that of matched laser propagation can be seen in the following arguments.

First, one can see that the matched laser propagation will not occur if the laser spot size is too large: as we discussed in previous section, the laser power needs to be larger than the power of relativistic self-focusing P_c . So in this case, the rear part of the pulse will tend to focus during propagation. This tendency

of focus can not stop until there is enough plasma density cavitation be formed. This focusing behavior is contradict with the assumption of matched propagation.

Second, the matched laser propagation will also not occur if the laser spot size is too small: in this case, the laser intensity tends to be too large to expel all the electrons inside the laser pulse, therefore the main part of the laser can not feel a channel of index of refraction because a real electron vacuum inside the laser.

So a matched propagation is only possible when the laser spot size matching the size of the channel, which is just the condition for the nice sheath to be formed.

To get eq.5.10, we assumed $a_0 \gg 1$ so that $P/P_c \gg 1$. But for $P/P_c = 1$, the above expressions give $a_0 = 2$ and $k_p R_m = 2\sqrt{2}$. Through PIC simulations, We find that the matching condition still holds for $a_0 \gtrsim 2$. In Fig.5.4, we show the matched blowout for the same parameters in Fig.5.3 at different propagation distances ($0.57Z_r$, $2.85Z_r$, $6.27Z_r$ and $10Z_r$). In this simulation, a plasma density channel with $\Delta n_c/n_p \sim 1/2$ was used to guide the leading part of the laser pulse (more discussion about guiding later).

5.5.2 Wake Excitation

For the matched laser profile, the theoretical model in chapter 2 can be used to describe the motion of the ion channel boundary (the back part where the plasma electrons are within a narrow sheath). For the regime interesting for LWFA, the blowout radius $R_m \gtrsim 3$ ($P/P_c \gtrsim 1$ and $a_0 \gtrsim 2$) so it is in the ultra-relativistic blowout regime: the ion channel is close to a spherical cavity of radius R_m ; the accelerating field E_z is nearly linear for most part of the ion channel and is with a normalized slope about $1/2$; The transverse fields E_r and

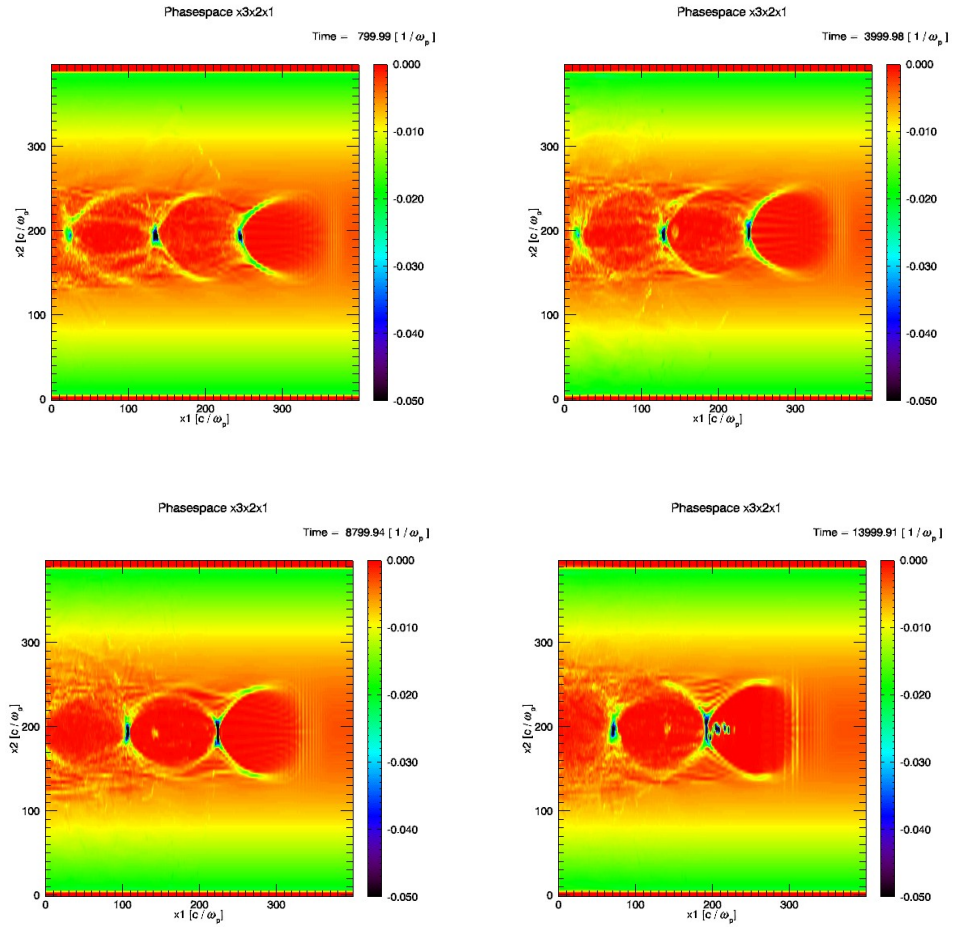


Figure 5.4: Plasma density plots for matched blowout of a laser driver, $P/P_c = 1$, $a_0 = 2$, $k_p W_0 = 2\sqrt{2}$, $k_p c\tau = \pi$ and $n_p/n_c = 0.00287$, (a) at $0.57Z_r$ (b) at $2.85Z_r$ (c) at $6.27Z_r$ (d) at $10Z_r$

B_θ are of the same magnitudes but with a different sign and linearly depend on the radius ($E_r = -B_\theta = r/4$).

Together with the matching condition, we can predict the maximum useful accelerating gradient E_{zm} for given laser power P and plasma density n_p .

$$eE_{zm}/mc\omega_p \approx \frac{k_p R_m}{2} \approx \sqrt{a_0} \approx \sqrt{2} \left(\frac{P}{P_c}\right)^{1/6} \quad (5.13)$$

5.5.3 Local Pump Depletion and Laser Front Etching

As the laser pulse propagates through the plasma, it excites the plasma wake thus loss part of its energy. In the blowout regime, the laser only strongly interacts with the plasma electrons near the front of the ion channel, where the plasma density is high. Within the ion channel, the electron density is near zero, therefore the laser loses very little energy there. Due to these reasons, the energy loss of laser is dominated by the loss at the front, therefore the front part of the laser will etch back during its propagation. This phenomena is called local pump depletion and was first observed by Decker and Mori [86] in 1D PIC simulation of high intensity ($a_0 \gg 1$) laser plasma interaction. It is worth noting that the local pump depletion for 2D or 3D is slightly different with that of 1D. In the 1D limit, plasma electrons can only move in the longitudinal direction so that the plasma density can never be zero. Indeed, 1D nonlinear theory and PIC simulations both show that the plasma density behind the laser driver is half the original plasma density. In the 2D or 3D limits, plasma electrons can also move transversely so that an ion channel can be formed. Despite this key difference, the high electron density region formed in the laser front by its snow plow effect is very similar in 1D, 2D and 3D (assuming that matched laser profiles are used such that significant transverse oscillation of laser profile can be avoid) and this is also the region where the laser lose most of its energy. This similarity between 1D and 2D/3D is mainly due to the fact that the ion channel has not been formed in this region.

Many PIC simulations were performed to check this similarity between 1D

and 2D/3D. For fixed plasma density and longitudinal laser profile, we vary the normalized laser vector potential a_0 from small to very large (for 2D/3D simulations, we use the matching condition to choose the laser spot size).

Two major conclusions can be drawn from these simulations. The first is that the laser loses energy similarly between 1D and 2D/3D for very high laser intensity, i.e., $a_0 \gg 1$. This is mainly due to the local pump depletion discussed before. This conclusion implies that we can use the 1D etching rate to estimate the 2D/3D etching rate. In Fig.5.5 and Fig.5.6, we compare the longitudinal laser profiles for two group of parameters in 1D and 3D after the lasers have lost a significant portion of their energy. In Fig.5.5, the initial laser vector potential a_0 is only 2 and the plasma density n_p is $0.00287n_c$. In the 3D case, a channel with $\Delta n_c/n_p = 1/2$ is used to guide the laser. In Fig.5.6, the initial laser vector potential a_0 is 40 and the plasma density n_p is $0.04n_c$. In both cases, the 3D laser fronts are quite similar to the 1D results (in the 3D $a_0 = 2$ case, a plasma density channel is used, so the comparison for this case is not rigorous. In this case the local pump depletion is also not rigorous because the plasma density spike in the laser front is not very sharp. But the main point here is to show that even in this case, 3D is not very different from 1D.)

The second conclusion is that the etching rate is independent of the intensity until a_0 reaches a plasma density dependent critical value and then it will drop for very larger a_0 . In ref.[86], Decker and Mori analyzed the laser front etching by using a 1D nonlinear model, and got an estimate of the etching rate, i.e., the etching velocity, as:

$$v_{etch} \simeq c \frac{\omega_p^2}{\omega_0^2} \quad (5.14)$$

We can see that this result has no dependence on the laser intensity, i.e., a_0 .

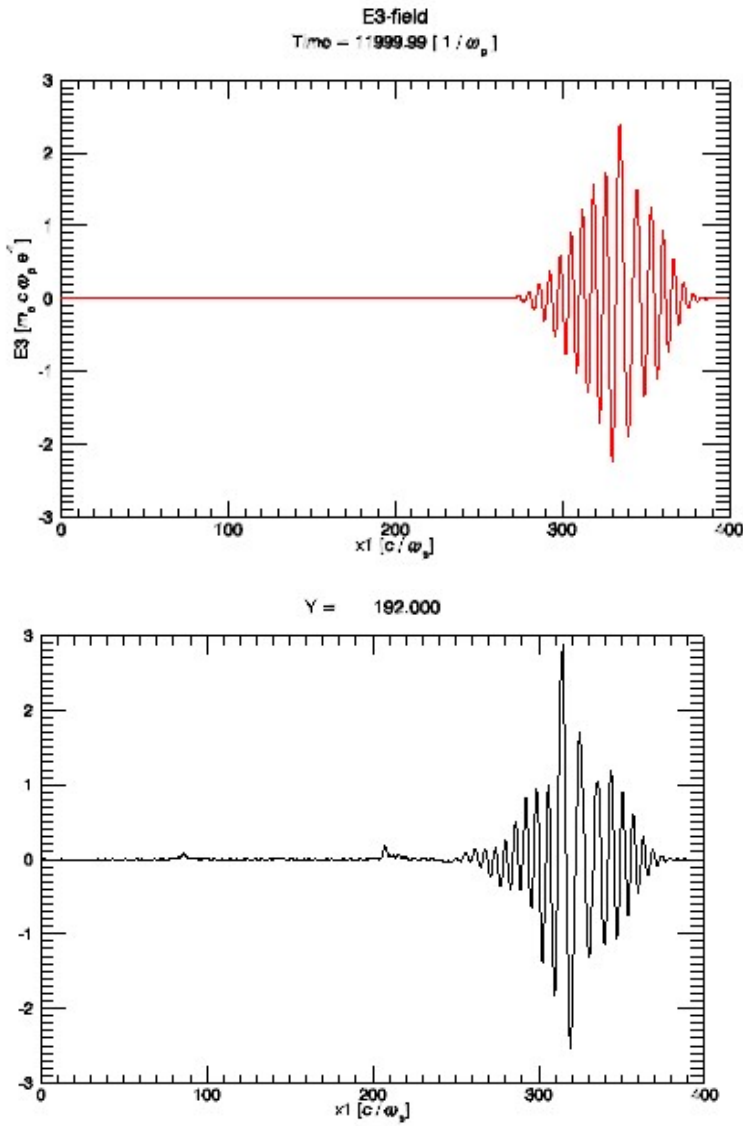


Figure 5.5: Lineouts of E_3 for 1D and 3D simulations for $a_0 = 2$ and $n_p/n_c = 0.00287$ at $t = 2500\omega_0^{-1}$ (a) 1D simulation (b) 3D simulation with laser spot size $k_p W_0 = 2\sqrt{2}$ and a plasma channel depth $\Delta n_c/n_p = 1/2$

In deed, two simple physical arguments can show how to get this. The first one is based on the 1D nonlinear wake field theory. For a nonlinear 1D plasma wake driven by a short laser pulse, the wake amplitude and the nonlinear wavelength

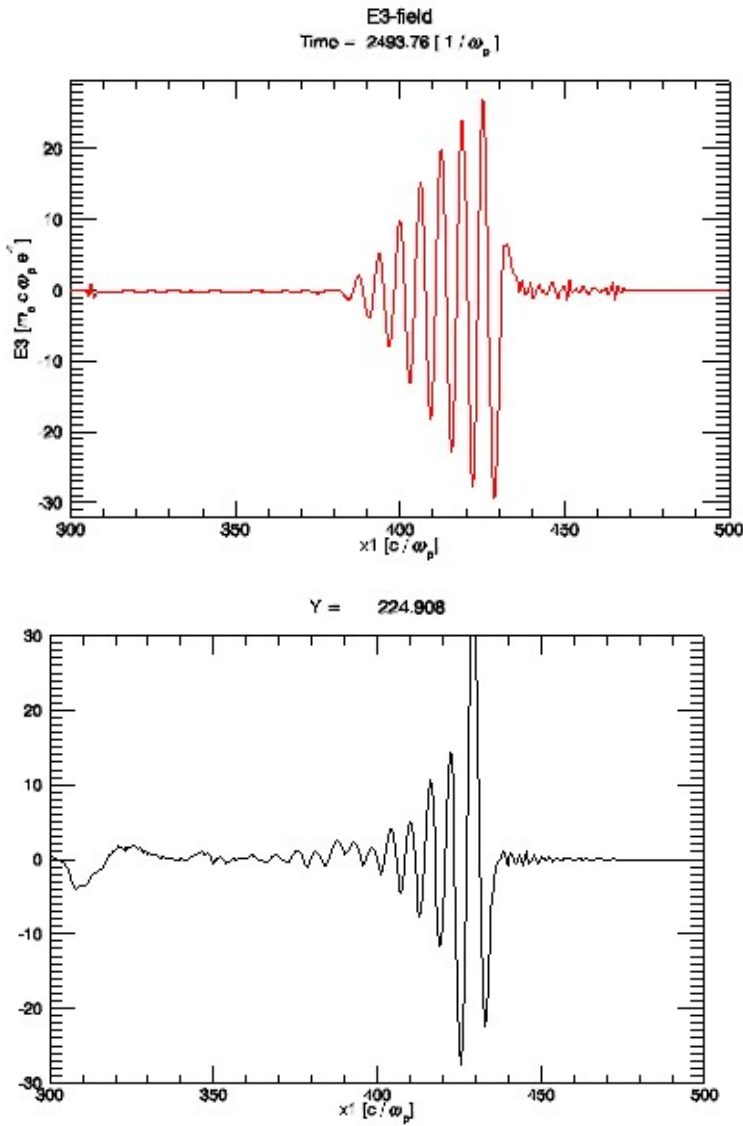


Figure 5.6: Lineouts of E3 for 1D and 3D simulations for $a_0 = 40$ and $n_p/n_c = 0.04$ at $t = 12000\omega_0^{-1}$ (a) 1D simulation (b) 3D simulation with matched laser spot size $k_p W_0 = 10$

are linearly proportional to the laser intensity a_0 . If one balances the energy inside the wake with the energy loss at the laser front, the above scaling of the etching rate can be deduced immediately. However the 1D nonlinear theory assumes a

very underdense plasma, i.e., $\omega_p/\omega_0 \ll 1$, therefore no limit on the laser intensity for this etching rate to be valid can be deduced directly. The second argument is based on single particle motion in a laser field. In a very underdense plasma ($\omega_p \ll \omega_0$), the influence of plasma on the laser is very small so roughly the single particle interaction between plasma electron and the laser can be used. In the 1D single particle limit and for large a_0 , the energy of the electrons is dominated by the longitudinal part rather than the transverse part : $P_\perp \sim a_0$, $P_z \sim a_0^2/2$ and $\gamma \sim 1 + a_0^2/2$. This implies that the energy loss rate is proportional to $n_p a_0^2$. On the other hand, the laser energy density is proportional $a_0^2 n_c$ (one can think laser as photon gas so the energy density is the photon number density $\omega_0 a_0^2$ times single photon energy $\hbar\omega_0$). Due to local pump depletion, the laser etching rate is obtain by $\frac{n_p a_0^2}{a_0^2 n_c}$. We can see the a_0^2 is cancelled leading to the independence of a_0 . In the above single particle picture, There is also no upper limit of a_0 because the laser is assumed to move with the speed of light in vacuum, c . Therefore, the a_0^2 scaling is valid for arbitrarily large a_0 . In a plasma, this scaling can only be approximately valid because the laser moves slower than the speed of light in vacuum. As shown in chapter 4, the particle energy scales as $p_\perp^2/2$ in a wave moving with finite γ_ϕ only if $v_\parallel < v_\phi$. If $p_\perp \sim \gamma_\phi$, $v_\parallel \sim v_\phi$, the energy gain will saturates. In the laser field, $p_\perp \sim a_0$, so this saturation transition occurs when $a_0 \sim \gamma_\phi \sim \frac{\omega_0}{\omega_p}$.

In Decker et al.'s work, they verified this etching rate by several 1D and 2D PIC simulations. Through numerous 1D and 3D PIC simulations, We find that this etching rate is valid in 1D and 3D and its valid range for intensity is roughly $2 \lesssim a_0 \lesssim 2\sqrt{\frac{n_c}{n_0}}$.

Due to this front etching, the laser will be depleted after a distance. We can get this so called pump depletion length as :

$$L_{etch} \simeq \frac{c}{v_{etch}} c\tau_{FWHM} \simeq \frac{\omega_p^2}{\omega_0^2} c\tau_{FWHM} \quad (5.15)$$

In an observing frame moving with c , the front of the laser, that excites the wake, moves backward as the pulse etches back with v_{etch} . The phase velocity of the wake can therefore be expressed as

$$v_\phi \simeq v_g - v_{etch} \simeq c[1 - 3\omega_p^2/(2\omega_0^2)] \quad (5.16)$$

where v_g is the linear group velocity of light in a very underdense plasma ($\omega_p^2 \ll \omega_0^2$). The reason to have this term is that the intensity of the very leading front of the laser is always small so it moves roughly with the linear group velocity.

With this phase velocity, we can easily estimate the dephasing length for trapped electrons traveling until they outrun the wave :

$$L_\phi \simeq \frac{c}{c - v_\phi} R \simeq \frac{2}{3} \frac{\omega_0^2}{\omega_p^2} R \quad (5.17)$$

Where R is the wave length of the accelerating field.

5.5.4 Guiding : Self-Guiding or Channel Guiding

Stable optical guiding of the short laser pulse over many Rayleigh lengths is a critical issue for plasma based acceleration. A light pulse can be guided with a nearly constant (matched) spot size by a plasma channel that has a parabolic refractive index/density profile with a maximum/minimum on axis. In the weakly nonlinear regime, the index of refraction in a plasma can be expanded as[85, 26]

$$\eta = ck/\omega \simeq 1 - \frac{1}{2} \frac{\omega_p^2}{\omega_0^2} \left(1 + \frac{\Delta n_c}{n_p} \frac{r^2}{w_0^2} + \frac{\Delta n}{n_p} - \frac{a_0^2}{8} \right) \quad (5.18)$$

where Δn_c parametrizes an external density channel, Δn is a density depletion from the transverse ponderomotive force and the term $a_0^2/8$ is due to relativistic mass corrections. The characteristic density change required to optically guide such a profile with little spot size oscillation is $\Delta n_c = 1/(\pi r_e w_0^2)$ [85], where $r_e = e^2/mc^2$ is the classical electron radius and w_0 is the laser spot size. If the density depression is normalized to the plasma density n_p , this condition becomes

$$\Delta n_c/n_p \simeq 4/(k_p w_0)^2 \quad (5.19)$$

An equivalent change to the index of refraction from relativistic mass corrections can also self-guide a laser if $a_0^2/8 > 4/(k_p w_0)^2$ or $P \geq P_c$, where $P_c = 17\omega_0^2/\omega_p^2[GW]$ is the critical power for relativistic self focusing [55]. As shown by Sun et al. [55] and the discussions in previous subsections, the electron blowout could also be achieved when $P \geq P_c$ and the spot size is sufficiently small (a few plasma skin depths). This will also enhance the effect of guiding. Unfortunately, the index of refraction in a plasma needs a distance on the order of c/ω_p to build up. This is because that the radiation pressure from the leading edge of an intense laser pushes plasma forward leading to a density compression that nearly cancels the relativistic mass increase to the index of refraction. Therefore, it is often thought that a short pulse laser $\tau \lesssim 1/\omega_p$ cannot be self-guided and some form of external optical guiding is needed. However, as described in ref.[86], for $P/P_c \gg 1$ a degree of self-guiding for short pulses is possible because the leading edge of the laser locally pump depletes before it diffracts and the back of the pulse is still guided in the ion column region.

This effect of self-guided propagation is seen in numerous 2D and 3D PIC simulations. These simulations also confirmed that for plasma density larger than $1 \times 10^{18} cm^{-3}$ and laser power $P/P_c \gtrsim 8$, the short pulse laser can be guided

by itself if the spot size is initially chosen as matched. A 3D simulation to show this will be given later.

For even lower plasma density, it is not currently affordable to test the self-guided propagation by fully 3D PIC simulations. However, we can get some roughly scaling based on the physical picture presented above.

we can start from to quasi-static theory where the index of refraction is

$$\eta \simeq 1 - \frac{1}{2} \frac{\omega_p^2}{\omega_0^2} \frac{1}{1 + \psi} \quad (5.20)$$

and it satisfies

$$\frac{\partial^2 \psi}{\partial \xi^2} + \frac{k_p^2}{2} \left[\frac{1 + a^2}{(1 + \psi)^2} - 1 \right] = 0. \quad (5.21)$$

As noted earlier $\frac{1}{1+\psi} - 1 \simeq -\psi$ must equal $4/(k_p w_0)^2$ in order for guiding to occur. For $|\psi| \ll 1$, we assume

$$\frac{\partial^2 \psi}{\partial \xi^2} \simeq -\frac{k_p^2}{2} a^2, \quad (5.22)$$

therefore $-\psi$ builds up to the necessary value in a distance $\Delta\xi$ which scales as

$$\Delta\xi \sim (k_p^2 w_0 a_0)^{-1} \sim (k_p a_0^{3/2})^{-1}. \quad (5.23)$$

The length of the laser that is lost due to diffraction each Rayleigh length (Z_R) will also scale as $(k_p a_0^{3/2})^{-1}$. Self guiding can be achieved if the length lost due to pump depletion in each Rayleigh length also scales the same way:

$$\frac{v_{etch}}{c} \simeq \frac{n_p}{n_c} \sim \frac{\Delta\xi}{Z_R} \Rightarrow a_0 \sim (n_c/n_p)^{1/5} \quad (5.24)$$

As we can see, this is a rather weak dependence on the plasma density. From PIC simulations for $n_p \gtrsim 1 \times 10^{18} cm^{-3}$, we can deduce the coefficient of this scaling roughly as 1.

5.5.5 Injection and Beam Loading

The electron beam riding on the wake can be either self-injected or externally injected from some other source. For self-injection, particles in the rear of the blowout region must be able to catch up with the wake. How the self-trapping processes occurs for a driven plasma wave has already been extensively discussed in chapter 4. The conditions can be summarized as the following two: one is that the field structure is asymmetric due to the existence of the driver (the decelerating part has a sinusoid structure but the accelerating part has a triangle structure and with a deep spike at the tail) so the electrons starting from the laser front can gain more acceleration than deceleration; the other is that the wakefield amplitude should be large enough such that the potential ψ can reach the trapping threshold ($\simeq -1$). To satisfy the latter condition in 3D wakes, simulations show that the blowout radius should be larger than $4 \sim 5$.

Indeed we can also analyze the trapping processes just based on physical pictures: In the blowout regime, two physical conditions need to be satisfied for trapping. first, the blowout radius should be large enough so that when the particles reach the rear of the ion channel, they move predominately in the forward direction with speed close to the speed of light. Second, at the rear portion of the ion channel, trajectory crossing occurs leading to a narrow sheath with the highest accelerating and focusing fields. Therefore, even though electrons initially have energy γ substantially below the wake's Lorentz factor γ_ϕ , they can easily achieve sufficient energy as they are accelerated while they slowly drift

backwards (relatively to the pulse) in the sheath. In our sample simulation (shown in next section), the effective γ of the wake is around 20 and the normalized blowout radius is around 4. The initial energy γ of those trapped electrons is substantially smaller than 20. For even lower plasma densities, we have also performed a number of simulations, where an electron beam with γ exceeding 10000 was used as the driver instead of a laser and we observed self-injected electrons in each case for a normalized blowout radius around 5. This indicates that for laser wavelengths in the $0.8\mu m$ range and plasma densities of interest, self-injection will always happen when we keep the normalized blowout radius around $4 \sim 5$.

As laser propagating, more and more electrons can get trapped in the rear region. When enough charge is accumulated there, the trapped charge may be able to absorb significant amount of energy inside the wake so stop further trapping. This effect is called beam loading and it can be used to estimate how much charge can be accelerated in the wake.

5.5.6 Possible Laser Plasma Instabilities and Laser Pulse Distortions

As we have mentioned before, one great advantage to operate in the blowout regime is the significantly reduced growth rate of various kinds of instabilities. Among these instabilities, some are well understood in the weakly nonlinear regime, for example Raman forward, Raman backward, envelope self-modulation, laser filamentation, laser hosing, laser asymmetrical self-focusing etc.; For these instabilities, although the basic coupling mechanisms do not change fundamentally, their growth rates are significantly changed due to the special characteristics of blowout regime. Most of the growth rate obtained from weakly nonlinear models are unable to give reasonable predictions in the blowout regime. There are

also some other instabilities which only exist in the blowout regime. One example is the electron beam hosing instability when an electron beam is loaded in the wake.

Generally it is very hard to analyze these instabilities theoretically in the blowout regime. There are at least three major difficulties: The first one is the non lamina nature of the plasma flow due to trajectory crossing. This makes it impossible to describe plasma motion by PDEs (partial differential equation). The second one is the highly nonlinear plasma motion due to both fluid and relativistic effects. The third one is the inherent 3D geometry, which makes the description of laser pulse also very difficult. Furthermore, different instabilities tend to couple together. So even in some cases the growth rates for certain instabilities can be derived (e.g., the electron hosing), the coupling between different instabilities and their nonlinear developments will still be too hard to be treated by any simple analytical model. Due to the above reasons, full scale 3D PIC simulations will be the major tool to understand the instabilities in the blowout regime.

Despite the unavailability of quantitative theoretical models, we can still get some rough qualitative understanding about why this regime is more stable comparing with weakly nonlinear regime. We can attribute this low growth of instabilities to the following three reasons:

The first one is the relativistic mass increasing when high intensity is used. The plasma electrons tend to respond slower so that the growth rate will be reduced. This argument is applicable for both 1D and 3D cases. Indeed in the 1D case, Decker et al. analyzed the reduced growth rates for several 1D instabilities.

The second reason is that the laser and the plasma only interact strongly at

the front part of the ion channel. and this part keep etching away due to the local pump depletion before the instabilities can real grow up. This argument is also applicable to 1D case.

The third one is that the major part of the laser is propagating inside an ion channel where the electron density is very low or even zero. In this region the laser plasma interaction can be ignored.

These arguments may well explain the very small growth of most destructive instabilities mentioned above. Indeed many of them are even not observed in full scale 3D simulations that have been done so far. For example, the Raman , the envelope self-modulation, filamentation are not observed and it seems they will play very little role in the blowout regime. For some others like laser hosing, asymmetrical self-focusing and electron hosing, the roles they can play are still not very clear although current 3D simulations do not show their growth.

Here we can show some observations from a group of 3D PIC simulations to see how stable this regime is. The parameters for these simulations are basically the same as we showed in Fig.5.1. A 30fs, 6TW laser propagates in a shallow plasma density channel with $n_p = 5 \times 10^{18} cm^{-3}$ and $\Delta n_c/n_p = 0.5$. For this laser power and plasma density, $P/P_c = 1$, therefore the matched laser spot size is chosen as $k_p W_0 = 2\sqrt{2}$. In this simulation, a clear blowout occur at the very beginning as shown in Fig.5.1 and the laser propagates stably for more than $10Z_r$ without noticeable oscillation of the laser centroid (the laser hosing).

Furthermore, we also did simulations with asymmetric spot sizes (10% difference in two transverse dimensions) or with non-Gaussian shape (two identical laser pulses with center off each other by half spot size). Both cases show no evidence of either laser hosing or asymmetrical self-focusing.

These simulations are very different with the predictions from weakly nonlin-

ear laser hosing theory. The growth rate of laser hosing for a short laser pulse in the weakly nonlinear regime is:

$$N_e = \frac{3\sqrt{3}}{4} (\alpha_3 \frac{P}{P_c} k_p^2 \xi^2 \frac{Z}{Z_r})^{1/3} \quad (5.25)$$

where $\alpha_3 = \sqrt{2}(2 - \frac{P}{P_c})^{-1/2}$. For the parameters of our simulations, the e-folding number for $k_p \xi \approx \pi$ is about 6.4. Even the initial noise of the laser centroid is very small (e.g., less than $0.001W_0$), the laser can still has large centroid oscillation (comparable to the spot size). However, in these simulations, we hardly see any oscillation of the centroid.

In the future, the stability for even longer distances (e.g., $100Z_r$) will be checked by simulations when they become affordable.

Other than instabilities, there are some other effects that may induce laser pulse distortion during laser propagation. Photon deceleration and GVD (group velocity dispersion) are two examples. Luckily, current simulations show that they may not significantly affect the accelerating structure until close to pump depletion. More detailed study is needed in the future.

5.6 Phenomenological Scaling and Its Verification by PIC Simulations

Based on the physics discussed in previous sections, we can draw the following conclusions: a practical LWFA should operate in the blowout regime with matched laser profile; the laser pulse guiding can be achieved by either self-guiding or plasma channel guiding; The accelerated electron beams can be either self-injected or external injected. In this section, we will derive a group of scaling laws and their coefficients for electron beam energy, beam charge and efficiency for

the blowout regime. These scaling laws give a recipe for how to extend the results from the recent experiments towards a more stable regime conducive to making an accelerator. These scaling laws suggests that by using near term lasers in the 0.1 to 3PW range it will be possible to generate of $1 - 13GeV$ mono-energetic electron beams with nC of charge in a single stage without the need for external guiding, and if external guiding is used, energies up to $120GeV$ can be achieved.

To verify our results, we have carried out many computer experiments using the 3D, particle-in-cell code OSIRIS [?], that explore a wide range of plasma densities, laser powers, and spot sizes. We highlight one simulation that is very relevant to near term experiments. In this simulation, a diffraction limited $30fs$ (FWHM) $0.8\mu m$ laser pulse containing 200 TW of power is focused to a spot size $w_0 = 19.5\mu m$ at the entrance of a $1.5 \times 10^{18} cm^{-3}$ density plasma to give a normalized vector potential of $a_0 = 4$. The laser is circularly polarized (with normalized vector potential $4/\sqrt{2}$ in each direction) and has a Gaussian transverse profile and a symmetric temporal profile of $10\tau^3 - 15\tau^4 + 6\tau^5$ where $\tau = \sqrt{2}(t - t_0)/\tau_{FWHM}$. The total plasma is $0.75cm$ long which corresponds to more than 5 Rayleigh lengths. The computational window of this simulation is of dimension $101.9 \times 127.3 \times 127.3\mu m^3$ which moves at the speed of light. The number of gridpoints is $4000 \times 256 \times 256 = 2.62 \times 10^8$. The resolution in the laser propagation direction z is $k_0\Delta z = 0.2$. We assume a preformed fully ionized plasma with uniform density profile. The resolution in the transverse direction is $k_p\Delta x = k_p\Delta y = 0.116$. We use 2 electrons per cell and a smooth neutralizing immobile ion background (the total number of particles is roughly 500 million). The total simulation time-steps is 300,000.

With given laser peak power P and the plasma density n_p , we need to choose the matched laser spot size for stable wake excitation. As discussed in last section,

the normalized vector potential a_0 and normalized laser spot size $k_p w_0$ can be calculated from the following formulas:

$$a_0 \simeq 2(P/P_c)^{1/3} \quad (5.26)$$

and

$$k_p w_0 \simeq 2\sqrt{2}(P/P_c)^{1/6} \quad (5.27)$$

With these proper chosen laser intensities and spot sizes, the laser pulses can be either self-guided or channel-guided over long interaction distance without significant variations. In figure 5.7, The stable self-guiding of an intense short pulse over five Rayleigh lengths is illustrated.

To achieve self-guiding, the laser power needs to be much larger than the critical power for relativistic self-focusing P_c . A rough condition is derived in last section:

$$a_0 \simeq 2(P/P_c)^{1/3} \gtrsim (n_c/n_p)^{1/5} \quad (5.28)$$

If the self-guiding condition is not satisfied, a plasma density channel needs to be used. To get the proper channel depth, we first calculate the matched laser spot size from the above formulas ($P/P_c \gtrsim 1$ is needed for this calculation to be meaningful), then we calculate the channel depth Δn_c from linear guiding formula:

$$\Delta n_c = \frac{4n_p}{(k_p w_0)^2} \quad (5.29)$$

Under the conditions for stable wake excitation, we can estimate the energy gain of a self-injected or external injected electron beam by using the obvious equation

$$\Delta E = qE_{LW}L_{acc} = \epsilon_{LW}l_{acc}mc^2 \quad (5.30)$$

where E_{LW} is the average accelerating field of the beam loaded wake, L_{acc} is the acceleration length, $\epsilon_{LW} \equiv eE_{LW}/(mc\omega_p)$ and $l_{acc} = \omega_p L_{acc}/c$.

The desired acceleration length is the dephasing length obtained in last section:

$$L_{acc} = L_\phi \simeq \frac{c}{c - v_\phi} R_m \simeq \frac{2\omega_0^2}{3\omega_p^2} R_m \simeq \frac{4\omega_0^2}{3\omega_p^2} \sqrt{a_0} k_p^{-1} \quad (5.31)$$

Based on the discussions on laser etching and pump depletion, we impose the condition

$$L_{etch} \gtrsim L_\phi \Rightarrow c\tau_{FWHM} \gtrsim 2R_m/3 \approx 4\sqrt{a_0}k_p^{-1}/3 \quad (5.32)$$

If the pulse is too short dephasing will not be reached, and the electron beam may have significant energy spread. We note that this condition is approximate, since the laser starts diffracting as soon as its intensity is insufficient to sustain self focusing and this happens before the pulse is completely pump depleted. Additionally the injected particles need to slightly pass the dephasing point (phase space rotation) so that the energy spread is minimum. On the other hand, the length of the pulse should not be too large, because the laser field could interact with the trapped electrons and degrade the beam quality.

ϵ_{LW} is the average accelerating field experienced by an electron, $\langle E_z \rangle$. From the discussions on the wakefield structure in last section, we know that for $a_0 \gtrsim 2$

and $k_p R_m \gtrsim 3$, the ion column roughly formed a sphere and that the accelerating field, for the most part, depends linearly on the distance from the middle of the sphere (figure 5.8(a)). This can be also seen in figures 1(a)-(c) where the region void of electrons roughly forms a circle and in figures 2(a),(b) where a lineout of $eE_z/(mc\omega_p)$ along the axis is shown.

The blowout region is roughly a sphere and the electrons are either self or externally injected at the rear, the electrons can travel a relative distance R_m before they dephase. The peak useful accelerating field is $eE_{z,max}/(mc\omega_p) = \sqrt{a_0}$ and because the wakefield is roughly linear, the average field is half of the peak:

$$\epsilon_{LW} \equiv eE_{z,max}/(2mc\omega_p) \simeq \sqrt{a_0}/2 \quad (5.33)$$

With the expressions for l_{acc} and ϵ_{LW} , We can therefore write the approximate equation for the energy gain as:

$$\begin{aligned} \Delta E &\simeq \frac{2}{3}mc^2 \left(\frac{\omega_0}{\omega_p}\right)^2 a_0 \\ &\simeq mc^2 \left(\frac{P}{m^2 c^5 / e^2}\right)^{1/3} \left(\frac{n_c}{n_p}\right)^{2/3} \\ \Delta E [GeV] &\simeq 1.7 \left(\frac{P[TW]}{100}\right)^{1/3} \left(\frac{10^{18}}{n_p[cm^{-3}]}\right)^{2/3} \left(\frac{0.8}{\lambda_0[\mu m]}\right)^{4/3} \end{aligned} \quad (5.34)$$

We can see that there is a much stronger dependence of the beam energy on the plasma density n_p than on the input laser power P . However, when the plasma density is lowered for fixed power, ensuring self-guided propagation of the leading edge of the laser is more challenging. This can be accomplished by plasma channels and to some degree by self-guiding. As we argue in last section, for self-guiding to occur P/P_c needs to increase as the plasma density decreases. On the other hand, if plasma channel is used, P/P_c can be kept as low as 1.

We can rewrite equation (5.34) in terms of the critical power for relativistic self-focusing, P_c :

$$\Delta E[GeV] \simeq 3.8 \left(\frac{P}{P_c} \right)^{-2/3} \frac{P[TW]}{100} \quad (5.35)$$

This equation reveals that for a constant ratio P/P_c the trapped particle energy scales linearly with the laser power. So we can simply scale one group of parameters to achieve higher energy by increasing the laser power and decreasing the plasma density by the same ratio.

The number, N , of electrons that are accelerated can be estimated from energy balance. Hence we examine the partition of field and particle energy within the first bucket. The fields inside the ion column have E_z , E_r , and B_ϕ components. In addition there is kinetic energy in the sheath. In a 3D linear or 1D nonlinear wake the fields and kinetic energy scale together. This is not the case for these 3D nonlinear wakes where an increasing percentage of energy ends up to the electron sheath for higher laser intensity. Integrating the field energy in the ion channel we find equipartition between the energy in the longitudinal field \mathcal{E}_l and the focusing fields \mathcal{E}_f :

$$\mathcal{E}_l \simeq \mathcal{E}_f \simeq \frac{1}{2}\mathcal{E} = \frac{1}{120}(k_p R)^5 \left(\frac{m^2 c^5}{e^2 \omega_p} \right) \quad (5.36)$$

The trailing particles can only recover the energy in the fields and much of the kinetic energy is left behind. By equating \mathcal{E} with the energy absorbed by N particles that travel across the ion channel (we assume the average field felt by these particle is $E_{z,max}/2$), we obtain:

$$N \simeq \frac{1}{30}(k_p R)^3 \frac{1}{k_p r_e} = \left(\frac{\beta^3}{\alpha} \right) \frac{8/15}{k_0 r_e} \sqrt{\frac{P}{m^2 c^5 / e^2}} \quad (5.37)$$

where $\alpha = k_p w_0 / (2\sqrt{a_0})$ and $\beta = k_p R / (2\sqrt{a_0})$. Using equation (5.10) $\alpha \simeq 1 \simeq \beta$ we obtain:

$$N \simeq \frac{8/15}{k_0 r_e} \sqrt{\frac{P}{m^2 c^5 / e^2}} \simeq 2.5 \cdot 10^9 \frac{\lambda_0 [\mu m]}{0.8} \sqrt{\frac{P [TW]}{100}} \quad (5.38)$$

The efficiency scales as the total energy \mathcal{E}_b in the accelerated electron beam (energy gain equation (5.34) times particle number from equation (5.37)) devived by the total laser energy \mathcal{E}_T (assuming $c\tau \simeq 2\sqrt{a_0}c/\omega_p$):

$$\Gamma \sim \mathcal{E}_b / \mathcal{E}_T \sim 1/a_0 \quad (5.39)$$

which indicates that a_0 , i.e., $(P/P_c)^{1/3}$ cannot be too large if one needs high efficiency.

For a $200TW$, $0.8\mu m$ pulse equation (5.38) predicts $0.6nC$ of charge. The charge measured from the simulation for the first bunch is $0.3nC$. We have also verified these scaling laws by monitoring how the wake is loaded by externally injected electron bunches.

As shown in figure 5.7(d), the acceleration process stops before the accelerating bunch dephases. This will not lead to any considerable modifications of the aforementioned formulas, particularly because the pump depletion length scales as the dephasing distance and the accelerating wakefield decreases as the trapped electrons approach the center of the sphere.

The beam energy seen in the simulation, 1.5 GeV, is close to that calculated theoretically from Eq. (5.34) which is (5.34) $\Rightarrow \Delta W \simeq 1.6GeV$. Using formulas (5.15)-(5.31) we see $L_\phi \simeq 1.31cm > 0.96cm \simeq L_T$ which is in agreement with our observation that pump depletion happened before dephasing. In fact, as mentioned earlier the pulse started diffracting at $0.75cm < 0.96cm$, that is to say

before all of its energy was lost. Therefore, even though eq. (5.34) is not strictly valid for our simulation the estimate from it is excellent.

In spite of the complexity of the physics associated with this interaction, the predictions by the simple formulas presented in this article are very close to 3D PIC simulation results. Good agreement is also achieved between these scaling laws and recent experimental results [60, 61, 62] which were slightly below the “threshold” for the blowout regime. To be in the regime identified by a spherical channel, one needs $a_0 \gtrsim 4$ or equivalently $P/P_c \gtrsim 8$ and $c\tau < 2\sqrt{a_0}c/\omega_p$ which leads to the condition that $P \gtrsim 30(\tau/30fs)TW$. These conditions can be relaxed for channel-guided lasers for which P/P_c may be smaller. It is then written as $a_0 \gtrsim 2$ or $P/P_c \gtrsim 1$. We present the comparison between the scaling law for the energy Eq. (5.34) and the aforementioned results in figure 5.10.

Other than the beam energy, charge, the quality of the electron beam is also very important for any practical application. In the regime presented here the self-injected electron bunches are highly localized in space with a half-width of the first bunch of only $\sim 10fs$, i.e. $1c/\omega_p$. Once a sufficient number of electrons have been trapped the trapping process terminates, as seen in figure 5.7(c). The first electron bunch reaches an energy of 1.5 GeV and its energy spectrum is presented in figure 5.8(c). The normalized emittances are shown in figure 5.9. They may be estimated as the product of the beam spot size, which roughly scales with $1/\sqrt{n_p}$, with the uncertainty in the momentum perpendicular to the acceleration direction, which scales with a_0 . These simple considerations show that as we move to lower densities in order to achieve higher energy particles the emittances of the self-injected electrons will increase. This suggests that for the electron beam to be useful for high energy physics or light source, external injection may be more attractive. As an interesting aside, simulations also reveal

the trapping and acceleration of a second distinct bunch in the second bucket (see figure 5.8(c)), which has a lower energy because the average electric field it experiences is smaller.

To summarize, the scalings derived above and the underlying physics predict that it is advantageous to use moderate intensities and very low plasma densities to increase the output energy and keep the efficiency high. The simulations also show that the injection process can be clamped and the energy spread of the electron beam is much less in the regime we are proposing, which indicates that this regime is also amenable to accelerating externally injected beams while maintaining good beam quality.

5.7 Comparison with the Scaling Based on Similarity Theory

It is interesting to point out the differences between the scaling laws we derived here with those obtain from a similarity theory by Gordienko and Puhkov (GP) [80]. In their work, they are more interested in the so called "bubble" regime where very high laser intensity ($a_0 \gg 1$) and high plasma densities ($n_p \sim 0.01 \sim 0.08n_c$) are used. They argued that for $a_0 \gg 1$ the speed of all plasma electrons is very close to the speed of light. Under this condition all quantities will scale with a single similarity parameter, $S \equiv \frac{n_p}{n_c a_0}$. The coefficients in front of the scalings are determined from simulations (or experiments). The resulting expressions are therefore only strictly valid so long as the laser's transverse and longitudinal profile, aspect ratio etc. remain the same. In contrast, our approach presented here is to use a phenomenological description. We identify the important physics as wake excitation (amplitude and phase velocity),

pump depletion (pulse evolution), dephasing (between particles and wake), and beam loading. We then use these concepts to develop expressions for predicting the number of electrons, the electron energy, and overall efficiency, including the coefficients.

It is instructive to compare the scaling laws described here for the blowout regime against those obtained in ref.[80] using a similarity theory for the “bubble” regime. The key assumption of ref.[80] was that $a_0 \gg 1$. For the energy gain, they obtained

$$E_{mono} \approx 0.65mc^2 \sqrt{\frac{P}{m^2 c^5 / e^2}} \frac{c\tau}{\lambda} \quad (5.40)$$

This formula also implies a dependence on plasma density because $c\tau \approx w_0 \approx \sqrt{a_0}c/\omega_p$ is assumed. Under these optimum conditions, formula (5.40) can be rewritten as

$$E_{mono} \approx 0.16mc^2 \frac{c\tau}{w_0} \left(\frac{P}{m^2 c^5 / e^2} \right)^{2/3} \left(\frac{n_c}{n_p} \right)^{1/3} \quad (5.41)$$

Comparing with the formulas obtained in last section, we can immediately notice the stronger dependence of the energy on the power in these formulas.

It turns out that the difference between the scaling laws presented here and those from similarity theory lie in the scaling for L_{acc} . We have argued in previous sections that L_{acc} is limited because the pulse pump depletes primarily by giving kinetic energy to the electrons. An electron at the front of the laser is pushed forward and to the side. As argued in ref. [86] and in previous sections, each electron gains an amount of energy that scales as $(a_0^2/2)mc^2$. Since the laser’s energy also scales as a_0^2 this “1D like” pump depletion distance is independent of laser intensity. However, for extremely large a_0 electrons can move forward

with a velocity greater than the velocity of the leading edge of the pulse; which is at most the linear group velocity. Equating the forward going velocity of a single electron to the linear group velocity gives an estimate for a critical value for the laser amplitude, $a_{0c} \approx 2\sqrt{n_c/n_p}$. We can see that for high plasma density $n_p/n_c \approx 0.01 \sim 0.08$ the critical value for a_0 is $a_{0c} \approx 20 \sim 8$, but for lower plasma densities $n_p/n_c \sim 0.001$, $a_{0c} \gtrsim 70$.

For laser amplitudes above this critical value the laser will pump deplete more slowly because the kinetic energy given to the each electron will no longer scale as a_0^2 . In this limit a constant percentage of the energy may go into the fields of the wake and $\Gamma \sim \text{constant}$ as predicted by ref. [80]. The pump depletion length, L_{pd} , can then be estimated from energy balance,

$$\frac{E_0^2}{8\pi} c\tau \approx \frac{E_z^2}{8\pi} L_{pd} \Rightarrow L_{pd} \approx \frac{a_0^2 \omega_0^2}{\epsilon^2 \omega_p^2} c\tau \approx \frac{1}{4} a_0 \frac{\omega_0^2}{\omega_p^2} c\tau \sim a_0 L_{etch} \quad (5.42)$$

which does depend on a_0 . Using this scaling for L_{acc} in equation (5.30) provides the same scaling for the particle energy as obtained from similarity theory. However, even for this high intensity limit dephasing will still occur because the leading edge cannot move faster than the linear group velocity of the highest frequency component, since at the very front the amplitude is small.

It may be interesting to see the differences between all available scaling laws for LWFA in just one table. In Table 5.1, we made such a list. These include the linear scaling laws in a 1996 paper. In this paper design formulas based on 1D linear theory was presented. This paper also gave a version of 1D nonlinear scaling. However this nonlinear version is incorrect. So a well known 1D nonlinear scaling is also listed in the table. We also list our scaling and the similarity scaling from GP.

Table 5.1: Comparison of Different Scaling Laws

	a_0	$k_p W_0$	ϵ	$k_p L_d$	$k_p L_{pd}$	$k_p \lambda_w$	γ_ϕ^*	$\Delta W/mc^2^{**}$
Linear (1996)	< 1	2π	a_0^2	γ_ϕ^2	$a_0^{-2}(\omega_0/\omega_p)^2$ $\omega_p\tau$	2π	ω_0/ω_p	$a_0^2(\omega_0/\omega_p)^2$ (use L_{dp})
Nolinear 1D (1996)	> 1	2π	a_0		$a_0^{-2}(\omega_0/\omega_p)^2$ $\omega_p\tau$			$a_0^{-1}(\omega_0/\omega_p)^2$ $\omega_p\tau$
Nolinear 1D	> 1	2π	a_0	$4\gamma_\phi^2 a_0$	$(\omega_0/\omega_p)^2 \omega_p\tau$	$a_0 2\pi$	(ω_0/ω_p) $a_0^{1/2}$	$a_0^2(\omega_0/\omega_p)^2$ (L_{pd} , $\omega\tau = a_0$)
Nolinear 3D Matched	> 2	$2a_0^{1/2}$	$a_0^{1/2}$	$\gamma_\phi^2 a_0^{1/2}$	$(\omega_0/\omega_p)^2 \omega_p\tau$	$4a_0^{1/2}$	(ω_0/ω_p) $/\sqrt{3}$	$\frac{4}{3}a_0(\omega_0/\omega_p)^2$
GP	> 20	$a_0^{1/2}$	$a_0^{1/2}$		$a_0(\omega_0/\omega_p)^2$ $\omega_p\tau$			$a_0^{3/2}(\omega_0/\omega_p)^2$ $\omega_p\tau$

5.8 Parameter Design for Future

We can easily extrapolate the blowout regime to 10GeV and beyond. As suggested by the scaling laws, if we keep P/P_c fixed, then the laser power and inverse of the density scale with the desired electron energy and the pulse length will scale as the electron energy to the 1/2 power. If we scale up our sample simulation, to obtain 15GeV we need a 2PW, 100fs laser and a plasma with density of $1.5 \times 10^{17} cm^{-3}$. From the discussions on self-guiding, we know that for this low plasma density and laser power, channel guiding is needed. If self-guiding is preferred for the same laser power, the scaling on self-guiding suggests that we can $P/P_c \simeq 28 \Rightarrow a_0 \simeq 6$ and a density $n = 4 \times 10^{17} cm^{-3}$. For these parameters stable self guiding should occur and lead to acceleration of $2nC$ charge at approximately 9GeV after 10cm of laser propagation. Carrying out a full-scale PIC simulation for the 10cm of propagation distance is beyond current capabilities. However, we have carried out a 3D PIC simulation for a short propagation distance to verify that electrons will still be self-injected. Results are shown in figure 5.11.

If both the technology for making meter scale ($0.1m \sim 1m$) low density plasma channels for guiding and for synchronized external injection are developed, then much higher energy gain can be achieved for the same laser power. For example, using $P/P_c \simeq 1$ and a plasma density channel with channel depth $\Delta n_c/n_p = 0.5$, a 10GeV electron beam with $0.7nC$ charge could be obtained with a 250TW, 100fs laser and a 43cm long plasma channel with a minimum density $n = 1.2 \times 10^{17} cm^{-3}$. Extrapolating the parameters further, we can predict that a 120GeV electron beam with $2nC$ charge can be generated by using a 3PW, 350fs laser and 18m long plasma channel with density $n = 1.0 \times 10^{16} cm^{-3}$.

In Table 5.2, we show a list of designs in two different setups for reaching the same energy scale. The first setup is using external guiding and external injection

by keeping $P/P_c = 1$ and $\Delta n_c/n_p = 60\%$. The third setup is using self-guiding and self-injection by choosing P/P_c just enough for self-guiding.

Table 5.2: Parameter Design for GeV and Beyond

$P(PW)$	$\tau(fs)$	$n_p(cm^{-3})$	$W_0(\mu m)$	$L(m)$	a_0	$\Delta n_c/n_p$	$Q(nC)$	$E(GeV)$
0.02	30	1×10^{18}	14	0.016	1.76	60%	0.18	0.99
0.10	30	2×10^{18}	15	0.009	3.78	0%	0.40	1.06
0.20	100	1×10^{17}	45	0.52	1.76	60%	0.57	9.9
2.0	100	3×10^{17}	47	0.18	5.45	0%	1.8	10.2
2.0	310	1×10^{16}	140	16.3	1.76	60%	1.8	99
40	330	4×10^{16}	146	4.2	7.6	0%	8	106
20	1000	1×10^{15}	450	500	1.76	60%	5.7	999
1000	1000	6.5×10^{15}	460	82	12.1	0%	40	1040

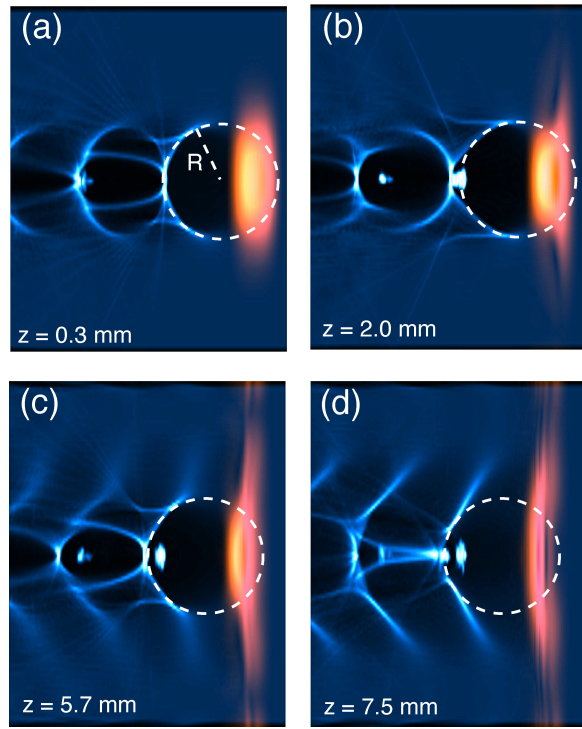


Figure 5.7: A sequence of 2-dimensional slices ($x - z$) reveals the evolution of the accelerating structure (electron density, blue) and the laser pulse (orange). Each plot is a rectangular of size $z = 101.7\mu\text{m}$ (longitudinal direction, z) and $x = 129.3\mu\text{m}$ (transverse direction, x). A broken white circle is superimposed on each plot to show the shape of the blown-out region. When the front of the laser has propagated a distance, (a) $z = 0.3\text{mm}$ the matched laser pulse has clearly excited a wakefield. Apart from some local modification due to beam loading effects, as seen in (b) this wakefield remains robust even as the laser beam propagates though the plasma a distance of 7.5mm (as seen in (c) and (d)) or 5 Rayleigh lengths. After the laser beam has propagated 2mm (as seen in (b)) into the plasma, one can clearly see self-trapped electrons in the first accelerating bucket. The radial and longitudinal localization of the self-trapped bunch is evident in part (c). After 7.5mm the acceleration process terminates as the depleted laser pulse starts diffracting.

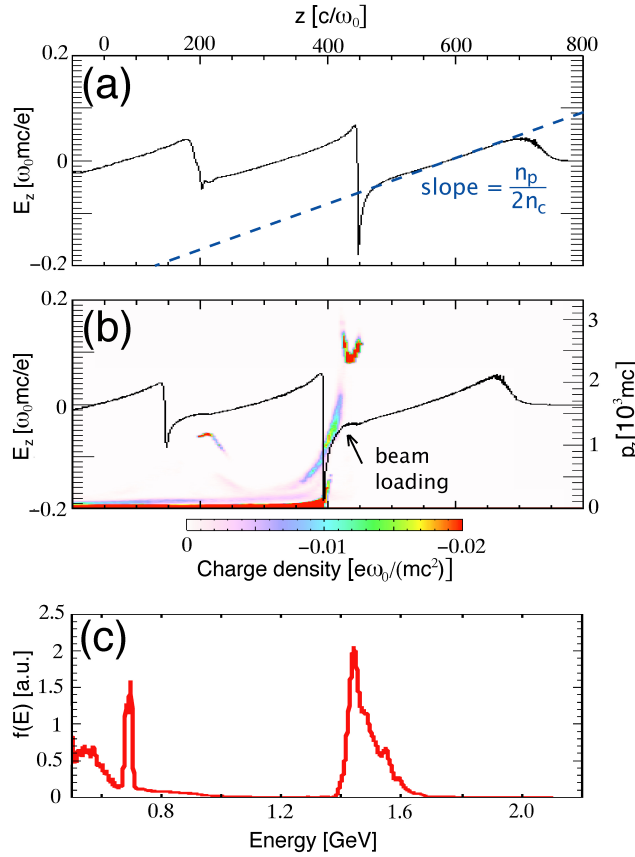


Figure 5.8: (a) A lineout of the wakefield along the z axis after $0.3mm$ shows that within the first bucket the slope of the wakefield is nearly constant and equal to $eE_z/(mc\omega_p) \simeq \xi/2$ where $\xi = (k_p(ct - z))$. After $5.7mm$ of propagation (b) the wakefield has been modified by beam loading (flattening of the wake between $400 - 450c/\omega_p$). This is corroborated by the p_z vx z plot that is superimposed on the lineout of the wakefield. Pictures (a) and (b) reveal that the acceleration mechanism is extremely stable during the simulation. The energy spectrum after $7.5mm$ (c) exhibits an isolated spike of $0.3nC$ at $1.5GeV$ with energy spread $\Delta\gamma/\gamma = 3.8\%$ corresponding to the first bucket and a second spike of $50pC$ at $700MeV$ with energy spread $\Delta\gamma/\gamma = 1.5\%$ corresponding to the second bucket.

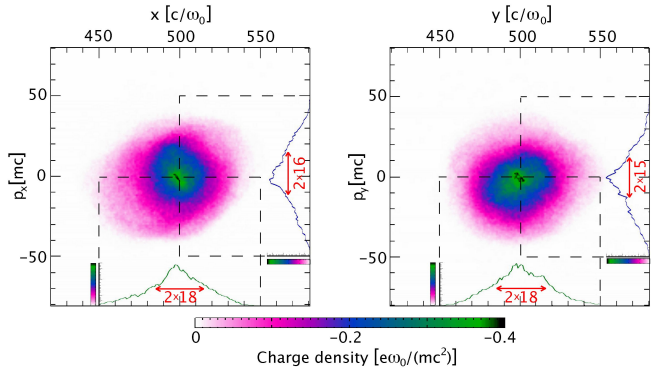


Figure 5.9: The normalized emittance $[\varepsilon_N]_i = \pi\sqrt{\langle\Delta p_i^2\rangle\langle\Delta x_i^2\rangle - \langle\Delta p_i\Delta x_i\rangle^2}$ (where Δp_i is normalized as indicated by the figure and the emittance is in units of Δx_i) and is the approximate area in phase space $p_i x_i$. For the pictures above which correspond to the first bunch this formula yields: $[\varepsilon_N]_x \simeq 35\pi \cdot mm \cdot mrad$ and $[\varepsilon_N]_y \simeq 29\pi \cdot mm \cdot mrad$. An upper limit for the emittance can be found by multiplying the typical divergences shown in the figure; this method leads to an overestimation which for this case is about 25%. For the second bunch of accelerated electrons (not shown in this figure) the emittances are significantly lower: $[\varepsilon_N]_x \simeq 10\pi \cdot mm \cdot mrad$ and $[\varepsilon_N]_y \simeq 11\pi \cdot mm \cdot mrad$.

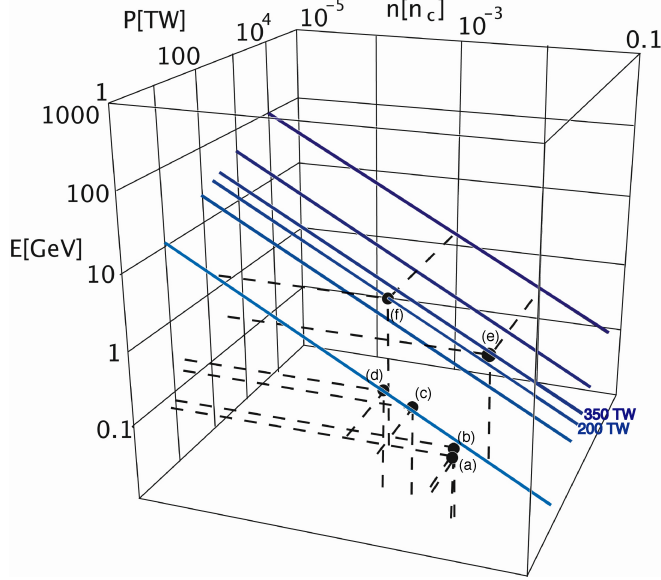


Figure 5.10: $E[GeV]$ vs. power $P[TW]$ and density n/n_c from equation 5.34 : The blue lines of constant power show the strong dependence of the energy of the self-trapped electrons to the density. The black points correspond to: (a) experiment [60], (b) experiment [61] which uses a channel for guiding, (c) experiment and 3D PIC simulation [62], (d) 3D PIC simulation [59] which uses a channel for guiding, (e) A 3D PIC simulation in [58], (f) 3D PIC simulation presented in this article. Each of these points is very close to one of the blue lines indicating agreement with our scaling law.

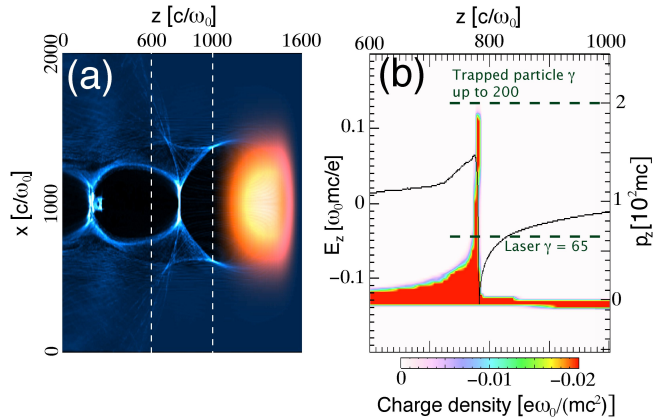


Figure 5.11: Picture (a) shows the laser electric field with orange on top of the electron density with blue after $0.4mm$ of propagation. The laser front is chosen sharper than the back because it has been found through simulations that this leads to more stable propagation. The blowout region is well formed. Picture (b) shows that particles at the rear of the ion channel have already reached velocities higher than the laser velocity and therefore are trapped. The region in z direction plotted in picture (b) corresponds to the z region between the broken lines in picture (a).

CHAPTER 6

Prospects for Plasma Based Acceleration in the Blowout Regime

6.1 Summary

The electron “cavitation” or “blowout” is a remarkable nonlinear phenomena in laser-plasma and beam-plasma interaction. It can occur naturally when an intense short-pulse laser or short ultra-relativistic electron beam interacts with a underdense plasma. In literature, the term “blowout regime” is used when this phenomena occurs. Recently, the blowout regime has attracted great interests in plasma based acceleration for accelerating electrons. Many important simulation and experiment results are reported for both LWFA and PWFA. Among them the following two are most exciting: the self-injected mono-energetic electron beams with energy range from $100MeV$ to GeV and with duration less than $50fs$, energy gain up to $42GeV$ of the tail of an incoming $42GeV$ electron beam in less than one meter. Clearly, there is much need for the understanding of the relevant physics in this regime. Indeed, much simulation work have been done to compare with experiments. However, there is little progress in the theoretical understanding of many important issues in this regime until very recently. The major reason for this is that this regime is highly nonlinear (e.g., relativistic effects) and highly non-lamina (trajectory crossing occurs) such that most

well-developed mathematic methods (e.g., PDEs and weakly nonlinear approximations) are not applicable to describe it. The motivation for this dissertation is to change the above situation. We developed a nonlinear theoretical framework that can address many important problems in the blowout regime. These include how the wake is excited and how to parametrize the blowout regime, how to optimize the wake fields for a given driver parameters and how to optimize the driver shape to achieve higher transformer ratio, how to describe beam loading, how to describe the electron hosing instability of short electron bunches, How to explain self-injection occurring in a multi-dimensional wake and How to scale the recent experimental results to higher energy and better beam quality. The major results are the following:

1. A nonlinear non-fluid theory for the excitation of multidimensional plasma wave wakes in the blowout regime is formulated. By using this theory one can predict the wakefield amplitudes and blowout radius in terms of the electron beam or laser beam parameters, as well as predict the nonlinear modifications to the wakes wavelength and wave form. For electron beam driver, a single parameter Λ , the normalized charge per unit length, is found to be able to characterize the major features of the channel shape and the wakefield. Two distinct regimes are identified, namely the non-relativistic blowout regime and the ultra-relativistic blowout regime. For the non-relativistic blowout regime, when linear fluid theory breaks down and how this leads to a saturation of the logarithmic divergence in the linear Greens function are shown. For the ultra-relativistic blowout regime, the requirements for forming a spherical wave form, i.e., bubble, are identified. The key differences between laser driver and electron beam driver are also discussed.
2. The optimum plasma density to obtain the largest wakefield for given

electron beam parameters is analyzed. It is shown that for recent and future electron beam parameters, the optimum density can be ten times larger than the prediction of linear theory. When the linear prediction is a good guide and when the nonlinear analysis must be used are discussed.

3. The beam loading issue in the blowout regime is discussed. A simple formula for the maximum number of particles that can be loaded in the wake is given. It is shown that much more charge can be loaded in the blowout regime than that the linear theory predicts.

4. The wake amplitude and transformer ratio for a linear ramped electron driver are derived. It is shown that high transformer ratio can be achieved in the blowout regime by using similar beam profile from linear theory.

5. The electron hosing instability in the blowout regime is analyzed by using a linear perturbation on the plasma electron blowout trajectory. The growth of the hosing instability is found to be affected by the plasma self-fields, the relativistic mass, the axial motion of plasma electrons and the position-dependent ion channel radius respectively. The new theory is fully relativistic and the growth rate for a electron beam with a simple current profile can be solved numerically. PIC simulations agree well with this new theory which predicts a smaller hosing growth for a non-adiabatically formed ion channel as in current plasma wakefield acceleration experiments than for a preformed ion channel case.

6. An extensive analysis of electron trapping and self-injection in arbitrary electromagnetic fields with translation symmetry is given. The general trapping condition and limit on energy gain are derived. Based on this analysis, the physical meaning of wavebreaking limit derived from 1D fluid theory is discussed. It is shown that the 1D wave breaking limits are not achievable in a system with a driver because particle trapping and significant loading of the wake will occur

far before the theoretical wave breaking limit is reached for both 1D and multi-dimensional wakefields. This analysis clarifies a subtle point that has confounded plasma physicists about the meaning of wave breaking for driven wakes for many years .

7. what is the possible parameter regimes for LWFA that might be useable in a real accelerator is discussed. Starting by considering requirements for any high energy physics accelerator regarding the stability, the number of accelerated electrons, their beam quality and the over all efficiency, the implications of the weakly nonlinear wakefield regime are presented. This exercise illustrates that the assumption of a weakly nonlinear wake is inconsistent with these requirements and that the blowout regime is the natural result. We then provide a phenomenological theory for LWFA and use it to obtain expressions that can be used to extrapolate this regime to higher energies, namely 1GeV -1Tev. We also present 3D PIC simulation results that are in agreement with our theory.

6.2 Future Work

Despite the significant progress of experiment, theory and simulation achieved recently in the research on plasma based acceleration, much remains to be done to justify plasma based acceleration as a viable technology for building accelerators. Regarding to the experimental technology, the improvement of the power and quality of the drivers and the inventions of new diagnostic methods are definitely among the most important thing to do. Regarding to the theory and simulation, many important issues still lack satisfactory answers. It is impossible for me to give a full review of these topics. Instead, I will just list a few topics that is closely related to the work in this dissertation.

First, systematic simulations for various laser-plasma and beam-plasma instabilities that may occur in the blowout regime should be pursued. For example, the electron hosing instability for asymmetric beam, the laser hosing, the laser asymmetric self-focusing et al.. Although most of these instabilities do not show significant effect in current simulations, they may play a role when $100GeV$ to TeV stages are considered. Based on these simulations, simple theoretical models may be constructed to identify key physical issues.

Second, it is very important to tailor the laser or electron beam parameters and the plasma parameters to achieve the best possible results. This is a critical step for building real machines. For example, relevant problems include how to choose the laser intensity and frequency profile to reduce the laser distortion, how to beam load the charged particle beam of sufficient charge at the right phase to achieve very small energy spread, how to change the plasma density profile (e.g., a density down ramp) to increase the energy gain from a LWFA et al.. Clearly, to answer questions like these needs a close interaction between theory and simulation and also a clear awareness of the feasibility of experimental technology.

Third, for plasma based acceleration to be useful for high energy physics, it is important to find out a way to efficiently accelerate positrons. It is clear that the blowout regime can not be used because the defocusing field inside the ion channel for positrons. A systematic research on what regime can be used to accelerate positron (similar to our analysis of the blowout regime) should be carried out.

Last, although it is shown in this dissertation that to efficiently accelerate large number of electrons ($\sim nC$) needs LWFA to operate in the blowout regime, the weakly nonlinear regime is still of interests when low charge (10s of pC) high

rep rate (kHz) system is considered. A systematic research on how to improve efficiency and stability for this kind of low charge system is definitely worth doing.

REFERENCES

- [1] A. Zee , ” Quantum Field Theory in a Nutshell”, Princeton University Press (March 10, 2003)
- [2] D. Strickland, G. Mourou, “Compression of amplified chirped optical pulses ”, Opt. Comm. 56, 219 (1985)
- [3] P. Maine, D. Strickland, P. Bado, M. Pessot, G. Mourou,“Generation of ultrahigh peak power pulses by chirped pulse amplification”, IEEE J. Quantum Electron. QE-24, 398 (1988)
- [4] G. Mourou, D. Umstadter, “Development and applications of compact high-intensity lasers”, Phys. Fluids B 4, 2315 (1992)
- [5] K. Yamakawa, P.H. Chiu, A. Magana, J.D. Kmetec, IEEE J. Quantum Electron. QE-30, 2698 (1994)
- [6] C. Joshi and P.B. Corkum, “Interactions of Ultra-Intense Laser Light with Matter”, Phys. Today 48, 36 (1995)
- [7] G. Mourou, C.P.J. Barty, M.D. Perry, “Ultrahigh-Intensity Lasers: Physics of the Extreme on a Tabletop”, Phys. Today 51, 22 (1998)
- [8] B.A. Remington, D. Arnett, R.P. Drake, H. Takabe, “Modeling Astrophysical Phenomena in the Laboratory with Intense Lasers”, Science 284, 1488 (1999)
- [9] D. Umstadter, “Review of physics and applications of relativistic plasmas driven by ultra-intense lasers”, Phys. Plasmas 8, 1774 (2001)
- [10] K. Yamanouchi, “Laser Chemistry and Physics: the Next Frontier ”, Science 295, 1659 (2002)
- [11] K.W.D. Ledingham, P. McKenna, R.P. Singhal, “Applications for Nuclear Phenomena Generated by Ultra-Intense Lasers”, Science 300, 1107 (2003)
- [12] S. Augst, D. Strickland, D.D. Meyerhofer, S.L. Chin and J.H. Eberly, “Tunneling Ionization of Noble Gases in a High-Intensity Laser Field”, Phys. Rev. Lett., 63, 2212-2215 (1989)
- [13] W. P. Leemans, C. E. Clayton, W. B. Mori, K. A. Marsh, A. Dyson, and C. Joshi, “Plasma physics aspects of tunnel-ionized gases”, Phys. Rev. Lett. 68, 321-324 (1992)

- [14] W. P. Leemans, C. E. Clayton, W. B. Mori, K. A. Marsh, P. K. Kaw, A. Dyson, C. Joshi, and J. M. Wallace, “Experiments and simulations of tunnel-ionized plasmas”, Phys. Rev. A 46, 1091-1105 (1992)
- [15] J. van Tilborg, C. B. Schroeder, C. V. Filip, Cs. Tth, C. G. R. Geddes, G. Fubiani, R. Huber, R. A. Kaindl, E. Esarey, and W. P. Leemans, “Temporal Characterization of Femtosecond Laser-Plasma-Accelerated Electron Bunches Using Terahertz Radiation”, Phys. Rev. Lett. 96, 014801 (2006)
- [16] C. Max, J. Arons and A. B. Langdon, “Self-modulation and self-focusing of electromagnetic waves in plasmas”, Phys. Rev. Lett., 33, 209-212 (1974)
- [17] W. L. Kruer, “The Physics of Laser Plasma Interactions”, MA: Addison-Wesley (1988)
- [18] T. M. Antonsen, Jr. and P. Mora, “Self-focusing and Raman Scattering of Laser Pulses in Tenuous Plasmas”, Phys. Rev. Lett., 69, 2204-2207, (1992)
- [19] W. B. Mori, C. D. Decker, D. E. Hinkel and T. Katsouleas, “Raman forward scattering of short-pulse high-intensity lasers”, Phys. Rev. Lett. 72, 1482-1485, (1994)
- [20] T. Katsouleas, S. Wilks, P. Chen, J. M. Dawson and J. J. Su, “Beam loading in plasma accelerators”, Particle Accelerators, Vol. 22, pp. 81-99 (1987)
- [21] A. Rousse, K. T. Phuoc, R. Shah, A. Pukhov, E. Lefebvre, V. Malka, S. Kiselev, F. Burgy, J.-P. Rousseau, D. Umstadter, and D. Hulin, “Production of a keV X-Ray Beam from Synchrotron Radiation in Relativistic Laser-Plasma Interaction”, Phys. Rev. Lett. 93, 135005 (2004)
- [22] S. Kiselev, A. Pukhov, and I. Kostyukov, “X-ray Generation in Strongly Nonlinear Plasma Waves”, Phys. Rev. Lett. 93, 135004 (2004)
- [23] C. G. Durfee, III and H. M. Milchberg, “Light pipe for high intensity laser pulses”, Phys. Rev. Lett. 71, 2409 - 2412 (1993)
- [24] H. M. Milchberg, T. R. Clark, C. G. Durfee III, T. M. Antonsen and P. Mora, “Development and applications of a plasma waveguide for intense laser pulses”, Phys. Plasmas 3, 2149 (1996)
- [25] P. Volfbeyn, E. Esarey, and W. P. Leemans, “Guiding of laser pulses in plasma channels created by the ignitor-heater technique”, Phys. Plasmas 6, 2269-2277 (1999)

- [26] W. B. Mori “The Physics of the Nonlinear Optics of Plasmas at Relativistic Intensities for Short-Pulse Lasers”, IEEE Journal of Quantum Electronics, Vol 33, No. 11, 1942 (1997)
- [27] T. Tajima and J.M. Dawson, “Laser Electron Accelerator”, Phys. Rev. Lett. **43**, 267-270 (1979)
- [28] C. Joshi, W. B. Mori, T. Katsouleas, J. M. Dawson, J. M. Kindel, and D. W. Forslund, Ultrahigh gradient particle acceleration by intense laser-driven plasma density waves, Nature, vol. 31 1, pp. 525-529 (1984)
- [29] P. Sprangle, E. Esarey, J. Krall, and G. Joyce, Propagation and guiding of intense laser pulses in plasmas, Phys. Rev. Lett., vol. 69, 2200-2203 (1992)
- [30] C. Coverdale, C. B. Darrow, C. D. Decker, W. B. Mori, K. C. Tzeng, K. A. Marsh, C. E. Clayton, and C. Joshi, Propagation of intense subpicosecond laser pulses through underdense plasmas, Phys. Rev. Lett., 74, 4659-4662 (1995)
- [31] C. E. Clayton, C. Joshi, C. Darrow, and D. Umstadter, “Relativistic Plasma-Wave Excitation by Collinear Optical Mixing”, Phys. Rev. Lett. 54, 2343-2346 (1985)
- [32] C. E. Clayton, K. A. Marsh, A. Dyson, M. Everett, A. Lal, W. P. Leemans, R. Williams, and C. Joshi, “Ultrahigh-gradient acceleration of injected electrons by laser-excited relativistic electron plasma waves”, Phys. Rev. Lett. 70, 37-40 (1993)
- [33] M. Everett, A. Lal, D. Gordon, C. E. Clayton, K. A. Marsh, and C. Joshi, Trapped electron acceleration by a laser-driven relativistic plasma wave, Nature, 368, 527-529 (1994)
- [34] V. Malka, S. Fritzler, E. Lefebvre, M.-M. Aleonard, F. Burgay, J.-P. Chambaret, J.-F. Chemin, K. Krushelnick, G. Malka, S. P. D. Mangles, Z. Najmudin, M. Pittman, J.-P. Rousseau, J.-N. Scheurer, B. Walton, A. E. Dangor, “Electron Acceleration by a Wake Field Forced by an Intense Ultrashort Laser Pulse”, Science Vol. 298, 1596-1600 (2002)
- [35] P. Chen, J. M. Dawson, Robert W. Huff, and T. Katsouleas, “Acceleration of Electrons by the Interaction of a Bunched Electron Beam with a Plasma”, Phys. Rev. Lett. **54**, 693-696 (1985); Phys. Rev. Lett. **55**, 1537 (1985)
- [36] S. Lee, T. Katsouleas, P. Muggli, W. B. Mori, C. Joshi, R. Hemker, E. S. Dodd, C. E. Clayton, K. A. Marsh, B. Blue, S. Wang, R. Assmann, F. J.

- Decker, M. Hogan, R. Iverson, and D. Walz, “Energy doubler for a linear collider”, Phys. Rev. ST Accel. Beams 5, 011001 (2002)
- [37] P. Muggli, S. Lee, T. Katsouleas, R. Assmann, F. J. Decker, M. J. Hogan, R. Iverson, P. Raimondi, R. H. Siemann, D. Walz, B. Blue, C. E. Clayton, E. Dodd, R. A. Fonseca, R. Hemker, C. Joshi, K. A. Marsh, W. B. Mori, and S. Wang, “Collective refraction of a beam of electrons at a plasma-gas interface”, Phys. Rev. ST Accel. Beams 4, 091301 (2001)
 - [38] S. Lee, T. Katsouleas, R. G. Hemker, E. S. Dodd and W. B. Mori, “Plasma-wakefield acceleration of a positron beam”, Phys. Rev. E 64, 045501 (2001)
 - [39] E. S. Dodd, R. G. Hemker, C.-K. Huang, S. Wang, C. Ren, W. B. Mori, S. Lee, and T. Katsouleas, “Hosing and Sloshing of Short-Pulse GeV-Class Wakefield Drivers”, Phys. Rev. Lett. 88, 125001 (2002)
 - [40] S. Wang, C. E. Clayton, B. E. Blue, E. S. Dodd, K. A. Marsh, W. B. Mori, C. Joshi, S. Lee, P. Muggli, T. Katsouleas, F. J. Decker, M. J. Hogan, R. H. Iverson, P. Raimondi, D. Walz, R. Siemann, and R. Assmann, “X-Ray Emission from Betatron Motion in a Plasma Wiggler”, Phys. Rev. Lett. 88, 135004 (2002)
 - [41] C. E. Clayton, B. E. Blue, E. S. Dodd, C. Joshi, K. A. Marsh, W. B. Mori, S. Wang, P. Catravas, S. Chattopadhyay, E. Esarey, W. P. Leemans, R. Assmann, F. J. Decker, M. J. Hogan, R. Iverson, P. Raimondi, R. H. Siemann, D. Walz, T. Katsouleas, S. Lee, and P. Muggli, “Transverse Envelope Dynamics of a 28.5-GeV Electron Beam in a Long Plasma”, Phys. Rev. Lett. 88, 154801 (2002)
 - [42] C. OConnell, F.-J. Decker, M. J. Hogan, R. Iverson, P. Raimondi, R. H. Siemann, D. Walz, B. Blue, C. E. Clayton, C. Joshi, K. A. Marsh, W. B. Mori, S. Wang, T. Katsouleas, S. Lee, and P. Muggli, “Dynamic focusing of an electron beam through a long plasma”, Phys. Rev. ST Accel. Beams 5, 121301 (2002)
 - [43] M. J. Hogan, C. E. Clayton, C. Huang, P. Muggli, S. Wang, B. E. Blue, D. Walz, K. A. Marsh, C. L. OConnell, S. Lee, R. Iverson, F.-J. Decker, P. Raimondi, W. B. Mori, T. C. Katsouleas, C. Joshi, and R. H. Siemann, “Ultrarelativistic-Positron-Beam Transport through Meter-Scale Plasmas”, Phys. Rev. Lett. 90, 205002 (2003)
 - [44] B. E. Blue, C. E. Clayton, C. L. OConnell, F.-J. Decker, M. J. Hogan, C. Huang, R. Iverson, C. Joshi, T. C. Katsouleas, W. Lu, K. A. Marsh, W. B.

- Mori, P. Muggli, R. Siemann, and D. Walz, “Plasma-Wakefield Acceleration of an Intense Positron Beam”, Phys. Rev. Lett. 90, 214801 (2003)
- [45] G. Rumolo, A. Z. Ghalam, T. Katsouleas, C. K. Huang, V. K. Decyk, C. Ren, W. B. Mori, F. Zimmermann, and F. Ruggiero, “Electron cloud effects on beam evolution in a circular accelerator”, Phys. Rev. ST Accel. Beams 6, 081002 (2003)
- [46] S. Deng, C. D. Barnes, C. E. Clayton, C. OConnell, F. J. Decker, O. Erdem, R. A. Fonseca, C. Huang, M. J. Hogan, R. Iverson, D. K. Johnson, C. Joshi, T. Katsouleas, P. Krejcik, W. Lu, K. A. Marsh, W. B. Mori, P. Muggli, and F. Tsung, “Plasma wakefield acceleration in self-ionized gas or plasmas”, Phys. Rev. E 68, 047401 (2003)
- [47] P. Muggli, B. E. Blue, C. E. Clayton, S. Deng, F.-J. Decker, M. J. Hogan, C. Huang, R. Iverson, C. Joshi, T. C. Katsouleas, S. Lee, W. Lu, K. A. Marsh, W. B. Mori, C. L. O’Connell, P. Raimondi, R. Siemann, and D. Walz, “Meter-Scale Plasma-Wakefield Accelerator Driven by a Matched Electron Beam”, Phys. Rev. Lett. 93, 014802 (2004)
- [48] M. J. Hogan, C. D. Barnes, C. E. Clayton, F. J. Decker, S. Deng, P. Emma, C. Huang, R. H. Iverson, D. K. Johnson, C. Joshi, T. Katsouleas, P. Krejcik, W. Lu, K. A. Marsh, W. B. Mori, P. Muggli, C. L. O’Connell, E. Oz, R. H. Siemann, and D. Walz, “Multi-GeV Energy Gain in a Plasma-Wakefield Accelerator”, Phys. Rev. Lett. 95, 054802 (2005)
- [49] W. Lu, C. Huang, M. Zhou, W. B. Mori and T. Katsouleas, “Limits of linear plasma wakefield theory for electron or positron beams”, Phys. Plasma **12**, 063101 (2005)
- [50] S. Deng, C. D. Barnes, C. E. Clayton, C. OConnell, F. J. Decker, R. A. Fonseca, C. Huang, M. J. Hogan, R. Iverson, D. K. Johnson, C. Joshi, T. Katsouleas, P. Krejcik, W. Lu, W. B. Mori, P. Muggli, E. Oz, F. Tsung, D. Walz, and M. Zhou, “Hose Instability and Wake Generation by an Intense Electron Beam in a Self-Ionized Gas”, Phys. Rev. Lett. 96, 045001 (2006)
- [51] W. Lu, C. Huang, M. Zhou, W. B. Mori and T. Katsouleas, “Nonlinear theory for relativistic plasma wakefields in the blowout regime”, Phys. Rev. Lett. **96**, 165002 (2006)
- [52] W. Lu, C. Huang, M. Zhou, M. Tzoufras, F. S. Tsung, W. B. Mori and T. Katsouleas, “A nonlinear theory for multidimensional relativistic plasma wave wakefields”, Phys. Plasmas 13, 056709 (2006)

- [53] D. K. Johnson, D. Auerbach, I. Blumenfeld, C. D. Barnes, C. E. Clayton, F. J. Decker, S. Deng, P. Emma, M. J. Hogan, C. Huang, R. Ischebeck, R. Iverson, C. Joshi, T. C. Katsouleas, N. Kirby, P. Krejcik, W. Lu, K. A. Marsh, W. B. Mori, P. Muggli, C. L. OConnell, E. Oz, R. H. Siemann, D. Walz, and M. Zhou, “Positron Production by X Rays Emitted by Betatron Motion in a Plasma Wiggler”, Phys. Rev. Lett. 97, 175003 (2006)
- [54] M. J. Hogan, C. D. Barnes, C. E. Clayton, F. J. Decker, S. Deng, P. Emma, C. Huang, R. H. Iverson, D. K. Johnson, C. Joshi, T. Katsouleas, P. Krejcik, W. Lu, K. A. Marsh, W. B. Mori, P. Muggli, C. L. OConnell, E. Oz, R. H. Siemann, , D. Walz and M. Zhou, “42-GeV Energy Gain in a Plasma-Wakefield Accelerator”, to be published in Nature
- [55] Guo-Zheng Sun, Edward Ott, Y. C. Lee, and Parvez Guzdar , “Self-focusing of short intense pulses in plasmas”, Phys. Fluids, 30, 526 (1987)
- [56] J. B. Rosenzweig, B. Breizman, T. Katsouleas, and J. J. Su, “Acceleration and focusing of electrons in two-dimensional nonlinear plasma wake fields”, Phys. Rev. A 44, R6189 (1991)
- [57] W. B. Mori et. al. aac proceedings
- [58] A. Pukhov and J. Meyer-ter-vehn, “Laser wake field acceleration: the highly non-linear broken-wave regime”, Appl. Phys. B: Lasers Opt. 74, 355 (2002)
- [59] F.S.Tsung, Ritesh Narang, W. B. Mori, C. Joshi, R. A. Fonseca, and L. O. Silva, “Near-GeV-Energy Laser-Wakefield Acceleration of Self-Injected Electrons in a Centimeter-Scale Plasma Channel”, Phys. Rev. Lett. 93, 185002 (2004)
- [60] S. P. D. Mangles, C. D. Murphy, Z. Najmudin et al., “Monoenergetic beams of relativistic electrons from intense laserplasma interactions”, Nature 431, 535 - 5388 (2004)
- [61] C.G.R Geddes, Cs. Toth, J. van Tilborg et al., “High-quality electron beams from a laser wakefield accelerator using plasma-channel guiding”, Nature 431, 538 - 541 (2004)
- [62] J. Faure, Y. Glinec, A. Pukhov et al., “A laserplasma accelerator producing monoenergetic electron beams”, Nature 431, 541 - 544 (2004)
- [63] Wim P. Leemans, Bob Nagler, Anthony J. Gonsalves, Csaba Tth, Kei Nakamura, Cameron G. R. Geddes, Eric Esarey, Carl B. Schroeder, and Simon M. Hooker, ”GeV electron beams from a cm-scale accelerator,” October issue of Nature Physics (2006)

- [64] Charles K. Birdsall and A.Bruce Langdon, “Plasma Physics Via Computer Simulation”, McGraw Hill Higher Education (1984)
- [65] A.I. Akhiezer and R.V. Polovin, “Theory of wave motion of an electron plasma”, JETP (U.S.S.R.) **30**, 915-928 (1956)
- [66] J.M. Dawson, “Nonlinear Electron Oscillations in a Cold Plasma ”, Phys. Rev. 113, 383-387 (1959)
- [67] T. P. Coffey, “Breaking of Large Amplitude Plasma Oscillations”, Phys. Fluids, 14, 1402 (1971)
- [68] T. Katsouleas and W. B. Mori, “Wave-Breaking Amplitude of Relativistic Oscillations in a Thermal Plasma ”, Phys. Rev. Lett., 61, 90, (1988)
- [69] W. B. Mori and T. Katsouleas, “Wavebreaking of Longitudinal Plasma Oscillations”, Physica Scripta T30, 127 (1990)
- [70] J. B. Rosenzweig, “Trapping, thermal effects, and wave breaking in the nonlinear plasma wake-field accelerator”, Phys. Rev. A 38, 3634 (1988)
- [71] J. B. Rosenzweig, “Multiple-fluid models for plasma wake-field phenomena”, Phys. Rev. A 40, 5249 (1988)
- [72] Z. M. Sheng and J. Meyer-ter-Vehn, “Relativistic wave breaking in warm plasmas”, Phys. Plasmas 4, 493 (1997)
- [73] C. B. Schroeder, E. Esarey and B. A. Shadwick, “Warm wave breaking of nonlinear plasma waves with arbitrary phase velocities”, Phys. Rev. E 72, 055401(R), 2005
- [74] W. Lu, Master thesis, UCLA (2004)
- [75] R.A.Fonseca et al., “OSIRIS: A Three-Dimensional, Fully Relativistic Particle in Cell Code for Modeling Plasma Based Accelerators”, In P.M.A. Sloot et al., editors, ICCS 2002, LNCS 2331, 342-351,(2002)
- [76] J.B. Rosenzweig, AIP Conference Proceedings 647, Melville, New York, 2002, Advanced Accelerator Concepts, Tenth Workshop, Mandalay Beach, California, 22-28, p.577 June (2002)
- [77] N. Barov and J.B. Rosenzweig, Phys. Rev. STAB 7, 061301 (2004)
- [78] K.V. Lotov, “Blowout regimes of plasma wakefield acceleration”, Phys. Rev. E 69, 046405 (2004)

- [79] I. Kostyukov and A. Pukhov, "Phenomenological theory of laser-plasma interaction in "bubble" regime", Phys. Plasma 11, 5256-5264 (2004)
- [80] S. Gordienko and A. Pukhov, "Scalings for ultrarelativistic laser plasmas and quasimonoenergetic electrons", Phys. Plasma 12,043109 (2005)
- [81] P. Sprangle, E. Esarey, and A. Ting, "Nonlinear theory of intense laser-plasma interactions", Phys. Rev. Lett. 64, 2011-2014 (1990)
- [82] D.H. Whittum, "Transverse two-stream instability of a beam with a Bennett profile", Phys. Plasmas 4, 1154 (1997)
- [83] P. Mora and T.M. Antonsen,Jr., "Kinetic modeling of intense, short laser pulses propagating in tenuous plasmas", Phys. Plasma, 4 217-229, (1997)
- [84] P. Sprangle, E. Esarey, J. Krall and A. Ting, IEEE Trans. Plasma Sci., 15, 145,(1987)
- [85] E. Esarey, P. Sprangle, J. Krall and A. Ting, IEEE Trans. Plasma Sci., 24, 145,(1996)
- [86] C. D. Decker, W.B.Mori, K.-C. Tzeng and T. Katsouleas, "The evolution of ultra-intense, short-pulse lasers in underdense plasmas",Phys. Plasmas 3, 2047 (1996)